DEGRADATION OF ATRAZINE UTILIZING TRIAZINE HYDROLASE (TRZN) FROM *ARTHROBACTER AURESCENS* TC1

By
Karla Diviesti

A thesis submitted to the Faculty and the Board of Trustees of the Colorado School of Mines in partial fulfillment of the requirements for the degree of Doctor of Philosophy (Quantitative Biosciences and Engineering)

Golden, Colorado
Date _____

Signed: _____
Karla Diviesti

Signed: _____
Dr. Richard Holz Thesis Advisor

Golden, Colorado
Date _____

Signed: _____
Dr. Nannette Boyle
Professor and Program Head
Quantitative Biosciences and Engineering

ABSTRACT

Triazine hydrolase (TrzN) from *Arthrobacter aurescens* TC1 is a Zn(II) dependent hydrolytic dehalogenase from the amidohydrolase super family. TrzN has 22 unique substrates. Most notably, TrzN can hydrolytically dechlorinate atrazine (2-chloro-4-ethylamino-6-isopropylamino-s-triazine) to its less toxic derivative hydroxyatrazine. Atrazine is a widely used synthetic herbicide which has an extensive list of potential environmental and health concerns. TrzN is a prime target for use in the engineering of biocatalysts for atrazine remediation. However, its catalytic and biochemical properties are not fully understood. This research project provides insight into the catalytic mechanism of TrzN as well as explores the enzymes use in biomaterials for atrazine degradation.

Insight into the catalytic mechanism of TrzN has been provided in chapter 2. Three amino acids (Thr325, Glu241, and His274) showed significant catalytic importance. Thr325 is essential for catalysis and data agreed that an essential bond is formed between the Thr325 oxygen and the Zn(II)-bound water moiety which likely stabilizes the water moiety for nucleophilic attack. The mechanism functions based on a two proton transfer system. First the His274 residue removes a proton form the Zn(II)-bound water moiety. The proton is shuttle from His274 to Glu241 which can then form a hydrogen bond with the triazole nitrogen on the atrazine ring positioning it for nucleophilic attack. In chapters 3 and 4, TrzN was immobilized in alginate, sol-gel, and mesoporous nanoparticle (MSN) biomaterials. All of the biomaterials were catalytically active and could degrade atrazine to hydroxyatrazine. Using enzymes as biocatalyst can traditionally be tricky, the inability to recover the catalyst and the enzymes inherent unstable nature makes the process costly and inefficient. Often, the solution to these short comings has been to immobilize enzymes in functional biomaterials. The biomaterials tested in these chapters were all able to be recovered and reused cyclically and over several weeks while maintaining or improving TrzN's stability. This research herein provides insight into a new avenue to design bioremediation methodologies for the removal of atrazine utilizing TrzN.

TABLE OF CONTENTS

LIST OF FIGURES

LIST OF TABLES

ACKNOWLEDGEMENTS

I would first like to acknowledge and thank Dr. Holz for accepting me into his lab and for his guidance and support as I worked through my project. His patience, mentorship, and humor created an environment where scientific exploration and continual education blossomed. I am very proud to be his first graduate student at the Colorado School of Mines and I am thankful for the opportunities and experiences he cultivated during my PhD studies. I would also like to acknowledge the NSF for the funding which made the work presented here possible.

I would like to thank my committee members Dr. Trewyn, Dr. Krebs, and Dr. Domaille for playing major roles in the completion of my degree. Their guidance contributed greatly to the work presented herein and I appreciate their insights, comments, and enlightening discussions. On the same note, I would like to thank the Colorado School of Mines Chemistry department and Quantitative Biosciences and Engineering program. Specifically, Dr. Cash and Dr. Boyle for playing integral roles in the implementation of the Quantitative Biosciences and Engineering program.

I am grateful for the relationships I built throughout my program with my fellow graduate students. Specifically, the “greenhouse gang”; Dr. Irene Ogutu, Dr. Amy Boncella, Callie Miller, Grayson Gerlich, Maya Mowery-Evans, Noha Alansari, Emily Sabo, Jesse Hudspeth, Bobby Santore, and Sarah Evans. Their presence was always a source of encouragement, and their discussions enabled me to carry out my work diligently. Lastly, their ability to keep plants alive in our office does not go unnoticed.

Finally, I am thankful for my family and friends. My mother Katherine Diviesti, my father Anthony Diviesti and my brother Michael Diviesti for the love and care throughout my studies and for contributing to who and what I am today. My friends Will McCaffrey, Micaela Seaver, Jose Ramirez, Valeria Vindas, Jessica O'Connell, Kassy Chessire, Nick Minella, and Mitchell Vallis for the continued support and for helping make Colorado my home.

CHAPTER 1

INTRODUCTION

1.1 General Introduction/Thesis Overview

An introduction to the ideas and principles that are the foundation for this research are presented here in Chapter 1. The backbone of this work focuses on the environmental contamination of halogenated aromatic compounds, specifically atrazine. The chapter proceeds with outlining the types of enzymatic dehalogenation reactions and provides background on why triazine hydrolase (TrzN) from *Arthrobacter aurescens* TC1 was chosen as the enzyme of interest for this work. The last section focuses on exploring how biomaterials can play a major role in the solution to atrazine bioremediation. The chapter concludes by outlining the research aims for this project.

1.2 Atrazine

Atrazine (2-chloro-4-ethylamino-6-isopropylamino-s-triazine) is a widely used synthetic herbicide that selectively controls broad leaf (dicot) weeds.[1] Atrazine is a chloro-triazine, which is a group of structurally similar herbicides that differ only in specific s-trazine 4- and 6-N-alkyl substituents while sharing a common mechanism of action by inhibiting mitochondrial respiration. This group of herbicides also includes; cyanazine, propazine, simazine, and terbuthylazine.[2] Initially registered in 1958 in Sweden by CIBA-GEIGY, atrazine was approved for use in the United States in the early 1960's.[1,3] Since then atrazine has become the second most abundantly applied herbicide, despite the environmental and health concerns.[2] The alarming potential toxic effects of atrazine resulted in its banishment from the European Union (EU) in

2004 with the committee citing "ubiquitous and unpreventable water contamination".[4] However in the United states, ~30,000 tons of atrazine is still applied annually.[3]

Controversy stems from atrazine's persistence and mobility in watersheds as it can be transported more than 1,000 km from its initial point of application.[5] Samples of atrazine have been found in soil, plantations, pastures, public water supply reservoirs, groundwater, streams, lakes, rivers, seas, and even glaciers in remote areas.[3,6] Atrazine's mobility can likely be attributed to its resistance to microbial decomposition and therefore stability in soil and water. A 2020 model developed for atrazine mobility indicated that variables such as crop type, geographic location, weight of atrazine applied, and soil type were factors contributing to the quantity of atrazine entering the watershed.[7] Moreover, atrazine's half-life in soil varies from 14 days to 4 years, and in water 6 months to several years.[3] These characteristics have made atrazine the most common pesticide contaminant of ground and surface water in the United States.[8]

Once in a watershed, atrazine has a wide breadth of negative effects. Starting at the bottom of the aquatic hierarchy, atrazine disrupts aquatic flora.[9] The concentration equivalent level of concern (CE- LOC) ranges from 1.9 to 26 μg/L. Aquatic fauna experience ~60% reduction in abundance with atrazine concentrations of 20 μg/L, and a similar ~60% inhibition of growth when atrazine concentrations in the aquatic soil are as low as 1 μg/kg sediment.[9] Algae from *Chlorella vulgaris* experiences inhibited electron transfer as soon as 1 hour after exposure to atrazine at concentrations as low as 1 μg/L.[3] Green algae consistently shows inhibition in growth and chlorophyll production at 10 μg/L of atrazine.[10] The subsequent decrease of primary production is directly related to a decrease in dissolved oxygen, carbon, nitrogen, phosphorous, and pH as well as an increase in suspended solids and calcium.[9] These fluctuations correlate directly to an unhealthy and unstable ecosystem.

Moving up in the food chain, atrazine is also toxic to higher eukaryotes such as crustaceans, insects, mollusk, fish, amphibians, and reptiles.[3] Frogs are some of the most heavily impacted organisms by atrazine. Male frogs exposed to atrazine exhibit feminization, depressed testosterone, decreased breeding gland size, demasculinized laryngeal development, suppressed mating behavior, reduced spermatogenesis, and decreased fertility.[11,12] In addition, zebra fish experience inhibition of the expression of neurotoxicity related genes suggesting atrazine is a neuroendocrine disruptor. Zebra fish also experience several developmental endpoints such as heartbeat, hatchability, and morphological abnormalities influenced by atrazine exposure in early life phases.[13] The EPA recognizes the impact of atrazine in aquatic environments, as outlined in the *Atrazine Proposed Interim Registration Review* published in December 2019. The agency expressed concern for atrazine concentrations in the watershed impacting aquatic plant communities and thus disrupting all levels of the food chain.[3]

Atrazine's abundance in numerous watersheds is a pipeline to direct and indirect human exposure. The Agency for Toxic Substances and Disease Registry (ATSDR) in 2003 warned that people in rural communities, near agricultural land, are at increased risk of atrazine exposure primarily through drinking water.[14] Quantifying the toxicity of atrazine to humans is difficult due to no available human toxicokinetic studies.[2] Therefore mammalian studies become the benchmark for potential toxicity in humans. Animal studies revealed atrazine-linked endocrine effects such as decreased semen quality, increased incidence of testicular cancers, and increased rates of developmental abnormalities in male and female reproductive tracts.[15] In 2000, the EPA Endocrine Disruptor Screening and Testing Advisory Committee recognized atrazine as an endocrine toxin in humans.[16] Although the literature has some gaps regarding the short and long term effects of atrazine on human health, what is apparent by existing research is that it is

imperative that solutions are explored to eradicate atrazine from the environment. One potential solution would be the abolition of atrazine from farming practices all together. The elimination of atrazine would not only improve human health and the environment, it would increase farm revenues with having an impact measured barely in pennies on consumer prices.[17] However in the current economic and social environment, targeting the biodegradation of atrazine is a more effective and easily implemented method of protecting water supplies while legislation is drafted to ban it.[1]

1.3 Enzymatic Dehalogenation

Dehalogenation is an elimination reaction where the leaving group is a halogen. In the case of atrazine, the leaving group would be a chlorine ion. It has been observed that hydrolytic dechlorination decreases or eliminates the herbicidal activities of chloro-s-triazines.[18] Within a bacterial system, enzymes catalyze dechlorination to utilize atrazine as a source of carbon or nitrogen.[19] The first bacterial dehalogenase was purified in 1960.[20] The biological origin of these enzymes remains unclear but some studies suggest the emergence of dehalogenases from precursor enzymes in response to large concentrations of xenobiotic halogenated substrates. Other theories propose pre-industrial emergence due to many different organohalogens occurring naturally, suggesting that corresponding dehalogenation activities exist in nature.[21] Clearly there are a few key enzymatic mechanisms for dehalogenation.

1.3.1 Reductive Dehalogenation

Reductive dehalogenation involves the removal of a halogen from a molecule with the concurrent addition of electrons. There are two variations of this reaction. The first is hydrogenolysis, which replaces the halogen with a hydrogen atom (Figure 1A). The second

process is vicinal reduction, also known as dihaloelimination, which is the removal of two halogens from adjacent carbon atoms with the formation of an additional bond between the carbon atoms (Figure 1B).[22]

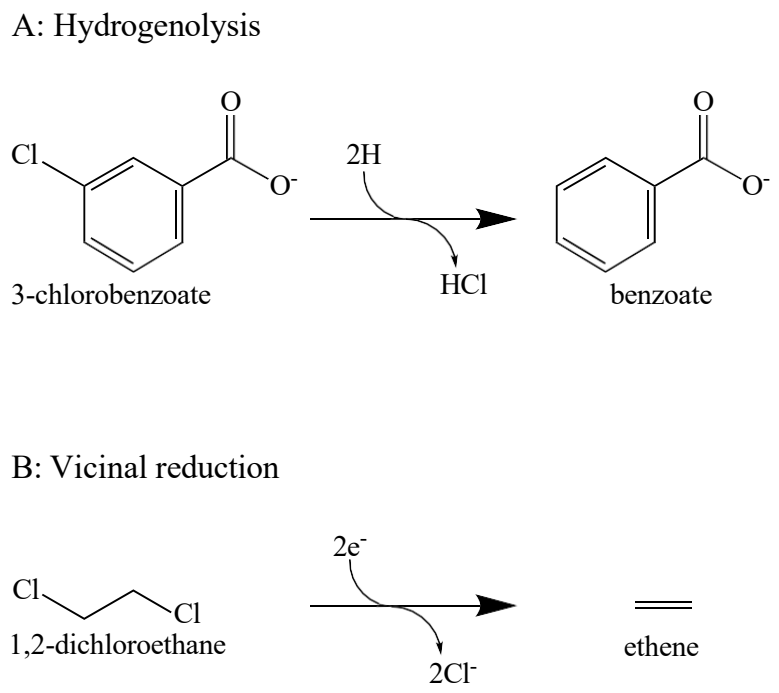

Figure 1.1. Examples of reductive dehalogenation. A. hydrogenolysis of 3-chlorobenzoate to benzoate. B. vicinal reduction of 1,2-dichloroethane to ethene.

The first purification of a reductive dehalogenase was in 1995 from *Desulfomonile tiedjei*.[23] Since then, a diverse class of enzymes has evolved with similar biochemical features despite having high sequence variability.[24] Reductive dehalogenase genes are typically composed of operons containing two proteins, the first being the active subunit and the second being a small putative membrane anchor protein. The anchor protein binds the active subunit to the outside of the cytoplasmic membrane.[24,25] The active subunit reductive dehalogenase is highly oxygen sensitive, contains two Fe-S clusters, and all but one known purified species contain a corrinoid cofactor.[24,26] Although a fascinating system, reductive dehalogenases do not

make good candidates to attack the current environmental crisis occurring with halogenated compounds due to their complexity and air sensitivity.[24]

1.3.2 Oxidative Dehalogenation

Oxidative dehalogenation is a non-respiratory dehalogenation process that results in the removal of halogens from an organic backbone with no energetic benefit to the organisms other than freeing organic carbon to be used catabolically.[27,28] This process involves the introduction of a single oxygen atom from the available molecular oxygen, which replaces the halogen with a hydroxyl group. The second oxygen atom is then usually reduced to form water.[29,30] Several mono- and dioxygenase systems can perform oxidative dehalogenation.[31] Many oxygenases non-specifically oxygenate haloaromatics and generate unstable intermediates from which the halogen is spontaneously eliminated.[28] For monooxygenation of halogenated aromatics, the majority of the reactions are catalyzed by flavin-dependent monooxygenases.[32] Dioxygenation varies slightly with the incorporation of two hydroxyl groups into organic substrates, with both oxygens still derived from available O_2 (Figure 1.2).[32] Similar to reductive dehalogenases as mentioned above, oxidative dehalogenation is fascinating, however, the complexity of the pathways involving co-factors again makes these systems less promising.

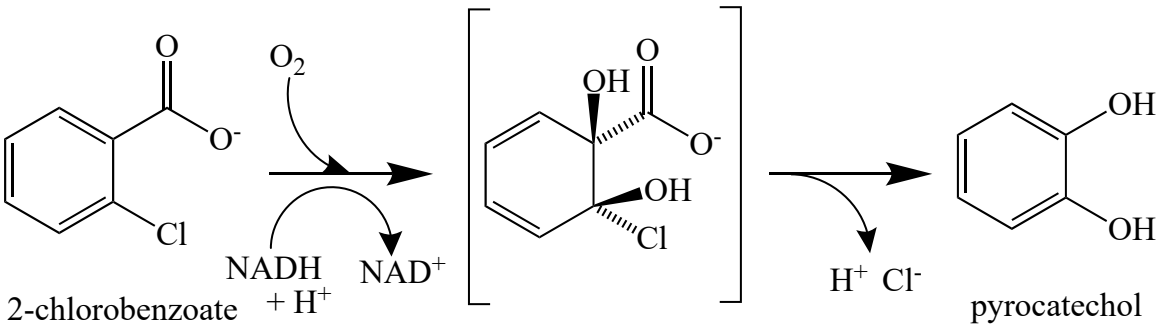

Figure 1.2. Dioxygenolytic dichlorination of 2-halobenzoate 1,2dioxygenase from Pseudomonas sp. 2CBS and Pseudomonas aeruginosa strain 142.

1.3.3 Thiolytic Dehalogenation

Thiolytic dehalogenation is a substitutive mechanism with glutathione as a co-factor where an unstable glutathione intermediate is hydrolyzed (Figure 3.).[20,31] These enzymes use reduced glutathione for nucleophilic displacement under mainly anaerobic conditions with no electron transfer.[33] There is a single example of aerobic thiolytic dehalogenation mediated by cytosolic glutathione.[34] Some studies refer to thiolytic dehalogenases as reductive dehalogenases due to their similar mechanisms, but for the point of this literature review they will be discussed separately. Well studied examples of thiolytic dehalogenation are glutathione S-transferases. This enzyme catalyzes the formation of an unstable S-chloromethyl glutathione intermediate that is subsequently hydrolyzed.[35] Dichloromethane dehalogenase (DcmA), a glutathione S-transferase, catalyzes a bimolecular nucleophilic substitution (S_N2) reaction releasing Cl^-, formaldehyde, and forms S-chloromethylglutathione that spontaneously hydrolyzes to glutathione.[36] As stated above with oxidative and reductive dehalogenases, thiolytic dehalogenases present fairly complex systems with cofactors that would not be strong candidates for bioremediation applications.

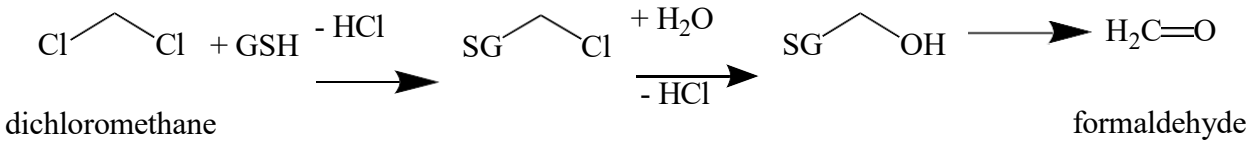

Figure 1.3. Thiolytic dehalogenation of dichloromethane catalyzed by glutathione transferase.

1.3.4 Hydrolytic Dehalogenation

Hydrolytic dehalogenation is the replacement of a halogen by a hydroxyl group derived from H_2O using nucleophilic substitution.[20,32] Commonly, hydrolytic dehalogenation is the first step in the aerobic degradation of halogenated aliphatic compounds. This initial step funnels the

haloaliphatic substrate into a central metabolic process, which allows bacteria to utilize the reaction products as a carbon source.[28] As recent as the 1990s, hydrolytic dehalogenation of aromatic compounds had been rarely described, likely due to haloaromatics resistance to nucleophilic displacement under physiological conditions. Some exceptions include bacterial isolates from the genera *Pseudomonas*, *Arthrobacter*, and *Corynebacterium*.[28] Since then, a small number of enzymes have been isolated, purified, and characterized that can hydrolytically dehalogenate aromatic substrates.

1.4 4-Chlorobenzoate Dehalogenase

One of the first hydrolytic dehalogenase enzyme systems to be purified was a 4-chlorobenzoate (4-CBA) dehalogenase. It was shown previously using ^{18}O labeled substrates, that multiple bacteria isolated from soil could hydrolytically dechlorinate 4-chlorobenzoate to 4-hydrobenzoate (4-HBA).[37] Looking closer at this system from *Pseudomonas* sp. strain CBS-3, the three proteins within this system operate in the following way for the removal of chlorine. 4-halobenzoate-coenzyme A ligase activates 4-chlorobenzoate in a coenzyme A, ATP and Mg^{2+} dependent reaction to 4-chlorobenzoyl-coenzyme A. Then the thioester intermediate is dehalogenated by the 4-chlorobenzoyl-coenzyme A dehalogenase. To finish, the coenzyme A is split off by a 4-hydroxybenzoyl-CoA thioesterase to form the dehalogenated product 4-hydroxybenzoate (Figure 4.).[38]

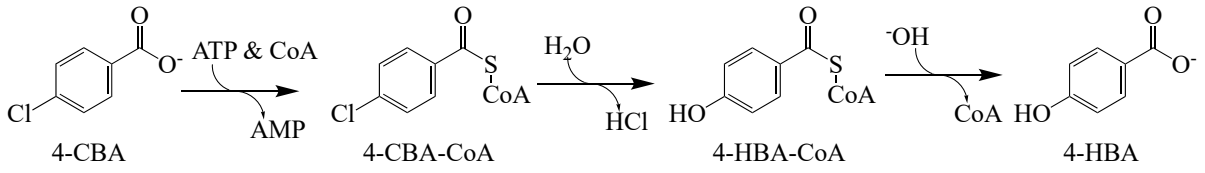

Figure 1.4. The hydrolysis of 4-CBA to 4-HBA was carried out by three enzymes.

Focusing on the 4-CBA-CoA dehalogenase, this enzyme is hypothesized to have evolved relatively recently due to its substrate, 4-CBA, which is not derived from a natural product and is known to be a byproduct of the oxidative biodegradation of 4-chlorobiohenyl, a synthetic pollutant.[39] The crystal structure suggests the enzyme is a flattened sphere shaped trimer with each subunit being overall very similar with two distinct domains (Figure 5.).[40]

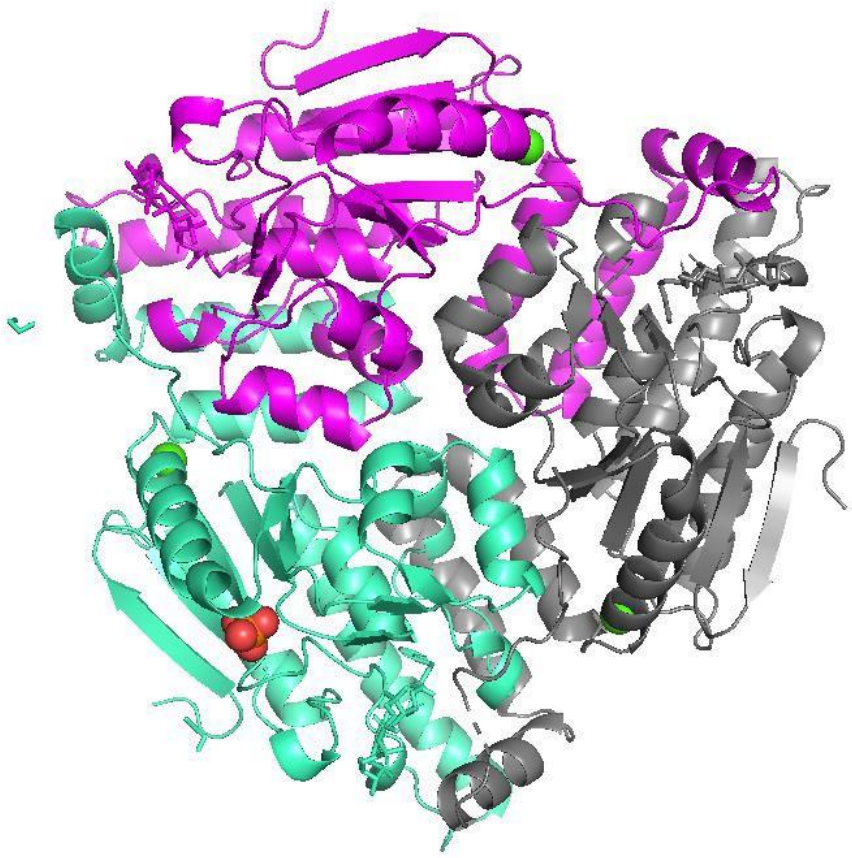

Figure 1.5. The trimer crystal structure of 4-CBA from *Pseudomonas* sp. strain CBS-3

The first domain is the catalytic domain stemming from the N-terminus and the second domain is smaller and likely responsible for the trimerization of the protein.[40] A two-step mechanism is proposed with the second step being the rate-limiting step. The first step is nucleophilic addition to the aromatic ring that utilizes an active site carboxylate, Asp145, as the attacking nucleophile. Trp137 is essential as a hydrogen bond donor to Asp145.[41] The second step cleaves the enzyme-aryl linkage by attacking the carbonyl carbon with H_2O as the nucleophile and His90 acting as the general base.[39,40,42] His90 serves another essential catalytic roles such as acting as a barrier between the solvent and the active site. Hydration of the active site inhibits the dissociation of Cl^- resulting in decreased activity. The residue is also important to regeneration of the active enzyme.[42] This system can be found in soil dwelling bacteria and other genera such as *Arthrobacte*r.[43,44]

1.5 Chlorothalonil Dehalogenase

For years, the 4-CBA-CoA dehalogenase was the only reported dehalogenase active on aromatic compounds. However, in 2010 a new hydrolytic dehalogenase for Chlorothalonil (2,4,5,6-tetrachloroisophthalonitrile; TPN) was characterized from the bacterial strain *Pseudomonas sp*. ctn-3 and appropriately named chlorothalonil hydrolytic dehalogenase (Chd).[45] From the amino acid sequence and secondary structure, it can be deduced that Chd is a member of the β-lactamase superfamily and displays the characteristic αβ/βα sandwich and conserved His-X-His-X-Asp-His motif with the first histidine being replaced with a serine.[45] Early reports suggested Chd is a monomer with a binuclear Zn(II) center.[46] However, this claim was quickly debunked and Chd is a homodimer (~72 kDa) with a mononuclear Zn(II) site in each active site as well as a structural Zn(II) at the interface between the two monomers (Figure 6).[47,48]

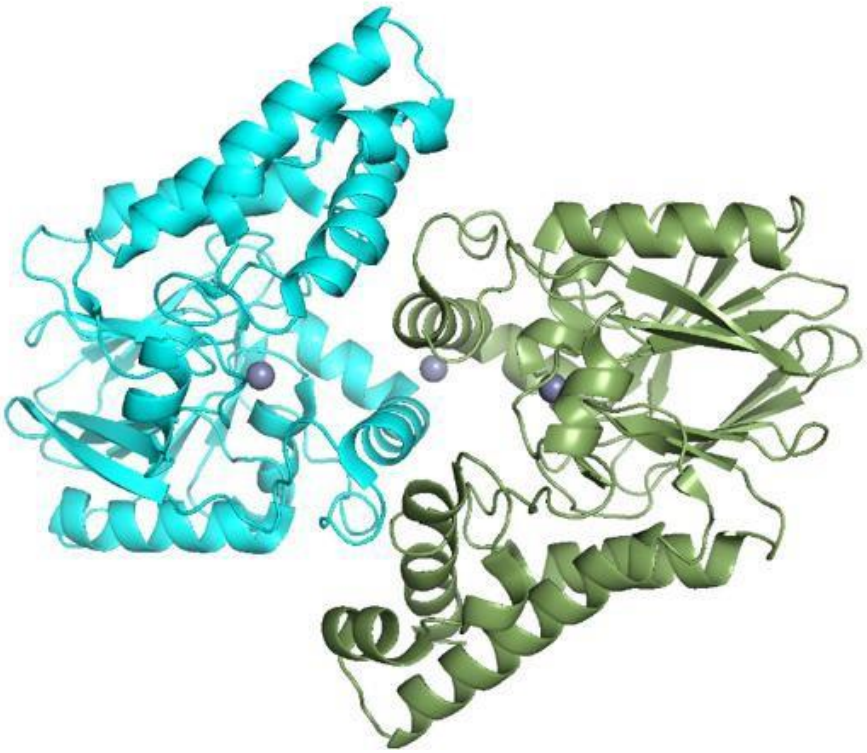

Figure 1.6. Crystal structure of the Chd homodimer from *Pseudomonas sp*. ctn-3. Grey spheres represent the Zn(II) ions.

The structural Zn(II) ion is located at the "top" of the protein and is not accessible to the bulk solvent. It resides in a tetrahedral geometry coordinated by the N^{ϵ} nitrogen atom of His143 and a carboxylate oxygen atom of Asp146 from each subunit. The structure suggests it assists in the formation of two bent channels that provide access to the catalytic Zn(II) ions.[48] The bent channel starts at the "bottom" of the protein and forms a Y-shaped path in which each branch of the Y connects to one of the catalytic Zn(II) ions and the shared single large channel is open to bulk solvent.[48] The Y channel is likely responsible for shuttling different reactants and products to and from the active site.

Looking more closely at the active site, the Zn(II) ion resides in a distorted trigonal bipyramid (TBP) geometry (Figure 1.7).[48] The catalytic Zn(II) ligands include the N^{ϵ} nitrogens of His117 and His257 in equatorial positions with a water/hydroxide oxygen. In the axial positions there are oxygen atoms from Asp116 and Asn216. Another important residue is His114, which presents itself in two alternate conformations. In conformation A, the N^{ϵ} nitrogen is hydrogen bound to the water/hydroxide oxygen atom and the nitrogen atom of Asn216. In conformation B, the hydrogen bond to the water/hydroxide oxygen is lost and possibly the hydrogen bond to Asn216 is lost as well.[48] In the past five years, serious headway has been made investigating the tertiary and quaternary structure of Chd; however, more work is needed to elucidate the purpose of the Y-shaped channel.

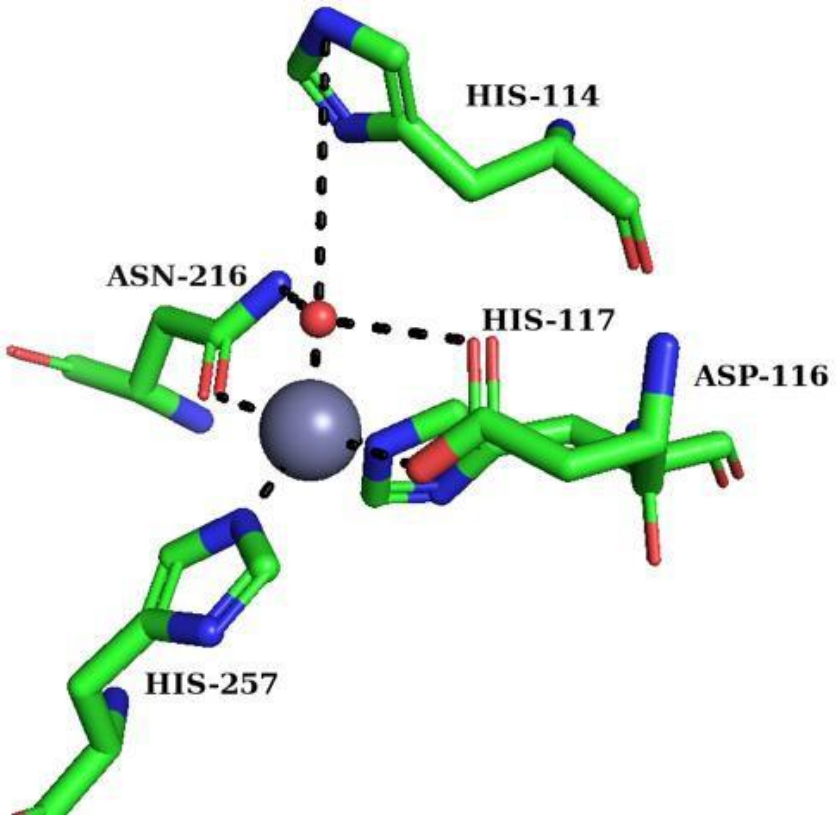

Figure 1.7. ChD active site. The grey sphere represents the catalytic Zn(II) ion and the catalytic water is shown as a red sphere.

Looking at the proposed mechanism, the first step in catalysis is the recognition of TPN by the large hydrophobic pocket of the Y-shaped channel that leads to the Zn(II) active site.[48] His114 and Trp227 sterically shape the conformation of the active site to recognize and orient TPN. TPN is positioned by a $\pi - \pi$ interaction with Trp227, a residue that is important for catalytic turnover.[45,48,49] Next, substrate docked in the active site suggest a hydrogen bond between the nitrogen atom of a TPN cyano group and the amide nitrogen of Asn216.[48,49] These docking studies showed an absence of favorable conformations for TPN to bind directly to the zinc center. This proposed hydrogen bonding interaction activates the ortho carbon for nucleophilic attack by removing electron density from the aromatic ring and simultaneously activating the coordinated water/hydroxide to function as the nucleophile.[48,49] His114 then deprotonates the metal-bound water with assistance from Asp116 and Asn227 forming a nucleophilic hydroxide moiety. Once the zinc-bound hydroxide is formed it can attack the activated ortho carbon of TPN forming an η-1-μ transition state complex. One proton is transferred in the transition-state likely due to the breaking of a water O-H bond and the protonation of His114.[47,48] The flexibility of the His114 may facilitate the formation of products and enable their release.[48] Once the products are released the Zn(II)-bound water molecule is replaced (Figure 8.).[48,49] The reaction has a k_{cat} value of 24 ± 2 s^{-1} and a K_m value of 110 ± 30 μM.[45–47]

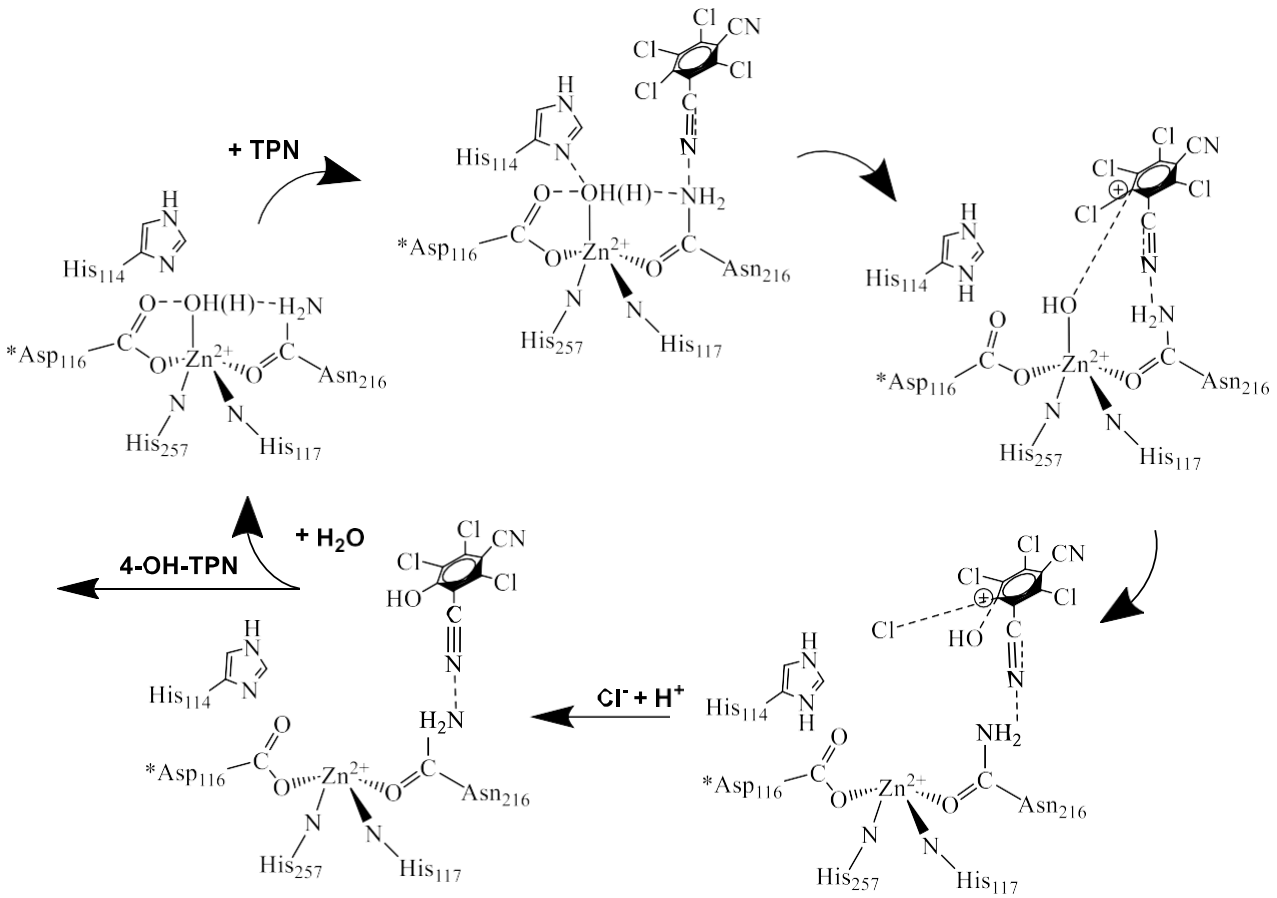

Figure 1.8. Catalytic mechanism for TPN hydrolysis by Chd.

Studies have shown that Chd can be used in remediation applications of chlorothalonil. Chd expressed from *Bacillus subtilis* WB800 can eliminate inhibition of 0.1 g/L chlorothalonil substantially when used as a pretreatment for grapes prior to fermentation using *Saccharomyces cerevisiae*.[50] Treatment with crude Chd, from a *B. subtilis* expression system, can partially eliminate TPN from wheat straw. This not only improves the efficiency of bioconversion by laccase and cellulose but also contributes to the utilization of lignocellulose resources.[51] Other studies have used whole bacterial cells, from *Pseudochrobactrum sp*. BSQ1 and *Massilia sp*. BLM18, for the degradation of TPN. The authors reported their bioaugmentation success is due to hydrolytic dehalogenation but fail to cite the enzyme responsible.[52] Overall, within the past 10

years, uncovering the mechanism of Chd and exploring its potential applications has opened opportunity for the exploration of other hydrolytic dehalogenase enzymes and their respective applications.

1.6 Atrazine Chlorohydrolase

Atrazine chlorohydrolase (AtzA) was originally characterized and purified in the late 1990s from *Pseudomonas* sp. strain ADP.[53] It is the first step in a 6-enzyme atrazine catabolic pathway with a broad substrate specificity (Figure 9.).[54,55]

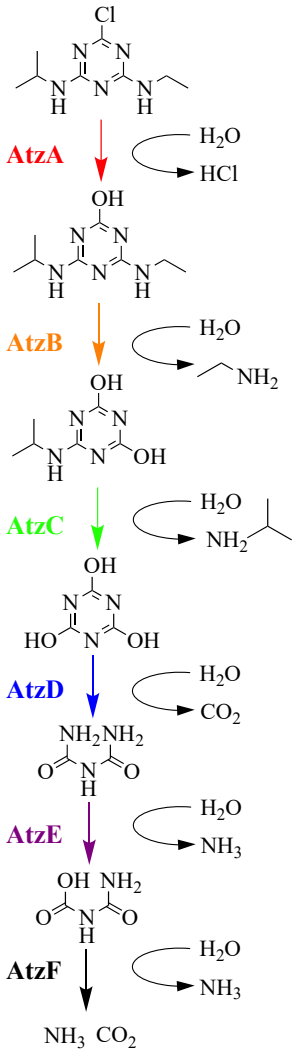

Figure 1.9. The 6-enzyme catabolic pathway of atrazine from *Pseudomonas* sp. strain ADP

AtzA is an Fe(II)-dependent homohexamer (~315 kDa) of the amidohydrolase superfamily that can catalytically dechlorinate atrazine to its nonherbicidal, less toxic derivative 2-hydroxyatrazine.[53,56,57] The hexamer is a trimer of dimers with the dimer interface being significantly larger than the individual protomer interfaces.[57] In each monomer, the active site is accessible via a long hydrophobic channel. The mononuclear metal center in the active site is coordinated by a subtype III amidohydrolase metal-binding motif consisting of His66, His68, His243, His276, and Asp327.[57,58] It is suggested that the Fe(II) is part of an octahedral conformation and is bound, but not tightly, within the active site.[57,59] Though early EPR data suggested a 5-coordinate binding site, the solved crystal structure elucidated an octahedral conformation.[57,58] The crystal structure uncovered a number of Ramachandran outliers within the active site. Of those, His66, His276, and Asp327 bind directly to the active site Fe(II). This results in strain within the active site. Glu251, which is in a region of weak electron density, is suggested to be mobile within the protein in order to allow substrate to enter and exit.[57] The substrate binding pocket appears to be ill-adapted for binding atrazine due to strained conformers of key amino acids, this, in combination with the low metal-binding affinity, results in a high probability of unproductive substrate binding.[57]

There are a few proposed mechanisms for AtzA. The first begins with $\pi - \pi$ stacking between the aromatic ring of the substrate and the hydrophobic pocket within the active site cavity (formed by Phe84, Trp87, and Leu88) in addition to hydrogen bonding to Glu246.[56] The Fe(II) ion and Asp327 are positioned to activate a solvent molecule producing the nucleophilic hydroxide. Specifically, Asp327 is proposed to deprotonate the coordinated water.[57] Nucleophilic attack on the C-4 carbon of the substrate results in a negatively charged tetrahedral intermediate

that is stabilized on the Fe(II)-coordinated aromatic N atom.[56] An interaction between the halide and Ser331 stabilizes the hydrogen bonding to Asn328 allowing the intermediate to breakdown, and the departure of the leaving group (Figure 10A).[56] The second mechanism is centered around a monodentate atrazine coordinating through the Cl atom and Fe(II) metal center.[57]

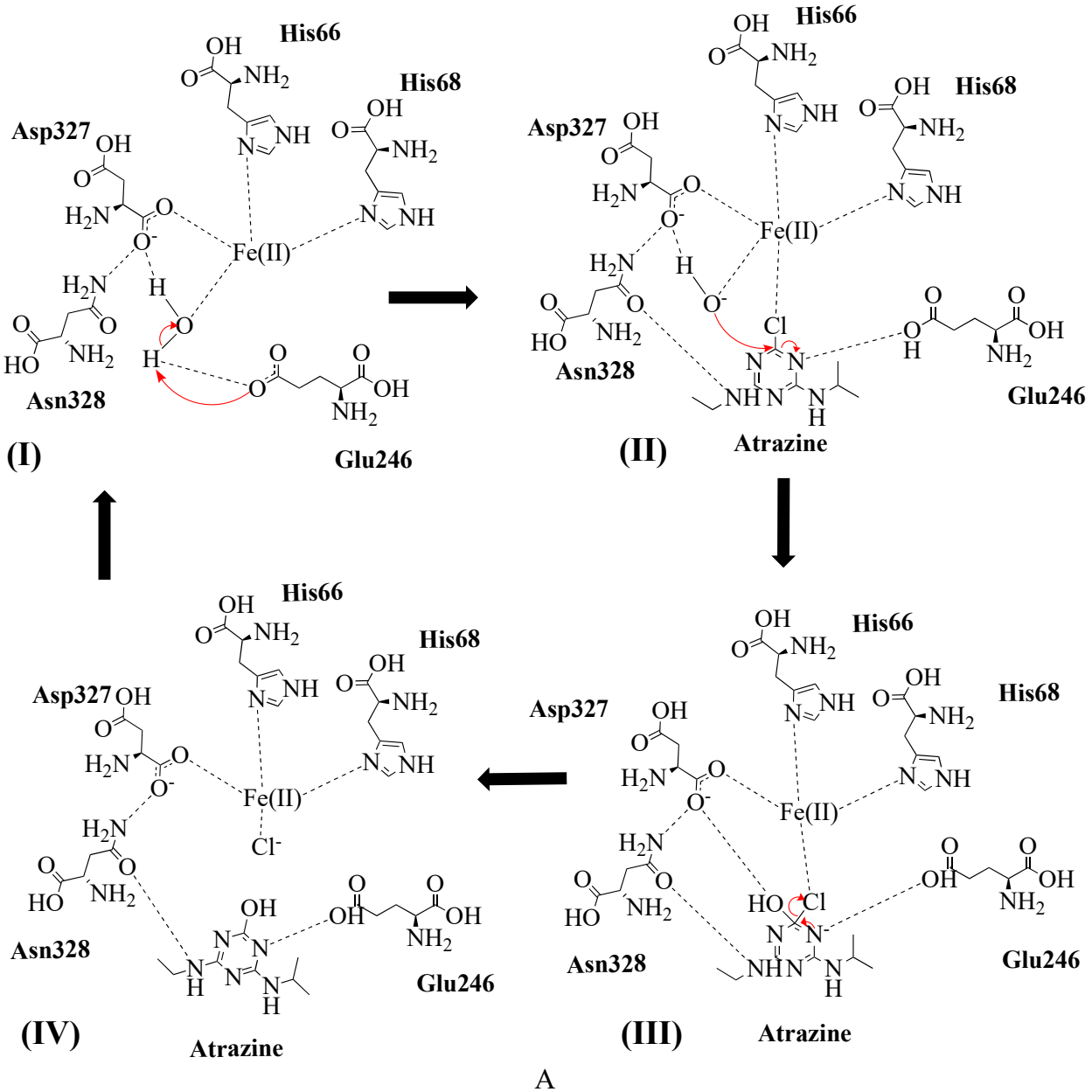

Figure 1.10. A. The first proposed mechanism of atrazine hydrolysis by AtzA which is distinctly characterized by the with $\pi - \pi$ stacking between the aromatic ring of the substrate. B. The second proposed mechanism of atrazine hydrolysis by AtzA centered around a monodentate atrazine coordinating through the Cl atom and Fe(II) metal center.

Figure 1.10 Continued

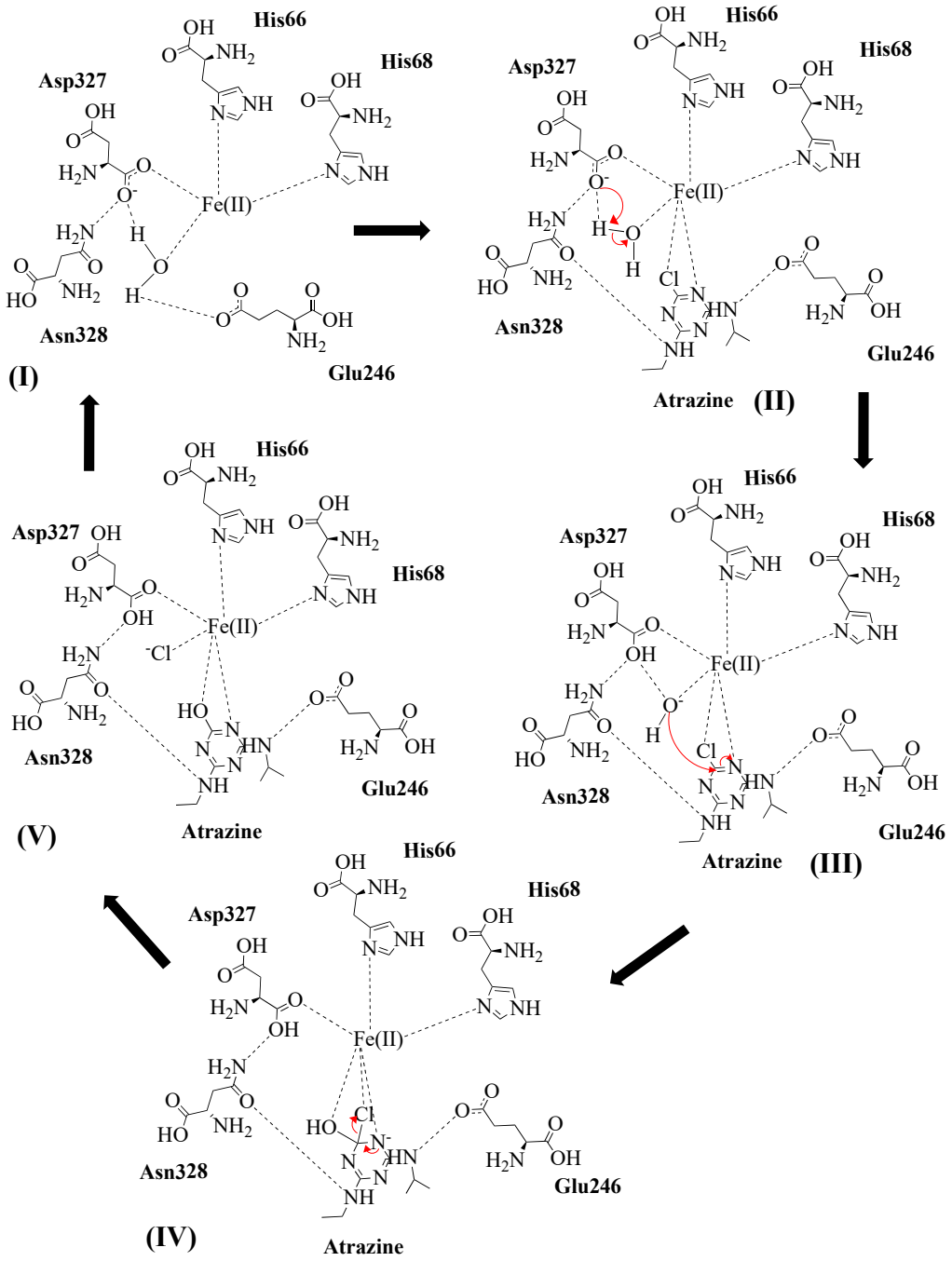

B

The coordinated water is deprotonated by Glu246, which then rotates to donate a hydrogen bond to a ring N atom of atrazine upon substrate binding. This N atom gains a negative charge in the tetrahedral intermediate. The protonated Glu246 then forms a stabilizing hydrogen bond with the intermediate (Figure 10B). The generation of the products is identical to the first proposed mechanism.[57] Michaelis-Menton kinetic data for AtzA provide a k_{cat} value of 2.2 s^{-1} and a K_m value of 153 μM. These values are only suggestions since the K_m value exceeds the solubility of atrazine.[56] Work is still necessary to pinpoint AtzA's exact catalytic mechanism and explore its kinetic potential.

AtzA's potential to be utilized in atrazine remediation strategies has been explored as early as at the late 1990s. Field studies showed that *E. coli* engineered to overproduce AtzA can be killed and used as a vessel to encapsulate AtzA and treat atrazine contaminated soil with 50-80% degradation after 8 weeks.[60] However, silica, and silica variations have been the material of choice for atrazine immobilization. Recombinant *E. coli* expressing AtzA was encapsulated in organically modified silica gels, were catalytically active.[61] Crude AtzA enzyme can also be immobilized within a sol-gel matrix and retain 40% of the non-immobilized activity for a three week period.[62] Similar to the sol-gel, AtzA was entrapped within a biomimetically synthesized silica that was catalytically active in diverse environmental conditions.[63] One study even utilized a modified bacterial atrazine inserted into transgenic grasses and alfalfa to degrade atrazine in contaminated soil. The results showed the grasses and alfalfa grew better in soils with atrazine and could degrade atrazine to hydroxyatrazine *in planta*.[64] Altogether, AtzA has shown to be a strong candidate for bioremediation in multiple different application techniques.

1.7 Triazine Hydrolase

Triazine hydrolase (TrzN) from *Arthrobacter* and *Nocardioides* spp. is a hydrolytic dehalogenase from the amidohydrolase superfamily with a broad substrate specificity originally purified in 2000.[65,66] The substrate specificity has been shown to include at least 22 unique s-triazine and pyrimidine ring compounds; one of those being atrazine.[67] TrzN is monomeric (~52 kDa) with a mononuclear four coordinate Zn(II) ion in the active site (Figure 11.).[65,66,68] The four coordinate active site forms an irregular tetrahedron geometry and is unique from other monometallic amidohydrolases, which typically present a five coordinate active site metal.[68,69] In the active site of TrzN from *Arthrobacter aurescens* TC1, there are four conserved histidine residues (His63, His65, His238, and His274) and Thr325. His63, His65, His238, and a water/hydroxide coordinate the metal center. Thr325 aligns with a conserved aspartate, which typically serves as a metal ligand in other monometallic superfamily members (Figure 12).[68]

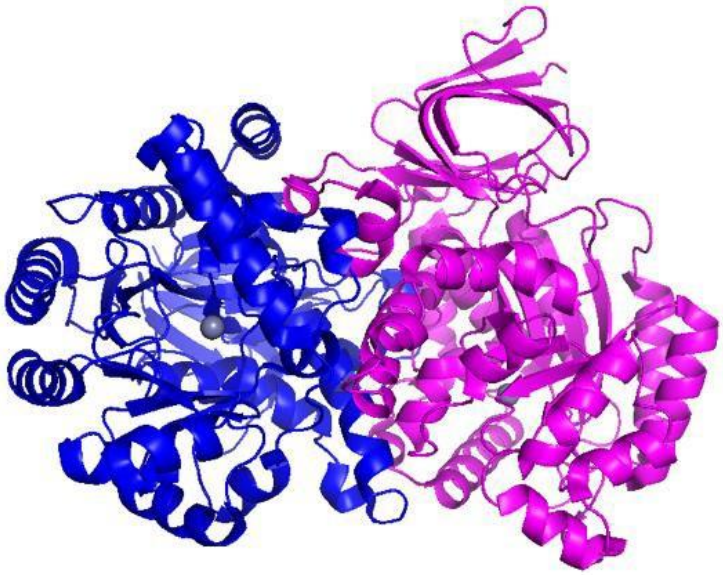

Figure 1.11. The overall crystal structure of TrzN from from *Arthrobacter aurescens* TC1. The Zn(II) ions are shown as grey spheres and the individual monomers are shown in blue and pink respectively.

However, the Thr325 oxygen is too far from the Zn(II) metal center to be a metal ligand. Instead, it is suggested this residue forms a hydrogen bond to the water/hydroxide that is bound to the Zn(II) active site helping position it for nucleophilic attack.[68] During atrazine catalysis, there is a proposed proton transfer to the atrazine ring prior to nucleophilic displacement, likely facilitated by Glu 241.[68,70] However, through mutagenesis, it was found that the presence of Glu241 is not necessary for catalysis implicating there are multiple protonation options.[71] It was suggested that the ring protonation provided significant catalytic enhancement with substrates containing an S-methyl or O-methyl leaving group. With a chloride leaving group, like atrazine has, catalysis could proceed reasonably efficiently without ring protonation.[68] TrzN has a k_{cat} value, with atrazine as the substrate, of $2.1 \pm 0.02\ s^{-1}$ and a K_m value of $19 \pm 1\ \mu M$.[65,68] The mechanism is still largely unknown and needs significantly more work to elucidate a final and comprehensive mechanism.

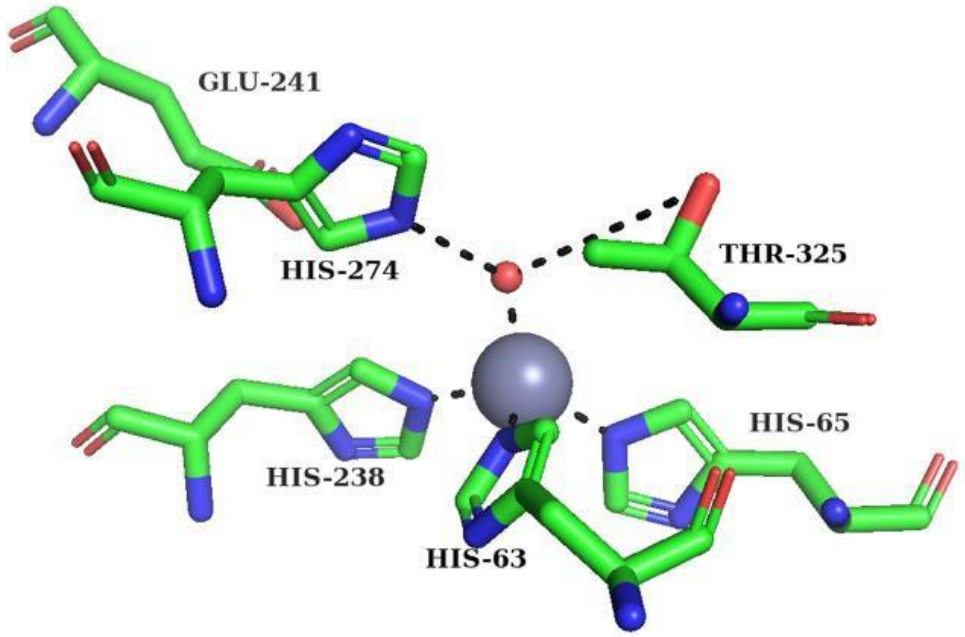

Figure 1.12. TrzN active site. The Zn(II) ion is shown as an orange sphere and the catalytic water is a red sphere.

It is important to note that one study revealed TrzN enzymes from different organisms with significant differences in their active site. TrzN from *Nocardioides* sp. strain MTD22 is very similar to TrzN from *Arthrobacter aurescens* TC1 due to Glu241 being in the same position surrounded by a hydrophobic and aromatic second-shell residues (Pro214 and Tyr215).[72] However TrzN from *Nocardioides sp*. strain AN3 contains a noncatalytic Gln241 residue at the equivalent position surrounded by hydrophilic residues (Thr214 and His215).[72] This study showed that the Gln241 containing TrzN variant is more stable but considerably less active. This is likely due to the tradeoff between enhanced catalysis and the thermodynamic "cost" of shielding the proton donating Glu241 residue by hydrophobic residues causing more activity and less stability.[72] This is currently the only study comparing different variants of TrzN.

AtzA and TrzN are the only two hydrolytic dehalogenases reported to dechlorinate atrazine to its less toxic derivative hydroxyatrazine. TrzN is better adapted to its physiological role than AtzA because AtzA has a substrate binding pocket that is under considerable strain and a substrate that is a poor fit.[57] Issues with TrzN arise from its solubility and ability to be expressed. The earliest studies of TrzN reported a 2.5 mg protein yield from a 5 L of *E. coli* culture.[67] However, a mutated strain of TrzN from *Arthrobacter aurescens* TC1(D38N/L131P/A159V) exhibited a 336-fold-increase in expression with the kinetic parameters changing minimally (k_{cat} 3.7 s^{-1} and K_m 53 μM) compared to wild-type (WT) TrzN.[69] The ability to be expressed in high quantities coupled with a broad substrate specificity makes TrzN a solid candidate for environmental remediation of halogenated aromatic compounds, specifically atrazine. Enriched cultures containing AtzA and TrzN have been previously implemented to degrade atrazine in ground water and showed high potential for atrazine hydrolysis. Bacterial strains containing TrzN can degrade atrazine at a >85% efficiency in both

aqueous solutions containing 500 mg/L atrazine and contaminated soil with an atrazine concentration of 300 mg/kg.[73] Other Arthrobacter bacterial strains demonstrated the ability to mineralize atrazine. Specifically, after 21 days, 60% of the original ^{14}C-ring-labelled atrazine was released as $^{14}CO_2$.[74] Only one instance of free enzyme remediation with TrzN has been reported. In this study, the addition of free TrzN to a holding dam with 157-170 μg/L of atrazine led to a >90% depletion in atrazine concentration after 4 hours.[75] The free-enzyme remediation results are promising, but the inability to recover the free enzyme after the reaction makes free enzyme remediation expensive and often inapplicable. In conclusion, TrzN is a prime candidate for bioremediation of halogenated aromatic compounds, specifically atrazine.

1.8 Biomaterials

Biocatalysis presents an opportunity to utilize enzymes in a wide range of applications that are frequently limited by evolution-led catalyst traits. Therefore it is necessary to tailor catalyst properties so they are optimal for the given reaction and application.[76] The utilization of biomaterials offers a diverse pool of options to tailor a biocatalyst with a specific enzyme and or application. Since its inception, the field of biomaterials has seen consistent growth in both medical and non-medical uses.[77] Specifically, the use of biomaterials for enzyme immobilization has picked up traction in recent years. Traditional methods of enzyme immobilization can be distinguished in to three groups; binding to a support (carrier), entrapment (encapsulation), and cross-linking.[78] Support binding can be physical, ionic, or covalent in nature. This low cost method is generally considered simple and convenient with noninvasive methods that enable enzyme binding to the support, which prevents enzyme leaking.[79] Disadvantages arise if the enzyme is irreversibly deactivated, then both the enzyme and the support are rendered useless.

These binding forces are also susceptible to changes in pH, temperature, and ionic strength which can effect stability.[78,79]

Entrapment is the inclusion of an enzyme in a polymer network.[78] The difference between entrapment and support binding can be a grey area, support binding often is correlated with a prefabricated support while entrapment requires the synthesis of a polymeric network in the presence of the enzyme.[78,80] Entrapment methods, compared to covalent and crosslinking methods, minimally change the structure of the protein and offer high operational stability. Limitations arise from potential enzyme leaking due to material breakdown or poor matrix interactions. Mass transport also becomes limiting if the substrate cannot diffuse through the matrix to the enzyme active site.[80] The third category of immobilization is crosslinking. Crosslinking is generally a two-step process. First, enzyme aggregates or crystals are formed using organic or inorganic precipitants. Then, the second step is the crosslinking of the aggregate or crystals. This is typically facilitated by targeting interactions between specific amino acids. The results is a carrier-less macroparticle.[78,80] New materials are being published every year that are derived from these core methods of immobilization.

As the library of immobilization materials expands, the fields in which biocatalysts become applicable have grown as well. Enzymatic bioremediation has been unsuccessful in industrialization due to the functional instability of free enzymes and the inability to recover and reused the catalyst.[81] Because of those limitations, bioremediation incorporating immobilized protein biocatalysts has been gaining traction in recent years as a green way to remove chemical compounds from an aqueous solution. This method of bioremediation has an advantage over microorganisms and phytoremediation due to higher activity for pollutant degradation coupled with less waste generation.[82] Pharmaceuticals are among the group of chemicals that continually

releases into nature and can effect human life.[83] Oxidative enzymes such as laccase have been immobilized using many different supports, such as functionalized Fe_3O_4 nanoparticles, mesoporous nanofibers, modified carbon nanotubes, and by carrier free magnetic cross-linked enzyme aggregates.[84–87] All of these methods reported a significant decrease in their targeted contaminant. Pharmaceuticals are just one of the many pollutants that are good candidates for bioremediation by immobilized enzyme biocatalysts. Other contaminants include; synthetic dyes, phenolic agents, polycyclic aromatic hydrocarbons, volatiles organic compounds, polychlorinated biphenyls, and pesticides.[81] The continual discovery of novel enzymes that degrade pollutants as well as the push for greener remediation alternatives has made the utilization of immobilized enzyme biocatalyst for bioremediations a rapidly expanding field.

1.9 Summary and Research Aims

Atrazine (2-chloro-4-ethylamino-6-isopropylamino-s-triazine) is a widely used synthetic herbicide that selectively controls broad leaf (dicot) weeds.[1] It is the second most abundantly applied pesticide and the most common pesticide contaminant of ground and surface water in the United States.[2,8] Atrazine's toxicity to the environment and human health has become a topic of great importance. One method of decreasing atrazine's toxicity is through hydrolytic dehalogenation.[18] Dehalogenation is an elimination reaction where the leaving atom is a halogen. In the case with atrazine, the leaving atom would be a chlorine ion replaced by an hydroxyl. There are a few key enzymatic mechanisms for dehalogenation, the first being reductive dehalogenation, which is a typically an anaerobic reaction that involves the removal of a halogen from a molecule with the concurrent addition of electrons to the molecule.[22] Oxidative dehalogenation is a second mechanism, a non-respiratory process, that results in the removal of halogens from an organic backbone with no energetic benefit to the organisms.[27,28] The third is

thiolytic dehalogenation, which is a substitutive mechanism with glutathione as a co-factor where an unstable glutathione intermediate is hydrolyzed.[20,31] Lastly, hydrolytic dehalogenation is the replacement of a halogen by a hydroxyl group derived from H_2O or hydroxide using nucleophilic substitution.[20,32]

Hydrolytic dehalogenation is the only biological dehalogenation mechanism to date that can detoxify atrazine. The first hydrolytic dehalogenase, for aromatic compounds, wasn't purified until the late 1990s.[28] Today there are still a limited number of known hydrolytic dehalogenases. These include 4-CBA-CoA dehalogenase, ChD, AtzA, and TrzN. TrzN is the most likely candidate to assist in the detoxification of atrazine in the environment because it has a broad substrate specificity, which includes atrazine, it is monomeric, and is well adapted to its physiological role.[57,65,67] However gaps still exist in the knowledge of TrzN's mechanism. TrzN has been implemented in previous atrazine remediation methods using whole cells and free enzyme,[73,75] but a true biomaterial incorporating TrzN has never been engineered. Therefore, in this thesis I examined the kinetics properties of TrzN from *Arthrobacter aurescens* TC1 to assist in elucidating the catalytic mechanism and establish conditions for TrzN to be utilized as a biocatalyts. Concurrently, I investigated TrzN's ability to be incorporated on and within different biomaterial structures to be used as a biocatalyst for the degradation of atrazine. Specifically, I have:

I. Provided clarity to the previously proposed TrzN mechanism through multiple kinetic studies using variables such as, pH, temperature, and H_2O/D_2O ratio.
II. Immobilized TrzN within an alginate bead, an alginate bead with a chitosan coating, and a TMOS sol-gel and investigated the ability of the biocatalysts to degrade atrazine under variable conditions.

III. Explored functionalized and non-functionalized mesoporous silica nanoparticles (MSN) as a solid support for TrzN. A wide breadth of running conditions were assessed for optimal atrazine degradation conditions.

1.10 References

(1) Ribaudo, M. O.; Bouzaher, A. Atrazine : Environmental Characteristics and Economics of Management. *Agric. Econ. Rep. Number 699* **1994**, No. 699, 16.

(2) Abass, K.; Pelkonen, O.; Rautio, A. Chloro-s-Triazines-Toxicokinetic, Toxicodynamic, Human Exposure, and Regulatory Considerations. *Curr. Drug Metab.* **2021**, *22* (8), 645–656. https://doi.org/10.2174/1389200222666210701164945.

(3) de Albuquerque, F. P.; de Oliveira, J. L.; Moschini-Carlos, V.; Fraceto, L. F. An Overview of the Potential Impacts of Atrazine in Aquatic Environments: Perspectives for Tailored Solutions Based on Nanotechnology. *Sci. Total Environ.* **2020**, *700*. https://doi.org/10.1016/j.scitotenv.2019.134868.

(4) Bethsass, J.; Aaron Colangelo. European Union Bans Atrazine, While the United States Negotiates Continued Use. *Int. J. Occup. Environ. Health* **2006**, *12* (3), 260–267.

(5) Thurman, E. M.; Cromwell, A. E. Atmospheric Transport, Deposition, and Fate of Triazine Herbicides and Their Metabolites in Pristine Areas at Isle Royale National Park. *Environ. Sci. Technol.* **2000**, *34* (15), 3079–3085. https://doi.org/10.1021/es000995l.

(6) Mast, M. A.; Foreman, W. T.; Skaates, S. V. Current-Use Pesticides and Organochlorine Compounds in Precipitation and Lake Sediment from Two High-Elevation National Parks in the Western United States. *Arch. Environ. Contam. Toxicol.* **2007**, *52* (3), 294–305. https://doi.org/10.1007/s00244-006-0096-1.

(7) Beaulieu, M.; Cabana, H.; Taranu, Z.; Huot, Y. Predicting Atrazine Concentrations in Waterbodies across the Contiguous United States: The Importance of Land Use, Hydrology, and Water Physicochemistry. *Limnol. Oceanogr.* **2020**, 2966–2983. https://doi.org/10.1002/lno.11568.

(8) Solomon, K. R.; Baker, D. B.; Richards, R. P.; Dixon, K. R.; Klaine, S. J.; Point, T. W. La; Kendall, R. J.; Weisskopf, C. P.; Giddings, J. M.; Giesy, J. P.; Lenwood W. Hall, J.; Williams, W. M. Ecological Risk Assessment of Atrazine In. *Environ. Toxicol.* **1996**, *15* (1), 31–76.

(9) Graymore, M.; Stagnitti, F.; Allinson, G. Impacts of Atrazine in Aquatic Ecosystems. *Environ. Int.* **2001**, *26* (7–8), 483–495. https://doi.org/10.1016/S0160-4120(01)00031-9.

(10) Lockert, C. K.; Hoagland, K. D.; Siegfried, B. D. Comparative Sensitivity of Freshwater Algae to Atrazine. *Bull. Environ. Contam. Toxicol.* **2006**, *76* (1), 73–79. https://doi.org/10.1007/s00128-005-0891-9.

(11) Hayes, T. B.; Khoury, V.; Narayan, A.; Nazir, M.; Parka, A.; Brown, T.; Adame, L.; Chan, E.; Buchholz, D.; Stueve, T.; Gallipeau, S. Atrazine Induces Complete Feminization and Chemical Castration in Male African Clawed Frogs (Xenopus Laevis). *Proc. Natl. Acad. Sci. U. S. A.* **2010**, *107* (10), 4612–4617. https://doi.org/10.1073/pnas.0909519107.

(12) Hayes, T. B.; Anderson, L. L.; Beasley, V. R.; De Solla, S. R.; Iguchi, T.; Ingraham, H.; Kestemont, P.; Kniewald, J.; Kniewald, Z.; Langlois, V. S.; Luque, E. H.; McCoy, K. A.; Muñoz-De-Toro, M.; Oka, T.; Oliveira, C. A.; Orton, F.; Ruby, S.; Suzawa, M.; Tavera-Mendoza, L. E.; Trudeau, V. L.; Victor-Costa, A. B.; Willingham, E. Demasculinization and Feminization of Male Gonads by Atrazine: Consistent Effects across Vertebrate Classes. *J. Steroid Biochem. Mol. Biol.* **2011**, *127* (1–2), 64–73. https://doi.org/10.1016/j.jsbmb.2011.03.015.

(13) Liu, Z.; Wang, Y.; Zhu, Z.; Yang, E.; Feng, X.; Fu, Z.; Jin, Y. Atrazine and Its Main Metabolites Alter the Locomotor Activity of Larval Zebrafish (Danio Rerio). *Chemosphere* **2016**, *148*, 163–170. https://doi.org/10.1016/j.chemosphere.2016.01.007.

(14) ATSDR. Public Health Statement Atrazine. *Agency Toxic Subst. Regist.* **2015**, No. September, 5–8.

(15) Pathak, R. K.; Dikshit, A. K. Atrazine and Human Health. *Int. J. Ecosyst.* **2012**, *1* (1), 14–23. https://doi.org/10.5923/j.ije.20110101.03.

(16) Fan, W. Q.; Yanase, T.; Morinaga, H.; Gondo, S.; Okabe, T.; Nomura, M.; Komatsu, T.; Morohashi, K. I.; Hayes, T. B.; Takayanagi, R.; Nawata, H. Atrazine-Induced Aromatase Expression Is SF-1 Dependent: Implications for Endocrine Disruption in Wildlife and Reproductive Cancers in Humans. *Environ. Health Perspect.* **2007**, *115* (5), 720–727. https://doi.org/10.1289/ehp.9758.

(17) Ackerman, F.; Whited, M.; Knight, P. Would Banning Atrazine Benefit Farmers? *Int. J. Occup. Environ. Health* **2014**, *20* (1), 61–70. https://doi.org/10.1179/2049396713Y.0000000054.

(18) Shimabukuro, R. H.; Swanson, H. R. Atrazine Metabolism, Selectivity, and Mode of Action. **1969**, *17* (2), 199–205.

(19) Bouquard, C.; Ouazzani, J.; Promé, J. C.; Michel-Briand, Y.; Plésiat, P. Dechlorination of Atrazine by a Rhizobium Sp. Isolate. *Appl. Environ. Microbiol.* **1997**, *63* (3), 862–866. https://doi.org/10.1128/aem.63.3.862-866.1997.

(20) Fetzner, S.; Lingens, F. Bacterial Dehalogenases:Biochemsitry, Genetics, and Biotechnological Applications. *Am. Soc. Microbiol.* **1994**, *58*, 641–685.

(21) De Jong, R. M.; Dijkstra, B. W. Structure and Mechanism of Bacterial Dehalogenases: Different Ways to Cleave a Carbon-Halogen Bond. *Curr. Opin. Struct. Biol.* **2003**, *13* (6), 722–730. https://doi.org/10.1016/j.sbi.2003.10.009.

(22) Mohn, W. W.; Tiedje, J. M. Microbial Reductive Dehalogenation. *Microbiol. Rev.* **1992**, *56* (3), 482–507. https://doi.org/10.1128/mmbr.56.3.482-507.1992.

(23) Ni, S.; Fredrickson, J. K.; Xun, L. Purification and Characterization of a Novel 3-Chlorobenzoate-Reductive Dehalogenase from the Cytoplasmic Membrane of Desulfomonile Tiedjei DCB-1. *J. Bacteriol.* **1995**, *177* (17), 5135–5139. https://doi.org/10.1128/jb.177.17.5135-5139.1995.

(24) Fincker, M.; Spormann, A. M. Biochemistry of Catabolic Reductive Dehalogenation. *Annu. Rev. Biochem.* **2017**, *86*, 357–386. https://doi.org/10.1146/annurev-biochem-061516-044829.

(25) Magnuson, J. K.; Romine, M. F.; Burris, D. R.; Kingsley, M. T. Trichloroethene Reductive Dehalogenase from Dehalococcoides Ethenogenes: Sequence of TceA and Substrate Range Characterization. *Appl. Environ. Microbiol.* **2000**, *66* (12), 5141–5147. https://doi.org/10.1128/AEM.66.12.5141-5147.2000.

(26) Van De Pas, B. A.; Smidt, H.; Hagen, W. R.; Van Der Oost, J.; Schraa, G.; Stams, A. J. M.; De Vos, W. M. Purification and Molecular Characterization of Ortho-Chlorophenol Reductive Dehalogenase, a Key Enzyme of Halorespiration in Desulfitobacterium Dehalogenans. *J. Biol. Chem.* **1999**, *274* (29), 20287–20292. https://doi.org/10.1074/jbc.274.29.20287.

(27) Temme, H. R.; Carlson, A.; Novak, P. J. Presence, Diversity, and Enrichment of Respiratory Reductive Dehalogenase and Non-Respiratory Hydrolytic and Oxidative Dehalogenase Genes in Terrestrial Environments. *Front. Microbiol.* **2019**, *10* (JUN), 1–14. https://doi.org/10.3389/fmicb.2019.01258.

(28) Leisinger, T.; Bader, R. Microbial Dehalogenation of Synthetic Organohalogen Compounds: Hydrolytic Dehalogenases. *Chimia (Aarau).* **1993**, *47* (4), 116. https://doi.org/10.2533/chimia.1993.116.

(29) Saghir, S. A.; Ansari, R. A.; Munir, S. T. *Fate of Chemicals Following Exposure III: Metabolism (Biotransformation)*, 4th ed.; Elsevier Inc., 2022. https://doi.org/10.1016/b978-0-12-824315-2.00050-6.

(30) Sobrado, P. Role of Reduced Flavin in Dehalogenation Reactions. *Arch. Biochem. Biophys.* **2021**, *697* (October 2020), 108696. https://doi.org/10.1016/j.abb.2020.108696.

(31) Fetzner, S. Bacterial Dehalogenation. *Appl. Microbiol. Biotechnol.* **1998**, *50* (6), 633–657. https://doi.org/10.1007/s002530051346.

(32) Pimviriyakul, P.; Wongnate, T. Microbial Degradation of Halogenated Aromatics : Molecular Mechanisms and Enzymatic Reactions. **2019**. https://doi.org/10.1111/1751-7915.13488.

(33) Chen, K.; Jian, S.; Huang, L.; Ruan, Z.; Li, S.; Jiang, J. Reductive Dehalogenation of 3,5-Dibromo-4-Hydroxybenzoate by an Aerobic Strain of Delftia Sp. EOB-17. *Biotechnol. Lett.* **2015**, *37* (12), 2395–2401. https://doi.org/10.1007/s10529-015-1932-z.

(34) Jörg, G.; Bertau, M. Fungal Aerobic Reductive Dechlorination of Ethyl 2-Chloroacetoacetate by Saccharomyces Cerevisiae: Mechanism of a Novel Type of Microbial Dehalogenation. *ChemBioChem* **2004**, *5* (1), 87–92. https://doi.org/10.1002/cbic.200300760.

(35) Van Pée, K. H.; Unversucht, S. Biological Dehalogenation and Halogenation Reactions. *Chemosphere* **2003**, *52* (2), 299–312. https://doi.org/10.1016/S0045-6535(03)00204-2.

(36) Chen, G.; Shouakar-Stash, O.; Phillips, E.; Justicia-Leon, S. D.; Gilevska, T.; Sherwood Lollar, B.; Mack, E. E.; Seger, E. S.; Löffler, F. E. Dual Carbon-Chlorine Isotope Analysis Indicates Distinct Anaerobic Dichloromethane Degradation Pathways in Two Members of Peptococcaceae. *Environ. Sci. Technol.* **2018**, *52* (15), 8607–8616. https://doi.org/10.1021/acs.est.8b01583.

(37) Scholten, J. D.; Chang, K.; Babbitt, P. C.; Charesr, H.; Sylvesrue, M.; Dunaway-mariano, D. Novel Enzymic Hydrolytic Dehalogenation of a Chlorinated Aromatic. **1990**, *253* (1986).

(38) Löffler, F.; Lingen, F.; Müller, R. Characterisation of 4-Chlorobenzoyl-Coenzyme A Dehalogenase from Pseudomonas Sp. CBS3. *Biodegradation* **1995**, *6*, 203–212.

(39) Yang, G.; Liang, P. H.; Dunaway-Mariano, D. Evidence for Nucleophilic Catalysis in the Aromatic Substitution Reaction Catalyzed by (4-Chlorobenzoyl)Coenzyme A Dehalogenase. *Biochemistry* **1994**, *33* (28), 8527–8531. https://doi.org/10.1021/bi00194a018.

(40) Henning, M. M.; Taylor, K. L.; Liu, R. Q.; Yang, G.; Xiang, H.; Wesenberg, G.; Dunaway-Mariano, D.; Holden, H. M. Structure of 4-Chlorobenzoyl Coenzyme A Dehalogenase Determined to 1.8 Å Resolution: An Enzyme Catalyst Generated via Adaptive Mutation. *Biochemistry* **1996**, *35* (25), 8103–8109. https://doi.org/10.1021/bi960768p.

(41) Lau, E. Y.; Bruice, T. C. The Active Site Dynamics of 4-Chlorobenzoyl-CoA Dehalogenase. *Proc. Natl. Acad. Sci. U. S. A.* **2001**, *98* (17), 9527–9532. https://doi.org/10.1073/pnas.161282698.

(42) Zhang, W.; Wei, Y.; Luo, L.; Taylor, K. L.; Yang, G.; Dunaway-Mariano, D.; Benning, M. M.; Holden, H. M. Histidine 90 Function in 4-Chlorobenzoyl-Coenzyme A Dehalogenase Catalysis. *Biochemistry* **2001**, *40* (45), 13474–13482. https://doi.org/10.1021/bi0114426.

(43) Crooks, G. P.; Copley, S. D. Purification and Characterization of 4-Chlorobenzoyl CoA Dehalogenase from Arthrobacter Sp. Strain 4-CB1. *Biochemistry* **1994**, *33* (38), 11645–11649. https://doi.org/10.1021/bi00204a028.

(44) Dunaway-Mariano, D.; Babbitt, P. C. On the Origins and Functions of the Enzymes of the 4-Chlorobenzoate to 4-Hydroxybenzoate Converting Pathway. *Biodegradation* **1994**, No. 5, 259–276.

(45) Wang, G.; Li, R.; Li, S.; Jiang, J. A Novel Hydrolytic Dehalogenase for the Chlorinated Aromatic Compound Chlorothalonil. *J. Bacteriol.* **2010**, *192* (11), 2737–2745. https://doi.org/10.1128/JB.01547-09.

(46) Chen, H.; Wang, H.; Wang, T.; Huang, S.; Zang, X.; Li, S.; Jiang, J. Identification of the Metal Center of Chlorothalonil Hydrolytic Dehalogenase and Enhancement of Catalytic Efficiency by Directed Evolution. **2016**, 2–9.

(47) Yang, X.; Bennett, B.; Holz, R. C. Insights into the Catalytic Mechanism of a Bacterial Hydrolytic Dehalogenase That Degrades the Fungicide Chlorothalonil. *J. Biol. Chem.* **2019**, *294* (36), 13411–13420. https://doi.org/10.1074/jbc.RA119.009094.

(48) Catlin, D. S.; Yang, X.; Bennett, B.; Holz, R. C.; Liu, D. Structural Basis for the Hydrolytic Dehalogenation of the Fungicide Chlorothalonil. *J. Biol. Chem.* **2020**, *295* (26), 8668–8677. https://doi.org/10.1074/jbc.ra120.013150.

(49) Yang, X.; Diviesti, K.; Miller, C.; Bennett, B.; Holz, R. C. Insights into the Catalytic Mechanism of the Chlorothalonil Dehalogenase from Pseudomonas Sp. CTN-3. *Front. Chem. Biol.* **2023**, *2* (February), 1–10. https://doi.org/10.3389/fchbi.2023.1105607.

(50) He, Q.; Huang, J.; Yang, X.; Yan, X.; He, J.; Li, S.; Jiang, J. Effect of Pesticide Residues in Grapes on Alcoholic Fermentation and Elimination of Chlorothalonil Inhibition by Chlorothalonil Hydrolytic Dehalogenase. *Food Control* **2016**, *64*, 70–76. https://doi.org/10.1016/j.foodcont.2015.12.028.

(51) Ye, B.; Luo, Y.; Zhong, B.; Zhu, J.; Huang, J.; Gu, J.; Jiang, J.; Yan, X.; He, J.; He, Q. High-Level Stable Expression of Gene for Preparation of Chlorothalonil Hydrolytic Dehalogenase and Its Application in Elimination of Chlorothalonil Inhibition on Bioconversion of Lignocellulosic Biomass. *J. Biosci. Bioeng.* **2020**, *130* (6), 630–636. https://doi.org/10.1016/j.jbiosc.2020.08.003.

(52) Xu, X. H.; Liu, X. M.; Zhang, L.; Mu, Y.; Zhu, X. Y.; Fang, J. Y.; Li, S. P.; Jiang, J. D. Bioaugmentation of Chlorothalonil-Contaminated Soil with Hydrolytically or Reductively Dehalogenating Strain and Its Effect on Soil Microbial Community. *J. Hazard. Mater.* **2018**, *351* (October 2017), 240–249. https://doi.org/10.1016/j.jhazmat.2018.03.002.

(53) De Souza, M. L.; Sadowsky, M. J.; Wackett, L. P. Atrazine Chlorohydrolase from Pseudomonas Sp. Strain ADP: Gene Sequence, Enzyme Purification, and Protein Characterization. *J. Bacteriol.* **1996**, *178* (16), 4894–4900. https://doi.org/10.1128/jb.178.16.4894-4900.1996.

(54) De Souza, M. L.; Newcombe, D.; Alvey, S.; Crowley, D. E.; Hay, A.; Sadowsky, M. J.; Wackett, L. P. Molecular Basis of a Bacterial Consortium: Interspecies Catabolism of Atrazine. *Appl. Environ. Microbiol.* **1998**, *64* (1), 178–184. https://doi.org/10.1128/aem.64.1.178-184.1998.

(55) Seffernick, J. L.; Johnson, G.; Sadowsky, M. J.; Wackett, L. P. Substrate Specificity of Atrazine Chlorohydrolase and Atrazine-Catabolizing Bacteria. *Appl. Environ. Microbiol.* **2000**, *66* (10), 4247–4252. https://doi.org/10.1128/AEM.66.10.4247-4252.2000.

(56) Scott, C.; Jackson, C. J.; Coppin, C. W.; Mourant, R. G.; Hilton, M. E.; Sutherland, T. D.; Russell, R. J.; Oakeshott, J. G. Catalytic Improvement and Evolution of Atrazine Chlorohydrolase. *Appl. Environ. Microbiol.* **2009**, *75* (7), 2184–2191. https://doi.org/10.1128/AEM.02634-08.

(57) Peat, T. S.; Newman, J.; Balotra, S.; Lucent, D.; Warden, A. C.; Scott, C. The Structure of the Hexameric Atrazine Chlorohydrolase AtzA. *Acta Crystallogr. Sect. D Biol. Crystallogr.* **2015**, *71*, 710–720. https://doi.org/10.1107/S1399004715000619.

(58) Seffernick, J. L.; McTavish, H.; Osborne, J. P.; De Souza, M. L.; Sadowsky, M. J.; Wackett, L. P. Atrazine Chlorohydrolase from Pseudomonas Sp. Strain ADP Is a Metalloenzyme. *Biochemistry* **2002**, *41* (48), 14430–14437. https://doi.org/10.1021/bi020415s.

(59) Noor, S.; Changey, F.; Oakeshott, J. G.; Scott, C.; Martin-Laurent, F. Ongoing Functional Evolution of the Bacterial Atrazine Chlorohydrolase AtzA. *Biodegradation* **2014**, *25* (1), 21–30. https://doi.org/10.1007/s10532-013-9637-2.

(60) Strong, L. C.; McTavish, H.; Sadowsky, M. J.; Wackett, L. P. Field-Scale Remediation of Atrazine-Contaminated Soil Using Recombinant Escherichia Coli Expressing Atrazine Chlorohydrolase. *Environ. Microbiol.* **2000**, *2* (1), 91–98.

(61) Benson, J. J.; Sakkos, J. K.; Radian, A.; Wackett, L. P.; Aksan, A. Enhanced Biodegradation of Atrazine by Bacteria Encapsulated in Organically Modified Silica Gels. *J. Colloid Interface Sci.* **2018**, *510*, 57–68. https://doi.org/10.1016/j.jcis.2017.09.044.

(62) Kauffmann, C.; Mandelbaum, R. T. Entrapment of Atrazine Chlorohydrolase in Sol-Gel Glass Matrix. *J. Biotechnol.* **1998**, *62* (3), 169–176. https://doi.org/10.1016/S0168-1656(98)00060-1.

(63) Ho, C. T.; Kang, S.; Hur, H. G. Enzymatic Properties of Atrazine Chlorohydrolase Entrapped in Biomimetic Silica. *J. Appl. Biol. Chem.* **2008**, *51* (4), 143–147. https://doi.org/10.3839/jabc.2008.024.

(64) Vail, A. W.; Wang, P.; Uefuji, H.; Samac, D. A.; Vance, C. P.; Wackett, L. P.; Sadowsky, M. J. Biodegradation of Atrazine by Three Transgenic Grasses and Alfalfa Expressing a Modified Bacterial Atrazine Chlorohydrolase Gene. *Transgenic Res.* **2015**, *24* (3), 475–488. https://doi.org/10.1007/s11248-014-9851-7.

(65) Shapir, N.; Pedersen, C.; Gil, O.; Strong, L.; Seffernick, J.; Sadowsky, M. J.; Wackett, L. P. TrzN from Arthrobacter Aurescens TC1 Is a Zinc Amidohydrolase. *J. Bacteriol.* **2006**, *188* (16), 5859–5864. https://doi.org/10.1128/JB.00517-06.

(66) Topp, E.; Mulbry, W. M.; Zhu, H.; Nour, S. M.; Cuppels, D. Characterization of S-Triazine Herbicide Metabolism by a Nocardioides Sp. Isolated from Agricultural Soils. *Appl. Environ. Microbiol.* **2000**, *66* (8), 3134–3141. https://doi.org/10.1128/AEM.66.8.3134-3141.2000.

(67) Shapir, N.; Rosendahl, C.; Johnson, G.; Andreina, M.; Sadowsky, M. J.; Wackett, L. P. Substrate Specificity and Colorimetric Assay for Recombinant TrzN Derived from Arthrobacter Aurescens TC1. *Appl. Environ. Microbiol.* **2005**, *71* (5), 2214–2220. https://doi.org/10.1128/AEM.71.5.2214-2220.2005.

(68) Seffernick, J. L.; Reynolds, E.; Fedorov, A. A.; Fedorov, E.; Almo, S. C.; Sadowsky, M. J.; Wackett, L. P. X-Ray Structure and Mutational Analysis of the Atrazine Chlorohydrolase TrzN. *J. Biol. Chem.* **2010**, *285* (40), 30606–30614. https://doi.org/10.1074/jbc.M110.138677.

(69) Jackson, C. J.; Coppin, C. W.; Carr, P. D.; Aleksandrov, A.; Wilding, M.; Sugrue, E.; Ubels, J.; Paks, M.; Newman, J.; Peat, T. S.; Russell, R. J.; Field, M.; Weik, M.; Oakeshott, J. G.; Scott, C. 300-Fold Increase in Production of the Zn2+-Dependent Dechlorinase TrzN in Soluble Form via Apoenzyme Stabilization. *Appl. Environ. Microbiol.* **2014**, *80* (13), 4003–4011. https://doi.org/10.1128/AEM.00916-14.

(70) Meyer, A. H.; Penning, H.; Elsner, M. C and N Isotope Fractionation Suggests Similar Mechanisms of Microbial Atrazine Transformation despite Involvement of Different Enzymes (AtzA and TrzN). *Environ. Sci. Technol.* **2009**, *43* (21), 8079–8085. https://doi.org/10.1021/es9013618.

(71) Schürner, H. K. V.; Seffernick, J. L.; Grzybkowska, A.; Dybala-Defratyka, A.; Wackett, L. P.; Elsner, M. Characteristic Isotope Fractionation Patterns in S -Triazine Degradation Have Their Origin in Multiple Protonation Options in the S -Triazine Hydrolase Trzn. *Environ. Sci. Technol.* **2015**, *49* (6), 3490–3498. https://doi.org/10.1021/es5055385.

(72) Sugrue, E.; Carr, P. D.; Scott, C.; Jackson, C. J. Active Site Desolvation and Thermostability Trade-Offs in the Evolution of Catalytically Diverse Triazine Hydrolases. *Biochemistry* **2016**, *55* (45), 6304–6313. https://doi.org/10.1021/acs.biochem.6b00731.

(73) LI, Q.; LI, Y.; ZHU, X.; CAI, B. Isolation and Characterization of Atrazine-Degrading Arthrobacter Sp. AD26 and Use of This Strain in Bioremediation of Contaminated Soil. *J. Environ. Sci.* **2008**, *20* (10), 1226–1230. https://doi.org/10.1016/S1001-0742(08)62213-5.

(74) El Sebaï, T.; Devers-Lamrani, M.; Changey, F.; Rouard, N.; Martin-Laurent, F. Evidence of Atrazine Mineralization in a Soil from the Nile Delta: Isolation of Arthrobacter Sp. TES6, an Atrazine-Degrading Strain. *Int. Biodeterior. Biodegrad.* **2011**, *65* (8), 1249–1255. https://doi.org/10.1016/j.ibiod.2011.05.011.

(75) Scott, C.; Lewis, S. E.; Milla, R.; Taylor, M. C.; Rodgers, A. J. W.; Dumsday, G.; Brodie, J. E.; Oakeshott, J. G.; Russell, R. J. A Free-Enzyme Catalyst for the Bioremediation of Environmental Atrazine Contamination. *J. Environ. Manage.* **2010**, *91* (10), 2075–2078. https://doi.org/10.1016/j.jenvman.2010.05.007.

(76) Burton, S. G.; Cowan, D. A.; Woodley, J. M. The Search for the Ideal Biocatalyst. *Nat. Biotechnol.* **2002**, *20* (1), 37–45. https://doi.org/10.1038/nbt0102-37.

(77) Ratner, B. D.; Bryant, S. J. Biomaterials: Where We Have Been and Where We Are Going. *Annu. Rev. Biomed. Eng.* **2004**, *6* (1), 41–75. https://doi.org/10.1146/annurev.bioeng.6.040803.140027.

(78) Sheldon, R. A. Enzyme Immobilization: The Quest for Optimum Performance. *Adv. Synth. Catal.* **2007**, *349* (8–9), 1289–1307. https://doi.org/10.1002/adsc.200700082.

(79) Liu, D. M.; Chen, J.; Shi, Y. P. Advances on Methods and Easy Separated Support Materials for Enzymes Immobilization. *TrAC - Trends Anal. Chem.* **2018**, *102*, 332–342. https://doi.org/10.1016/j.trac.2018.03.011.

(80) Imam, H. T.; Marr, P. C.; Marr, A. C. Enzyme Entrapment, Biocatalyst Immobilization without Covalent Attachment. *Green Chem.* **2021**, *23* (14), 4980–5005. https://doi.org/10.1039/d1gc01852c.

(81) Sellami, K.; Couvert, A.; Nasrallah, N.; Maachi, R.; Abouseoud, M.; Amrane, A. Peroxidase Enzymes as Green Catalysts for Bioremediation and Biotechnological Applications: A Review. *Sci. Total Environ.* **2022**, *806*, 150500. https://doi.org/10.1016/j.scitotenv.2021.150500.

(82) Somu, P.; Narayanasamy, S.; Gomez, L. A.; Rajendran, S.; Lee, Y. R.; Balakrishnan, D. Immobilization of Enzymes for Bioremediation: A Future Remedial and Mitigating Strategy. *Environ. Res.* **2022**, *212*, 113411. https://doi.org/https://doi.org/10.1016/j.envres.2022.113411.

(83) Lignin, K.; Demuner, I. F.; Colodette, J. L.; Demuner, A. J.; Jardim, C. M. Biorefinery Review: Wide-Reaching Products Through Kraft Lignin. *BioResources* **2019**, *14* (3), 7543–7581.

(84) Shi, L.; Ma, F.; Han, Y.; Zhang, X.; Yu, H. Removal of Sulfonamide Antibiotics by Oriented Immobilized Laccase on Fe3O4 Nanoparticles with Natural Mediators. *J. Hazard. Mater.* **2014**, *279*, 203–211. https://doi.org/10.1016/j.jhazmat.2014.06.070.

(85) Xu, R.; Si, Y.; Wu, X.; Li, F.; Zhang, B. Triclosan Removal by Laccase Immobilized on Mesoporous Nanofibers: Strong Adsorption and Efficient Degradation. *Chem. Eng. J.* **2014**, *255*, 63–70. https://doi.org/10.1016/j.cej.2014.06.060.

(86) Xu, R.; Tang, R.; Zhou, Q.; Li, F.; Zhang, B. Enhancement of Catalytic Activity of Immobilized Laccase for Diclofenac Biodegradation by Carbon Nanotubes. *Chem. Eng. J.* **2015**, *262*, 88–95. https://doi.org/10.1016/j.cej.2014.09.072.

(87) Yang, J.; Lin, Y.; Yang, X.; Ng, T. B.; Ye, X.; Lin, J. Degradation of Tetracycline by Immobilized Laccase and the Proposed Transformation Pathway. *J. Hazard. Mater.* **2017**, *322*, 525–531. https://doi.org/10.1016/j.jhazmat.2016.10.019.

CHAPTER 2

KINETIC ANALYSIS OF THE TRIAZINE HYDROLASE FROM *ARTHROBACTER AURESCENS* TC1: INSIGHTS INTO THE CATALYTIC MECHANISM

Karla Diviesti[a], Maya Mowery-Evans[a], and Richard C. Holz[a,b]

2.1 Abstract

In order to gain insight into the catalytic mechanism of Triazine Hydorlase (TrzN), the pH and temperature dependence of the kinetic parameters k_{cat}, K_m, and k_{cat}/K_m along with the solvent isotope effect were examined for TrzN from *Arthrobatcer aurescens* TC1. TrzN was found to exhibit unique curves for plots of relative activity vs pH over pH values 4-10 for the hydrolysis of atrazine and was found to display maximal activity at pH between 7.5 and 8. Fits of these data provided a pK_{ES1} value of 3.6 ± 0.03, a pK_{ES2} value of 10.8 ± 0.1 (k'_{cat} 21.4 ± 0.1), a pK_{E1} 6.9 ± 0.2 (k'_{cat}/K'_m 0.85 ± 0.03). Proton inventory studies indicate that two protons are transferred during catalysis. Since TrzN is stable to 35 °C, an Arrhenius plot was constructed by plotting ln(k_{cat}) vs 1/T, providing an E_a of 16.7 ± 0.3 kJ/mol. ΔH° of ionization values were also determined. Based on the data, pK_{ES1} and pK_{E1} can be assigned to Glu24, pK_{ES2} is assigned to Thr325, while pK_{E1} is likely associated with either His274 or the Zn(II)-bound water moiety. Given the data, Glu241, Th325, and His274 are essential residues for catalytic activity and the data agrees with the current proposed mechanism for TrzN.

[a]Department of Chemistry, Colorado School of Mines, Golden, CO 80401 U.S.A
[b]Quantitative Biosciences and Engineering Program, Colorado School of Mines, Golden, CO 80401 U.S.A

2.2 Introduction

Triazine hydrolase from *Arthrobacter aurescens* TC1 (TrzN, EC 3.8.1.8) catalyzes the irreversible dechlorination of atrazine to its less toxic derivative hydroxyatrazine under physiological conditions (scheme 2.1).[1] Atrazine (2-chloro-4-ethylamino-6-isopropylamino-s-triazine) is a water-soluble herbicide that functions by inhibiting photosynthesis in targeted plants. Approximately 30,000 tons are applied annually which results in heavy surface runoff into surrounding aquatic environments.[2–4] Atrazine is toxic to the environment and humans, exposure has been linked to lung and kidney diseases, cardiovascular damage, retinal degeneration, and cancer.[5–8] Because of this, atrazine has been banned in the European Union since 2003; however, widespread use in the US has continued.[7,8] Hence the bioremediation of atrazine has become a topic of significant importance. TrzN has shown to have great potential as a catalyst for the bioremediation of atrazine contaminated sites.[8,9] Recently it was shown that TrzN immobilized within different biomaterials can successfully dechlorinate atrazine.[10,11] However, little information is known about the catalytic mechanism of TrzN and how that contributes to its success as a biocatalyst.

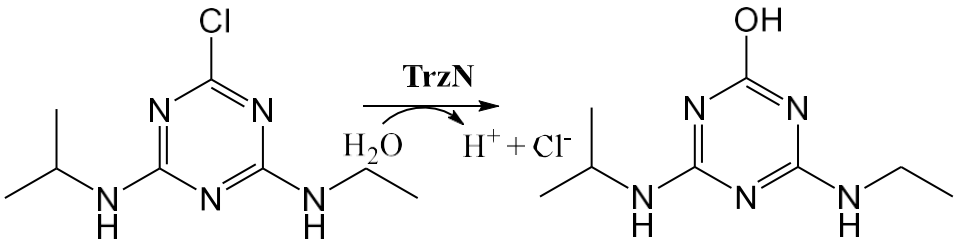

Scheme 2.1 Hydrolysis of atrazine to hydroxyatrazine and chloride by TrzN.

TrzN is a Zn(II) dependent hydrolytic dehalogenase from the amidohydrolase superfamily with at least 22 unique s-triazine and pyrimidine substrates.[12,13] TrzN is catalytically active as a monomer (~51 kDa) with a four coordinate Zn(II) in the active site. The active site

forms an irregular tetrahedral geometry and is unique from other monomeric amidohydrolases, which typically present a five coordinate active site metal ion.[12,14,15] X-ray crystallographic studies on TrzN reveal His63, His65, His238, and a water/hydroxide as metal ligands.[16] In other monometallic superfamily members, there is a conserved aspartate at position 325, which typically serves as the fifth metal ligand; however, in TrzN, position 325 aligns with a Thr whose oxygen atom is too far (3.3Å) from the Zn(II) metal center to be metal ligand.[14] Overall, the active site is narrow with just enough space to fit atrazine.[13]

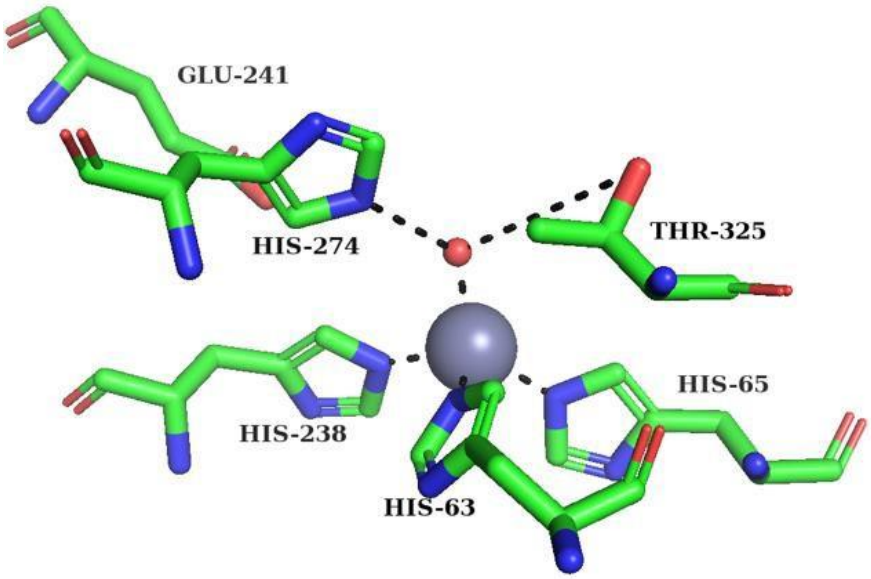

Figure 2.1. TrzN Active site. The Zn(II) ion is shown as an orange sphere and the catalytic water is a red sphere.

Currently, the proposed catalytic mechanism for the hydrolysis of atrazine by TrzN suggests that substrate recognition is the first step in catalysis.[13] Substrate recognition is likely assisted by Met82 and Tyr215, two residues within the active site that form hydrophobic

interactions with the N-alkyl moieties of atrazine.[13] His274 is proposed to function as the general acid/base in catalysis by removing a proton from the Zn(II)-bound water moiety. This proton is transferred to Glu241, which forms a hydrogen bond with the atrazine triazole nitrogen atom. However, the presence of Glu241 is not necessary for catalysis implying there are other residues that may play a role in the catalytic deprotonation/protonation process.[14,17,18] Thr325, although too far to be a metal ligand, is suggested to form a hydrogen bond to the Zn(II)-bound water moiety helping to position it near the ortho carbon of atrazine for nucleophilic attack.[14] In addition, the hydrogen bonding interactions of Glu241 and Glu68 with atrazine would reduce electron density in the triazole ring, activating the ring for nucleophilic attack by the Zn(II)-bound hydroxide. The products Cl^-, hydroxyatrazine, and H^+ are released, and the Zn(II)-bound water molecule is replaced (Figure 2.2). In order to gain additional insight into the proposed catalytic mechanism of the hydrolysis of atrazine by TrzN, the kinetic parameters k_{cat} and K_m were examined as a function of pH and temperature. The dependence of k_{cat} was also obtained at various D_2O concentrations to gain insight into the number of protons transferred in the transition-state. Combination of these data provide additional support for the proposed catalytic mechanism of atrazine hydrolysis by TrzN.

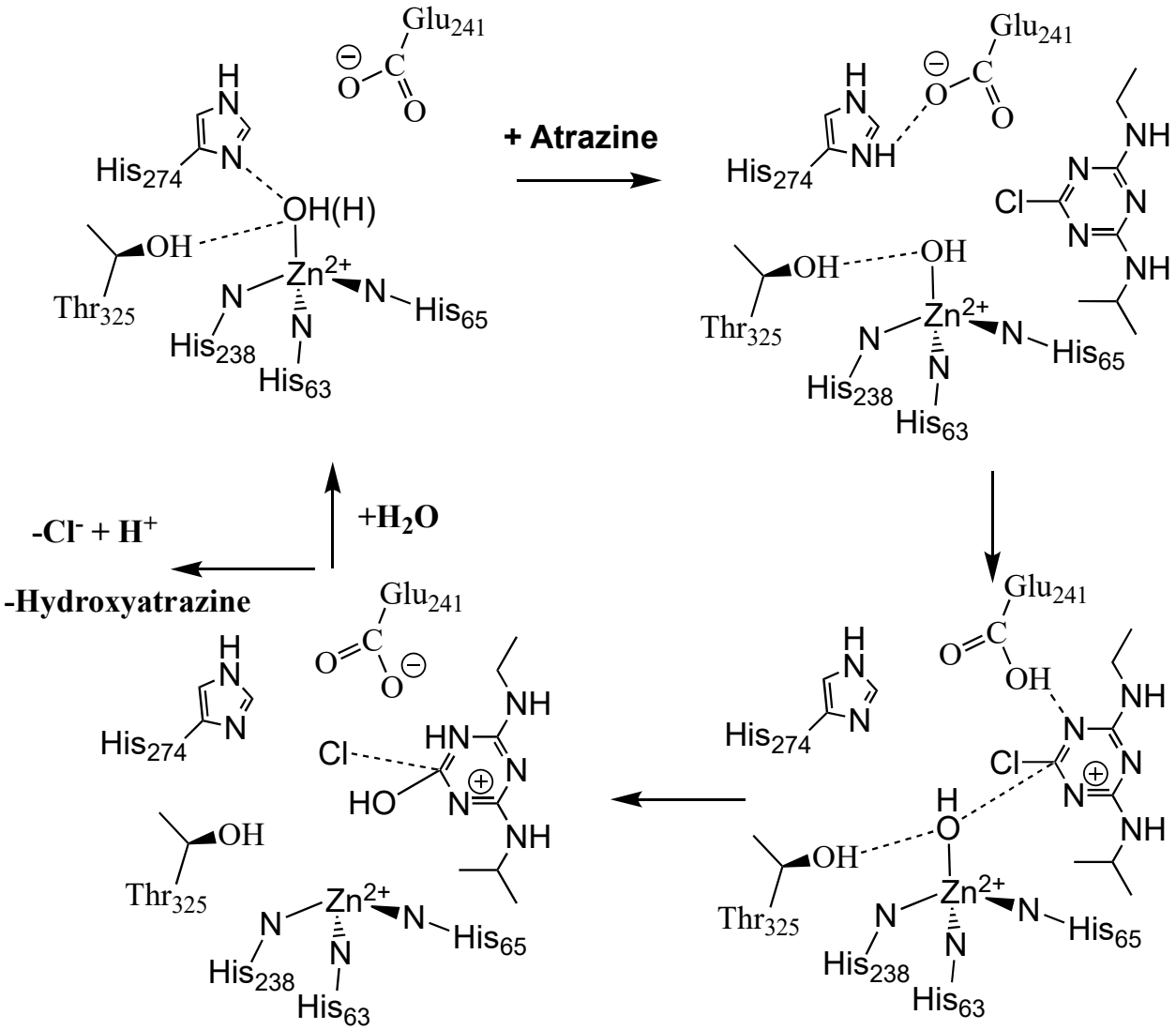

Figure 2.2. Proposed mechanism of the degradation of atrazine by TrzN

2.3 Results

2.3.1 pH Profiles Of The Kinetic Parameters

At pH of 7.0 and 20°C, a k_{cat} value for TrzN towards the substrate atrazine was observed to be 22.6 ± 2 s^{-1} with a K_m value of 34.7 ± 4 μM, and a k_{cat}/K_m value of 0.66 ± 0.04 s^{-1} μM^{-1}. The previously reported kinetic values for TrzN with the D38N, L131P, and A159V mutations at pH 7.0 and 20°C using atrazine as the substrate revealed a k_{cat} value of 3.7 s^{-1}, a K_m value of 53 μM, and a k_{cat}/K_m of 0.07x10^5 s^{-1} μM^{-1}.[19] The previously reported kinetic constants were obtained from protein purified by IMAC that likely still contained the His_6-tag, which is required for IMAC purification, as no mention of its cleavage was made.[23] Without removing the His_6-tag, at pH 7.0 and 20°C, in our hands, a k_{cat} value of 6.4 ± 1 s^{-1}, K_m value of 16.4 ± 5 μM, and a k_{cat}/K_m value of 0.46 ± 0.09 s^{-1} μM^{-1} was obtained. These data indicate a significant decrease in activity for His_6-tagged TrzN compared to values obtained after the removal of the His_6-tag.[10,19]

TrzN was found to exhibit a bell shaped curve for relative activity vs pH between 3.0 and 10.0 with a maximum catalytic activity observed between pH 7.5 and 8, is in good agreement with previous studies.[16] Plots of log(k_{cat}), log(k_{cat}/K_m) and log(K_m) vs pH were prepared and fit to eqs. 1 and 2 using the Visual Enzymatics 2010 plug in for Igor Pro 9 (Figure 4)[24]: where k'_{cat} is the theoretical maximal velocity, k'_{cat}/K'_m is the theoretical maximal catalytic efficiency,

$$\log(k_{cat}) = \log\left(\frac{k'_{cat}}{1+\frac{H}{K_{ES1}}+\frac{K_{ES2}}{H}}\right) \tag{2.1}$$

$$\log(k_{cat}/K_m) = \log\left(\frac{\frac{k'_{cat}}{K'_m}*\frac{H}{K_{E2}}}{\left(1+\frac{H}{K_{E3}}*\left(1+\frac{H}{K_{E1}}\right)\right)}\right) \tag{2.2}$$

K_{ES1} is the ionization constant of the ES complex, which affects the acidic side of the pH curve, while K_{ES2} reflects the basic side. K_{E1} and K_{E2} are ionizable groups on the enzyme and K_{E3} is an ionizable group for the free enzyme or free substrate in the pH range examined (Scheme 2).[24,25] Inspection of the plot of log(K_m) vs pH (Figure 4) shows two distinct sections. Log(K_m) values are relatively unchanged between pH values 4.0-5.5 and then decrease in a linear fashion from pH 6.0-10.0. Because log(K_m) is pH dependent, the plots of log(k_{cat}) vs pH and log(k_{cat}/K_m) vs pH reveal different pK_a values (Table 1). Table 1 also shows the ionization constants calculated for chlorothalonil dehalogenase (Chd) the only other hydrolytic dehalogenase that has been kinetically examined.[20] A plot of log(k_{cat}) vs pH provided an exponential curve that was fit to eq. 1 (Figure 4). Fits to eq. 1 provided a pK_{ES1} value of 3.6 $\pm$ 0.03, a pK_{ES2} value of 10.8 $\pm$ 0.1, and a k'_{cat} of 21.4 $\pm$ 0.1 s^{-1}. The plot of log(k_{cat}/K_m) vs pH provided an S-shaped curve that was fit to eq 2, providing a pK_{E1} value of 6.9 $\pm$ 0.2 (Figure 4).

2.3.2 Solvent Isotope Effect Studies

Solvent isotope effect studies were performed on TrzN using atrazine as the substrate at pH 7.5 by substituting hydrogen with deuterium. k_{cat} values for atrazine were measured at several different ratios of H_2O/D_2O and the results were plotted as atom fraction of deuterium vs rate ratio (V_n/V_1) where V_n is the observed k_{cat} at n fraction of D_2O whereas V_1 is the observed velocity in D_2O (Figure 5).[21,25] Proton inventories and fractionation factors were obtained by fitting the experimental data to equations derived from the Gross-Butler equation (Figure 2).[21,25,26] These data deviate from linearity and was best fit to eq. 4, suggesting that there are at least two protons transferred in the rate-limiting step with fractionation factors ϕ_1 and ϕ_2 equal to 0.57 (Figure 5).

Scheme 2

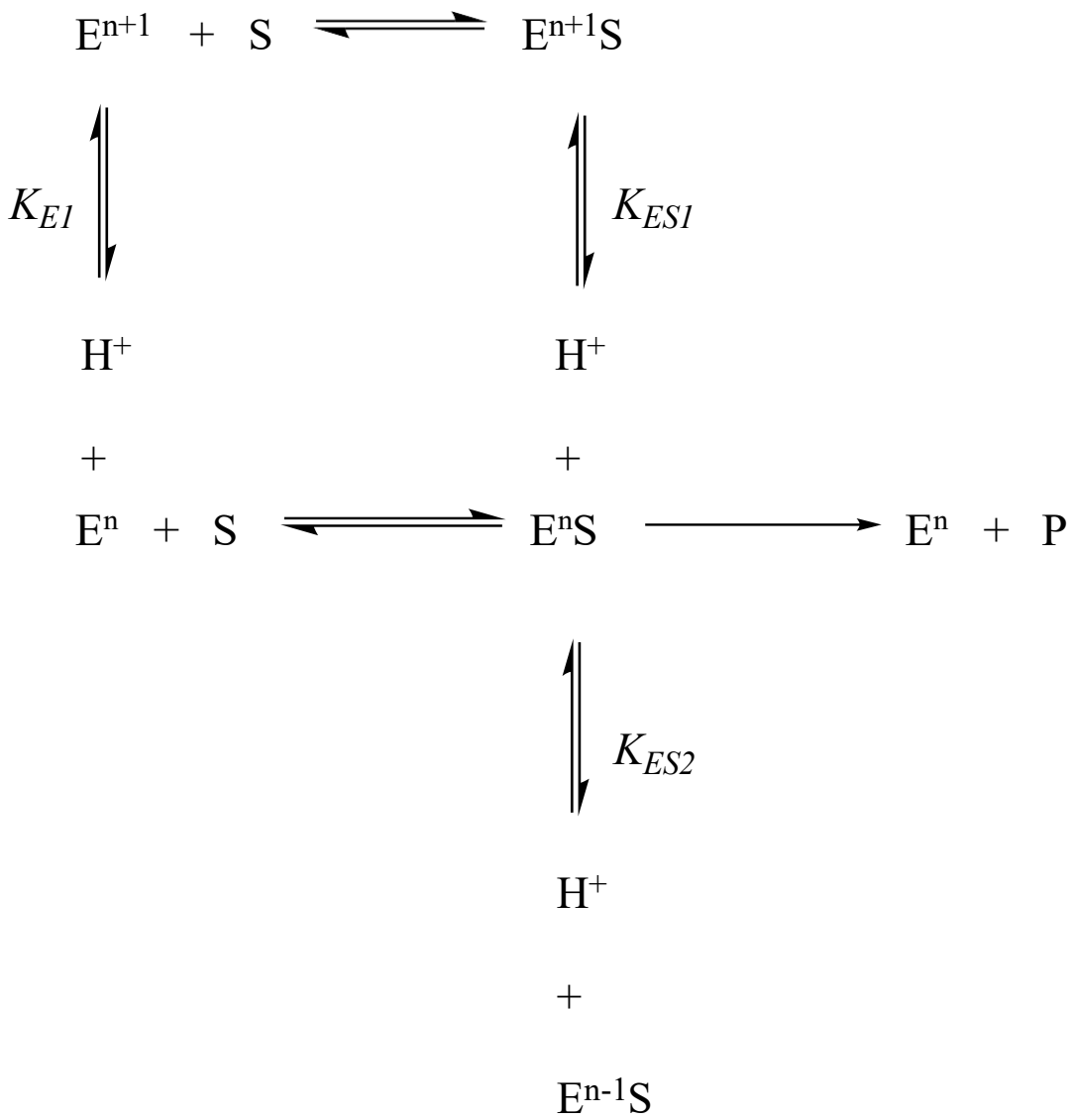

Scheme 2.1 Hydrolysis of atrazine to hydroxyatrazine and chloride by TrzN.

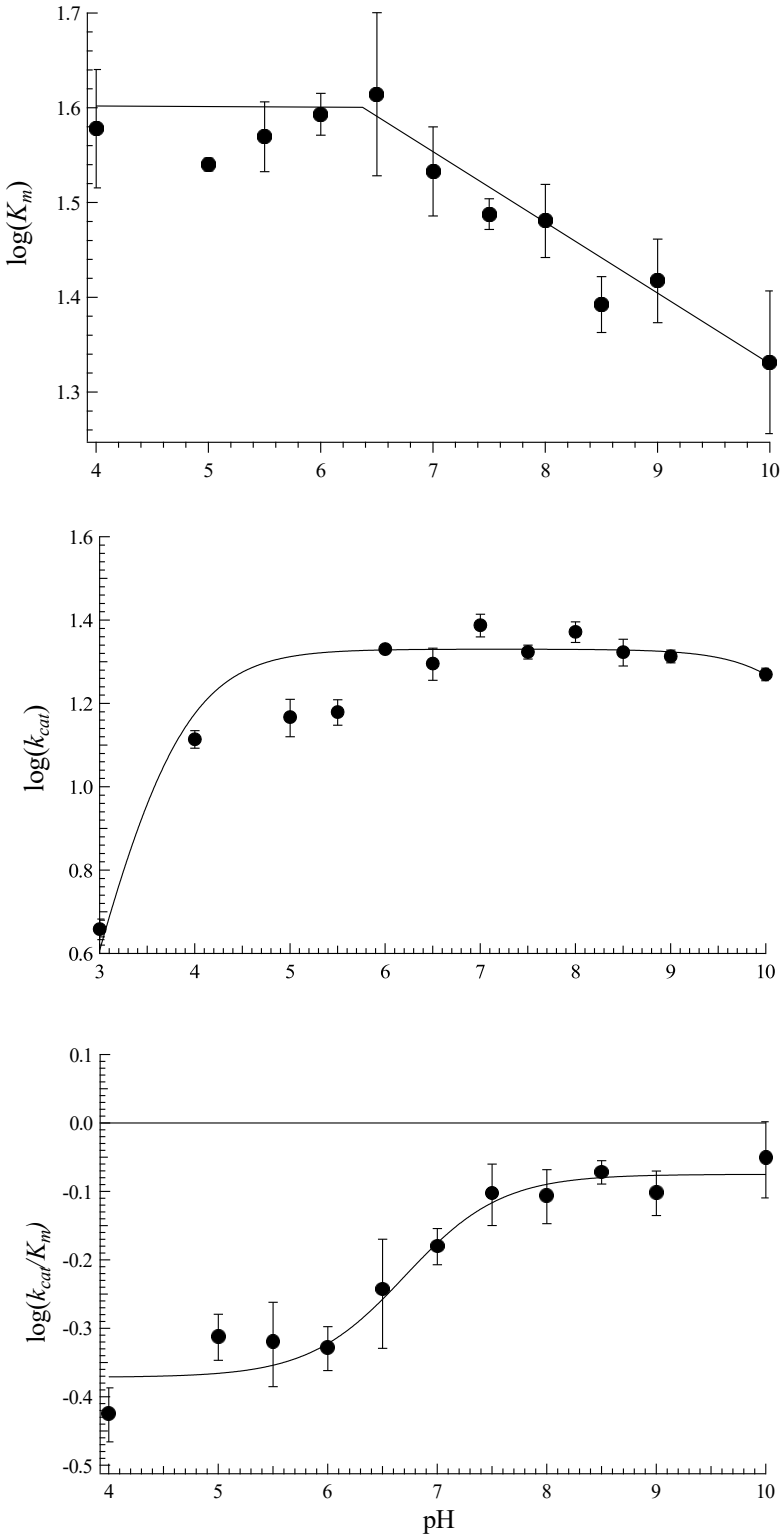

Figure 2.3. Effects of pH on the kinetic parameters of the hydrolysis of atrazine by TrzN between pH 4.0 and 10.0. The K_m decreases linearly in with pH in two distinct groups, one from 4.0 to 5.5 and the second from 6.0 to 10.0. The pH dependence of k_{cat} is fit to eq 1, and the pH dependence of k_{cat}/K_m is fit to eq 2. The kinetic constants obtain from the fits are listed in Table

Table 2.1. Ionization constants for atrazine hydrolysis by TrzN and Chd

	TrzN	**Chd**[a]
	k_{cat} vs pH	
pK_{ES1}	3.6 ± 0.03	5.4 ± 0.2
pK_{ES2}	10.8 ± 0.1	9.9 ± 0.1
k'_{cat} (s^{-1})	21.4 ± 0.1	24 ± 2
	k_{cat}/K_m vs pH	
pK_{E1}	6.9 ± 0.2	5.4 ± 0.3
pK_{E2}	N/A	9.5 ± 0.1
k'_{cat}/K'_m ($s^{-1}\mu M^{-1}$)	0.85 ± 0.03	220 ± 10

[a] Data taken from reference 20

Because the largest deviation for the theoretical proton inventory curves occurs at the atom fraction of 0.5, calculation of the midpoint partial solvent isotope effect helps in determining the number of protons involved in the catalytic reaction.[27,28] The following equations are derived from Elrod, allowed the calculation of the midpoint partial solvent isotope effects when the experimental data was obtained at different atom fractions:

$$\text{one proton: } \frac{V_m}{V_1} = (1 - n_m)(V_0 - V_1) + n_m \tag{2.3}$$

$$\text{two proton: } \frac{V_m}{V_1} = [(1 - n_m)(V_0 - V_1)^{\frac{1}{2}} + n_m]^2 \tag{2.4}$$

$$\text{general solvation: } \frac{V_m}{V_1} = (V_0 - V_1)^{1-n_m} \tag{2.5}$$

where n_m = 0.5 (the H_2O/D_2O ratio at the midpoint), V_m/V_1 equals the midpoint partial solvent isotope effect, V_0/V_1 represents the total isotope effect (velocity in 100% H_2O/velocity in 100% D_2O). The experimental and calculated midpoint partial isotope effects are presented in Table 2. The presence of D_2O lowered the catalytic activity of TrzN resulting in an overall isotope effect of 1.43. The k_{cat}/K_m value in 100% D_2O at pH 7.5 is 0.54 $\pm$ 0.04 (in 100% H_2O the k_{cat}/K_m value is 0.79$\pm$ 0.08), which is similar to what has been reported for other metal dependent amidohydrolases.[29–31] The midpoint partial solvent isotope effect calculations do not strongly distinguish between one or two protons transferred, or even generalized solvent effects (Table 2.2).

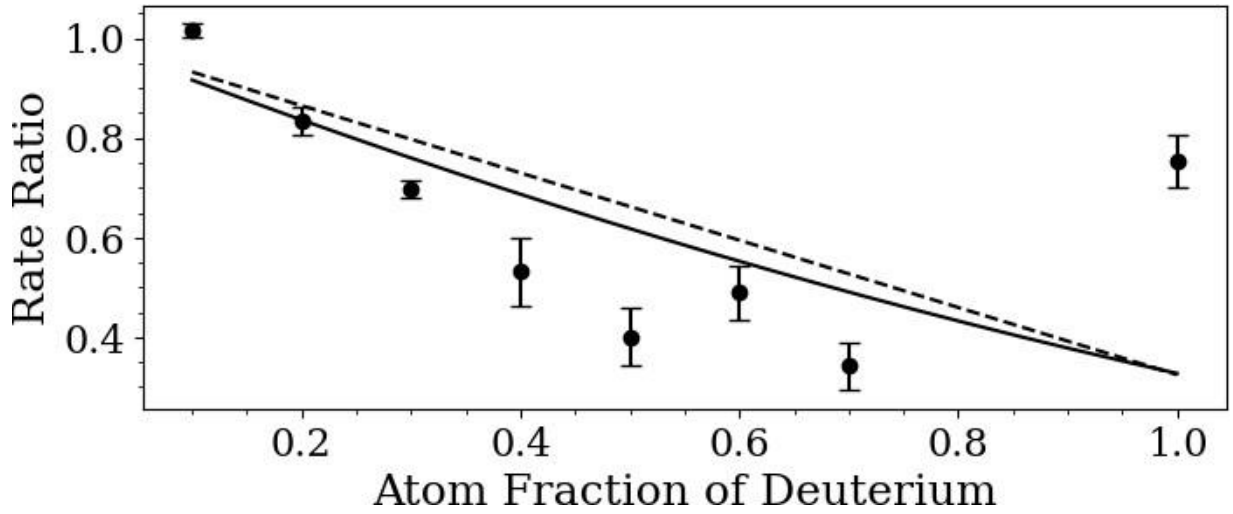

Figure 2.4. Plot of V_n/V_1 vs atom fraction of deuterium of TrzN at pH 7.5. V_n/V_1 is defined as the velocity at *n* atom fraction of deuterium over velocity in water. The dashed line represents a fit to the Gross-Butler equation and the solid line is a linear fit.

Table 2.2. Comparison of experimental midpoint solvent isotope effects with calculated midpoint solvent isotope effects of TrzN and ChD

			Calculated midpoint solvent isotope effects		
	V_0/V_1	Midpoint solvent isotope effect V_m/V_1	One proton	Two protons	Generalized solvation changes
TrzN	1.43	0.53	1.22	1.21	1.97
Chd[a]	N/A	2.98	2.99	4.03	2.34

The experiment was carried out using atrazine as the substrate at pH 7.4. Experimental and theoretical midpoint isotope effects were calculated for 0.5 atom fraction of deuterium
[a] Data Taken from reference 20

2.3.3 Temperature Dependence

TrzN has shown to be catalytically active at temperatures up to 80°C.[10] Therefore, the hydrolysis rate of atrazine was measured in triplicate between 4 and 80°C at 8 substrate concentrations ranging from 5 μM to 150 μM in 0.1 M sodium phosphate buffer pH 7.0. From these data, k_{cat} and K_m values were derived by fitting the experimental data to the Michaelis-Menten equation at each temperature studied. k_{cat} linearly increased until 35°C after which it steadily decreased until 80°C where a k_{cat} value of 14.4 ± 0.6 s^{-1} was observed, which is ~56% of the maximum activity observed at 35°C (k_{cat} = 25.8 ± 0.2 s^{-1}) (Figure 6). An Arrhenius plot was constructed between 4 and 35°C (278 and 308 K) by plotting ln(k_{cat}) vs. 1/T (Figure 7). A linear plot was obtained, indicating that the rate-limiting step does not change as temperature is

increased within this temperature range.[24] The activation energy, E_a, was calculated from the slope of the line as the slope of an Arrhenius plot is equal to $-E_a/R$, where R = 8.3145 J K^{-1}. The E_a for temperatures between 278 and 308 K was found to be 16.7 $\pm$ 0.3 kJ/mol. Other thermodynamic parameters were calculated by the following equations: where k_b,

$$\Delta G^{\ddagger} = RTln(\frac{k_{cat}h}{k_bT}) \tag{2.6}$$

$$\Delta H^{\ddagger} = E_a - RT \tag{2.7}$$

$$\Delta S^{\ddagger} = (\Delta H^{\ddagger} - \Delta G^{\ddagger})/T \tag{2.8}$$

h, and R are the Boltzman, Planck, and gas constants, respectively (Table 3).[21,24] A plot of ln(1/K_m) vs 1/T (Figure 8) revealed a flat line K_m did not change between 278 and 308 K indicating that there is little or no enthalpy (ΔH°) change. The calculated ΔH° based off the slope of the linear regression was 0.57 $\pm$ 2 kJ/mol. In addition, the following thermodynamic parameters were also calculated ΔG° was 8.8 $\pm$ 0.2 kJ/mol and ΔS° was -0.027 $\pm$ 0.006 kJ/mol (Table 3):

$$\Delta G^{\circ} = -RTln(\frac{1}{K_m}) \tag{2.9}$$

$$\Delta S^{\circ} = (\Delta H^{\circ} - \Delta G^{\circ})/T \tag{2.10}$$

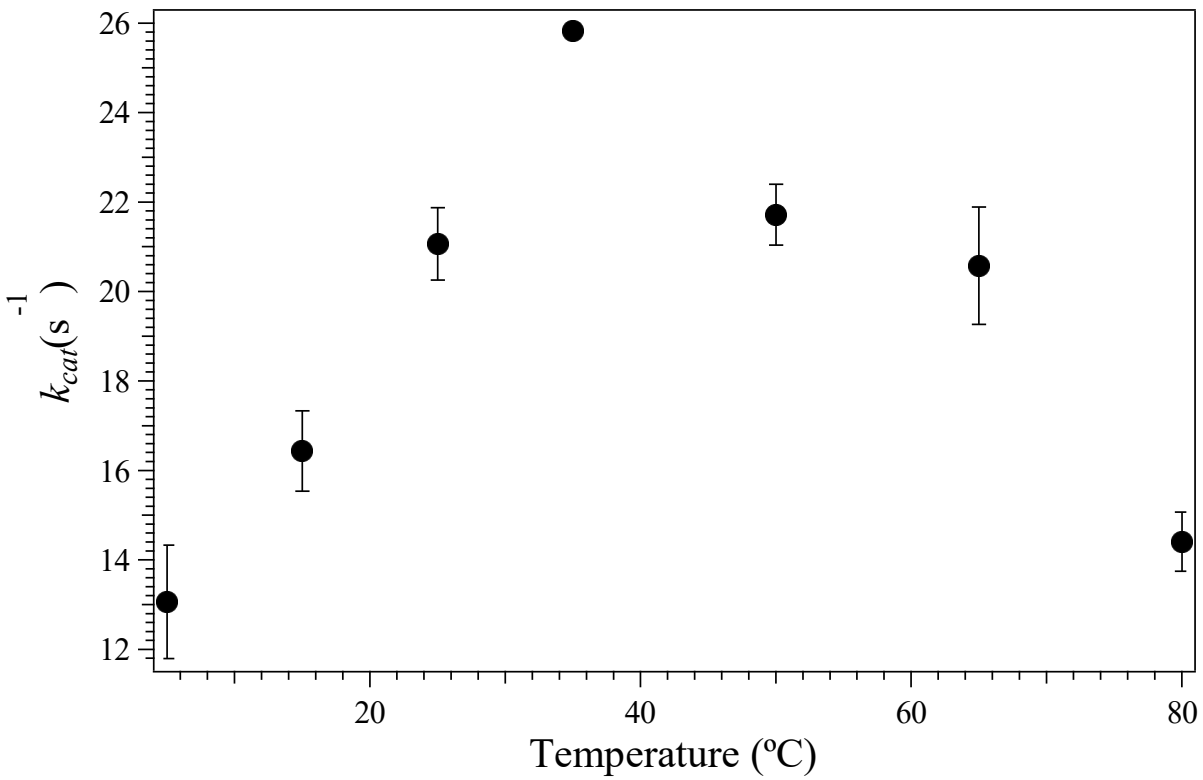

Figure 2.5. Plot of k_{cat} vs pH of the hydrolysis of atrazine by TrzN in 0.1 M sodium phosphate buffer, pH 7.0 over a temperature range of 5°C to 80°C.

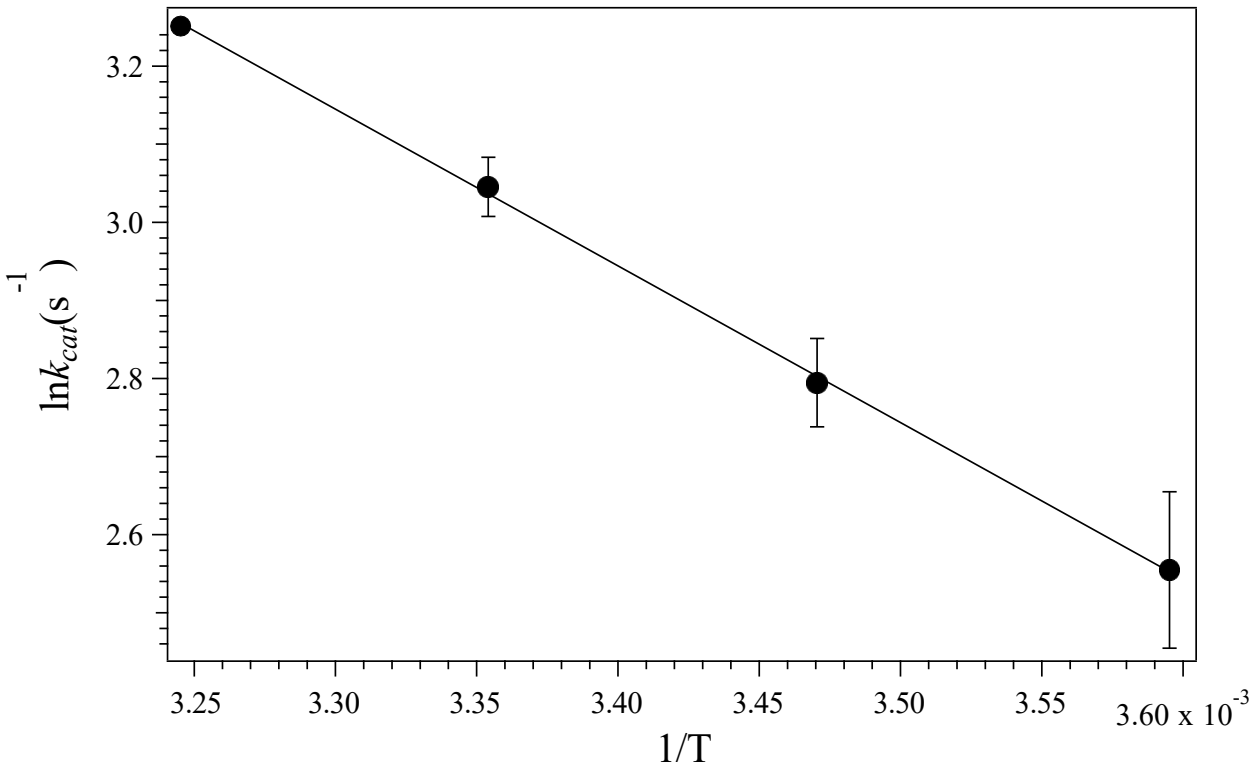

Figure 2.6. Arrhenius plot of the hydrolysis of atrazine catalyzed by TrzN at four different temperatures between 5°C and 35°C. The solid line is a linear fit to the data.

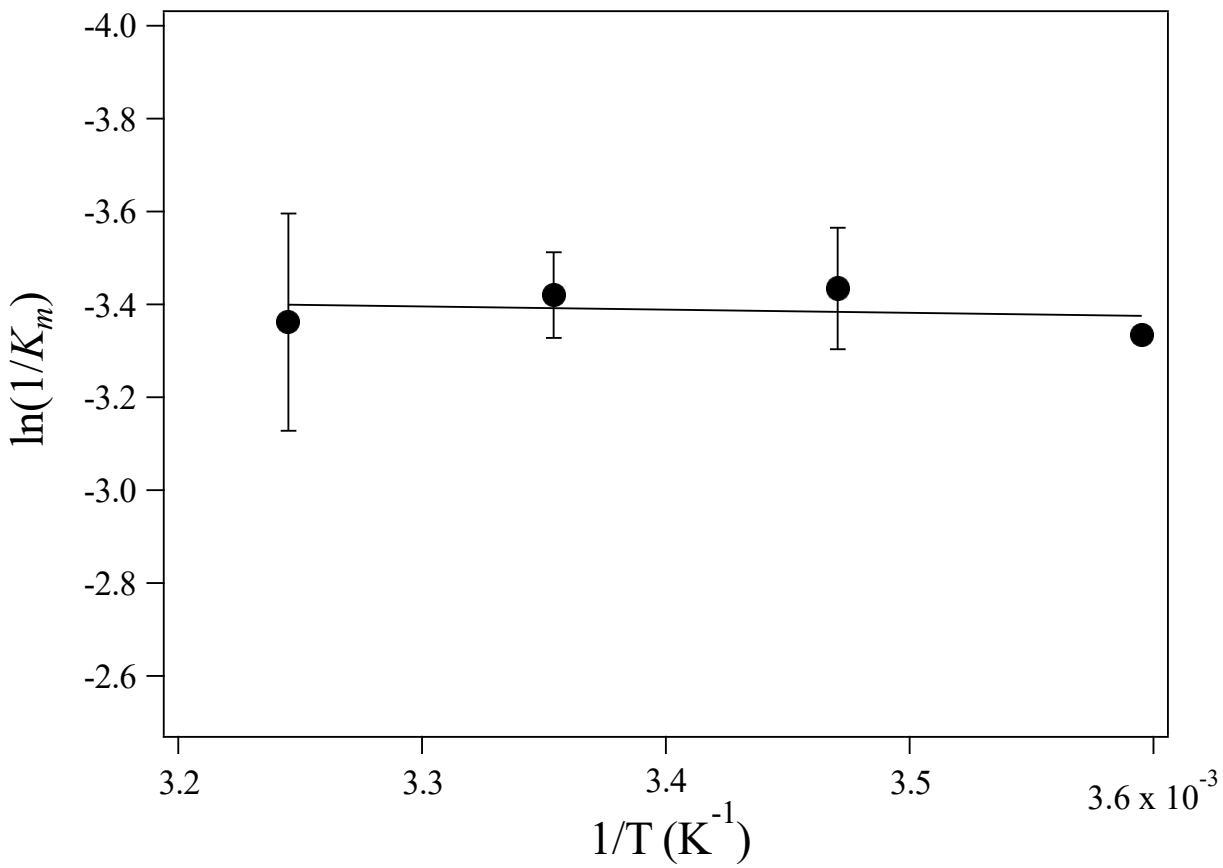

Figure 2.7. plot of ln(1/K_m) vs 1/T for the hydrolysis of atrazine at four different temperatures between 5°C and 35°C. The solid line is a linear fit to the data.

Table 2.3. Thermodynamic properties of atrazine hydrolysis by TrzN at 25°C

		TrzN
E + S → ES	ΔG° (kJ/mol)	8.75 ± 0.3
	ΔH° (kJ/mol)	0.57 ± 2
	ΔS° (kJ/mol)	-0.027 ± 0.006
ES → (ES·EP)‡	$\Delta G^{\ddagger}$ (kJ/mol)	65.5 ± 0.1
	$\Delta H^{\ddagger}$ (kJ/mol)	14.2 ± 2.2
	$\Delta S^{\ddagger}$ (kJ/mol)	-0.17 ± 0.01
	E_a (kJ/mol)	16.7 ± 0.3

2.4 Discussion

TrzN is a promising target for atrazine degrading biomaterials as it has previously been shown to be an effective biocatalyst when immobilized on solid supports.[10,11] However, improvement in biocatalyst engineering for TrzN is hampered by the lack of mechanistic detail. A catalytic mechanism was previously proposed based on a combination of X-ray crystallography, site directed mutagenesis, carbon and nitrogen isotope data, and substrate docking studies.[13,14,17] Briefly, catalysis begins with substrate recognition of atrazine,[14] and His274 is proposed to remove a proton from the Zn(II) bound water moiety and shuttle that proton to Glu241 which then further shifts it to the substrate triazole nitrogen atom. Glu68 is also proposed to form a hydrogen bond with the N-alkyl nitrogen atom of atrazine.[13] The ortho carbon atom is then primed for nucleophilic attack by the Zn(II)-bound hydroxide.[14,17] While this mechanism is logical based on the current data, aspects such as proton transfer have not been meaningfully explored. Therefore, the catalytic mechanism of TrzN was examined kinetically in order to gain a deeper understanding of the functional amino acids in the active site.

The kinetic parameters k_{cat}, K_m, and k_{cat}/K_m for the hydrolysis of atrazine as a function of pH were examined. Inspection of the plot of log(K_m) vs pH indicates that K_m is unchanged between pH values 4.0-5.5 but then decreases linearly from pH 6.0-10.0. It is likely that the observed pK_a between 6-7, where the transition in the graph occurs, is due to either substrate ionization, which perturbs the ability of atrazine to bind to TrzN, or the depronation of a free enzyme residue that perturbs substrate binding.[32] A plot of log(k_{cat}) vs pH exhibits a bell-shaped curve and the fit of these data to eq. 1, revealed one catalytically competent ionizable group with a pK_{ES1} value of 3.6 $\pm$ 0.03 that must be deprotonated in the ES complex and another with pK_{ES2} of 10.8 $\pm$ 0.1 that must be protonated to facilitate catalysis. Assignment of the observed pK_{ES}

values is difficult but previously reported substrate docking studies for TrzN with atrazine suggested that Glu241 is protonated during catalysis and its protonated carboxylic acid forms a hydrogen bond with the N-3 atom of atrazine.[13] *Seffernick et al.*[33,34] also suggested Glu241 was protonated at neutral pH and had an abnormally high pK_a in the vicinity of 8.5.[14] However, the pK_a commonly reported for glutamic acid is ~4, which is close to the observed pK_{ES1} value of 3.6 $\pm$ 0.03.[25,35] Enzymes with catalytically important Glu residues have been assigned pK_a's as high as 6.8, which is still significantly lower than the value of 8.5 suggested by *Seffernick et al.*[33,34] As such, the observed pK_{ES1} value observed herein is proposed to be due to the Glu241 sidechain being deprotonated making it available to accept a proton from the His274. In the MACiE data base, a database of over 200 enzyme reaction mechanisms, glutamic acid is frequently reported in numerous mechanism to act as a proton shuttle with pK_a values in the 3.5 to 6 range, in agreement with the observed pK_{ES1} value for TrzN.[36]

An alternative assignment of pK_{ES1} would be His274, however, a typical pK_a of histidine is ~6.5, but a >2 unit decrease in pK_a values for His residues have been observed as a result of either electrostatic or hydrogen bonding contributions from other residues. For example, in carbonic anhydrases (CA), which are sequentially and mechanistically similar to TrzN, active site His residues have been proposed to shuttle protons from the Zn-bound water; however, the pK_a value reported for the active site His residue in CA is significantly higher (7.2 $\pm$ 0.1) than the observed pK_{ES1} for TrzN.[37] Likewise, in Chd, a pK_{ES1} value of ~5.4 was reported and suggested to be due to an active site His or Glu, similar to what is described above for TrzN (Table 2).[20] Combination of all of these data suggest that the pK_{ES1} observed for TrzN is most likely due to Glu241 suggesting it is depronated allowing it to accept a proton from the His274 and subsequently being able to transfer that proton to the triazole nitrogen of the atrazine ring.[18]

With the assignment of the observed pK_{ES1} value of 3.6 $\pm$ 0.03 to Glu241, the question of which active site residue(s) is responsible for the observed pK_{ES2} value of 10.8 $\pm$ 0.1. One possibility is Thr325, which forms a hydrogen bond to the Zn(II)-bound water molecule (2.6 Å). In other amidohydrolase superfamily members, this residue is replaced with a conserved aspartic acid residue, which functions as an active site Zn(II) ligand. In TrzN, Thr325 is too far from the metal to be a ligand; however, it was suggested to help position the Zn(II) bound water moiety for depronaton by His274.[14] The p*K*a value of Thr residues is typically >11, which is in the range of the observed pK_{ES2} value of 10.8 $\pm$ 0.1. When this residue is mutated to a aspartate or glutamate there is no detectable activity, likely due to the inability of aspartate or glutamate to form an hydrogen bond to the Zn(II)-bound water moiety as they are deprotonated. On the other hand, when Thr325 was mutated to a serine residue, TrzN was still active albeit with a 17-fold reduction in k_{cat}.[14] Serine lacks the methyl group on the β carbon that threonine has but can still form an hydrogen bond, suggesting that the hydrogen bond between the OH group if Thr325 is necessary for catalysis. During kinetic analysis, TrzN had no quantifiable activity at pH 11, corroborating that deprotonation of Thr325 would prevent hydrogen bond formation with the Zn(II)-bound water moiety, which would result in a loss of activity. Comparison of the observed pK_{ES2} value for TrzN with that of Chd, (9.9 $\pm$ 0.1), which was proposed to be due to the deprotonation of the leaving group or an active site residue such as an Arg or Lys.[20] Alternatively, it was also suggested that the observed pK_{ES2} for Chd might be due to the deprotonation of a metal-bound water molecule. Therefore, an alternative assignment for pK_{ES2} in TrzN would be the leaving group or the Zn(II)-bound hydroxide; however, with the close proximity of Thr325 to the Zn(II)-bound hydroxide and its requirement for catalysis, it is most likely that the observed pK_{ES2} is due to Thr325.

Inspection of the plot of log(k_{cat}/K_m) vs pH indicates a clear S-shaped model with a pK_{E1} value of 6.9 $\pm$ 0.8 which are enzyme-centered ionizable groups that are involved in catalysis (Scheme 2).[25] . The most likely candidate for this pK_a is His274 as the observed pK_{E1} value is within the typical range for pK_a values observed for catalytically important for His residues.[38,39] Alternatively, the observed pK_{E1} value could also possibly be due to the Zn(II)-bound water moiety as the pK_a of the Zn(II)-bound water moiety in CA, which has a similar active site to TrzN, was reported to be 7.0.[40] These data suggest an enzyme-centered residue needs to be protonated for substrate to securely bind to the active site, but when its deprotonated, the catalytic efficiency increases suggesting this residue needs to be deprotonated for full catalytic activity even if the substrate is less securely bound in the active site. Given the proposed mechanism for TrzN as well as the X-ray structure of the Glu241Asn mutant enzyme bound by the substrate analog atratone, which reveals the hydrogen bonding network between His274 and Glu241 with a triazine ring nitrogen atom of atratone, its most likely the that observed pK_{E1} value is likely due to His274.[16]

Kinetic isotope effect studies provide a simple way to gain insight into the nature of the rate-limiting step and also provide information about the transition-state.[41] The intrinsic primary isotope effect, k_H/k_D, is related to the symmetry of the transition-state for that step (*i.e.* the larger the isotope effect, the more symmetrical the transition-state) with the theoretical limit being 9 at 37°C in the absence of tunneling effects. For the simplest case, in which a single proton produces the solvent isotope effect, a plot of atom fraction of deuterium *vs*. V_n/V_0 is linear, where V_n is k_{cat} at a particular fraction of deuterium and V_0 is k_{cat} in buffer containing 0% D_2O. The solvent isotope effect of TrzN using atrazine as a substrate was examined at pH 7.5 by substituting hydrogen (^1H) with deuterium (^2H). The presence of D_2O lowered the catalytic

activity of TrzN resulting in a solvent isotope effect of 1.43. Solvent isotope effects close to 1 often correlates to the stiffness of the solvent-exchangeable hydron not being altered in the transition state of a subsequent rate-limiting step.[31] For TrzN, V_n/V_1 deviates from linearity and the best fit to a model for two protons being transferred in the transition-state with identical fractionation factors of 0.57; however, It has previously been shown that displacement of a Zn(II)-bound water can be correlated to fractionation factors of 0.35-0.54.[42] A two proton transfer system is in good agreement with the transfer of a proton from the Zn(II)-bound water moiety to His274 and then His274 shuttling a proton to Glu241, which then can form an hydrogen bond to a triazole nitrogen of the atrazine ring. However, It has previously been hypothesized that TrzN has alternative paths for proton exchange since catalysis can proceed without Glu241, suggesting there are multiple protonation options.[14,17,18] When Glu241 is mutated to residues unable to shuttle protons, activity with atrazine as the substrate is still observed, albeit eleven-fold lower than WT.

Comparison of the solvent isotope data obtained for TrzN and those reported for Chd suggest the two hydrolytic dehalogenases proceed by different catalytic mechanisms as only one proton is transferred in the transition-state of Chd, with a fractionation factor of 0.17, whereas two are transferred for TrzN.[20] The proposed catalytic mechanism of Chd, similar to TrzN, involves substrate binding near the active site Zn(II) metal center but no direct substrate-Zn(II) bonding interaction. In Chd, a proton is transferred from a Zn(II)-bound water molecule to an active site His residue forming the nucleophilic hydroxide.[20,43] This is similar to the proposed mechanism of TrzN except that atrazine contains a triazole ring so a second proton transfer occurs in order to form a hydrogen bond between Glu241 and an N atom of the triazole ring. Overall, the solvent isotope data, coupled with the results from the pH studies, supports that two

protons are transferred during hydrolysis of atrazine using TrzN. Previously reported nitrogen isotope fractionation data, suggested an alternative path for proton transfer, which comes from a second, non-nucleophilic, water molecule in the active site that is 2.83 Å (Glu241 is 3.3 Å) from the atrazine ring nitrogen.[18] This active site water molecule could take the place of Glu241 or in its presence, could help activate the triazole ring of atrazine towards nucleophilic attack by the Zn(II)-bound hydroxide group.

The activation energy (E_a) for the activated $ES^{\ddagger}$ complex determined from an Arrhenius plot between 4 and 35 ºC and was found to be 16.7 ± 0.3 kJ/mol. The enthalpy of activation was calculated to be 14.2 ± 2.2 kJ/mol while the entropy of activation was found to be -0.17 ± 0.01 kJ/mol at 25°C. The positive enthalpy is indicative of a conformation change upon substrate binding, which is likely due to bond formation and breaking during the nucleophilic attack on the ortho carbon by the Zn(II)-bound hydroxide.[21] The negative entropy value suggests some molecular motions are lost upon $ES^{\ddagger}$ complex formation. These motions are likely due to hydrogen bond formation between catalytically relevant active site residues and active site water molecules and/or the triazole ring nitrogens of the substrate atrazine. Previous docking studies suggest that Thr325, Gly326, and Glu68 form a hydrogen bonding network with the substrate and Glu241, Pro214, and Tyr214 form a hydrogen bonding network with other water molecules.[13] The observed K_m values between 278 and 308 K did not change, indicating a ΔH° value near zero (0.57 ± 2 kJ). ΔH°corresponds to the standard enthalpy change and the fact that it is near zero indicates that the formation of the Michaelis complex at 25°C is neither endothermic or exothermic.[24] Using the observed ΔH°value, ΔG° was calculated to be 8.75 ± 0.3 kJ and ΔS° was -27 ± 6 J/mol. Based on these data, the formation of the ES complex is in rapid equilibrium as substrate binding/dissociation is very rapid compared to the breakdown of the ES

complex. A near zero ΔH° value has been observed previously in monomeric thermostable proteins,[44] and it was suggested that the enzyme system is largely unchanged and the enthalpy of substrate dissociation remains constant within the temperature range examined.[45,46]

In conclusion, the data presented herein provide insight into the proposed catalytic mechanism for TrzN (Figure 2). The pH studies of the kinetic constants k_{cat}, K_m and k_{cat}/K_m provide two ionizable groups, one with p$K_a \approx 3.6$ and one with a p$K_a \approx 10.8$, which were assigned to the active site residues Glu241 and Thr325. A third pK_a at ≈ 7, that is enzyme centered, was assigned to His274. Solvent kinetic isotope effect studies indicate that two protons are transferred in the transition-state, likely due to the breaking of a Zn(II)-bound water O-H bond by His274 and the transfer of this proton to Glu274 which shuttles it to a triazole nitrogen of the substrate atrazine. The observed E_a of ≈ 17 suggests a conformational change in the ES complex, which is in good agreement with proposed bond formation and breaking. This conformational change, which can be identified by a positive change in enthalpy, could also be correlated to the bond formation and breaking during the nucleophilic attack on the ortho carbon by the Zn(II)-bound hydroxide. The pH data also suggest that the protonation of Thr325 is critical to catalysis, suggesting that without the stabilizing bond formed between Thr325 and the Zn(II)-bound water moiety nucleophilic attack is unlikely to occur. Taken together, the data reported herein supports the previously proposed catalytic mechanism with direct evidence for the catalytic roles of His271, Glu274, and Thr325 and the transfer of two proton in the transition-state.

2.5 Materials and Methods

2.5.1 Chemicals

The gene for TrzN was synthesized by Genscript (Piscatawat, NJ). All chemicals used in this study were purchased from commercial sources and were of the highest quality available.

2.5.2 Expression and Purification of Recombinant TrzN

The gene from *Arthrobacter aurescens* TC1 that encodes for TrzN with the D38N, L131P, and A159V mutations with a polyhistidine (His_6) affinity tag engineered onto the N terminus with a Tobacco Etch Virus (TEV) cleavage site was synthesized with optimized *Escherichia coli* codon between the Ndel and Xhol restriction sites of kanamycin-resistant pET28a(+) in order to create a TrzN/pET28a(+) plasmid. The TrzN/pET28a(+) plasmid was transformed into E. coli BL21(DE3) competent cells (Stratagene) and was expressed and purified as previously reported.[10,19] Briefly, a 100 mL LB-Miller starter culture was inoculated from a single colony with 50 µg/mL kanamycin. A 12 L culture was inoculated from this starter using 10 mL/L supplemented with 5 µM isopropyl ß-d-1-thiogalactopyranoside (IPTG) and grown at 37°C for 48h.[10,19] Cells were harvested by centrifugation at 7000 rpm 4°C, for 15 min. The cells were resuspended at 2 mL per gram of buffer A (50 mM NaH_2PO_4, 500 mM NaCl, 10 mM imidazole, 1.5 mM *tris(2-carboxyethyl)phosphine (TCEP), 10% glycerol,* pH 8.0) then lysed by sonication on ice in three 10 min (30s on, 45s off) intervals using a 21W Misonex sonicator 3000. Cell debris was removed by centrifugation at 17,500 rpm, 4°C, for 40 min. The protein was purified by immobilized metal affinity chromatography (IMAC) using Ni-NTA (nickel-nitrilotriacetic acid) Superflow Cartridges (Qiagen). The column was equilibrated with buffer A and the crude protein extract was loaded onto the IMAC column. Unbound protein was eluted

with 15 column volumes (CV) of buffer A at a flow rate of 2 mL/min. Elution of TrzN was initiated with 15 CV of 3% buffer B (buffer A with 500 mM imidazole). Elution finished with a linear gradient (3-100%) of buffer B over 20 CVs at a flow rate of 2 mL/min. Peak fractions were pooled and resuspended in 50 mM HEPES pH 7.5 and concentrated with an Amicon Ultra-15 centrifugal filter device with a molecular weight cutoff (MWCO) of 30,000 (Millipore). Sodium dodecyl sulfate-polyacrylamide gel electrophoresis (SDS-PAGE) reveals a single polypeptide band at ~51 kDa, consistent with previous studies (Figure 3). The protein concentration was determined by UV-Vis absorbance at 280 nm (ε_{280} = 61,670 $M^{-1}cm^{-1}$) and with a Coomassie (Bradford) Protein Assay Kit (Thermo Scientific).[10,12,19]

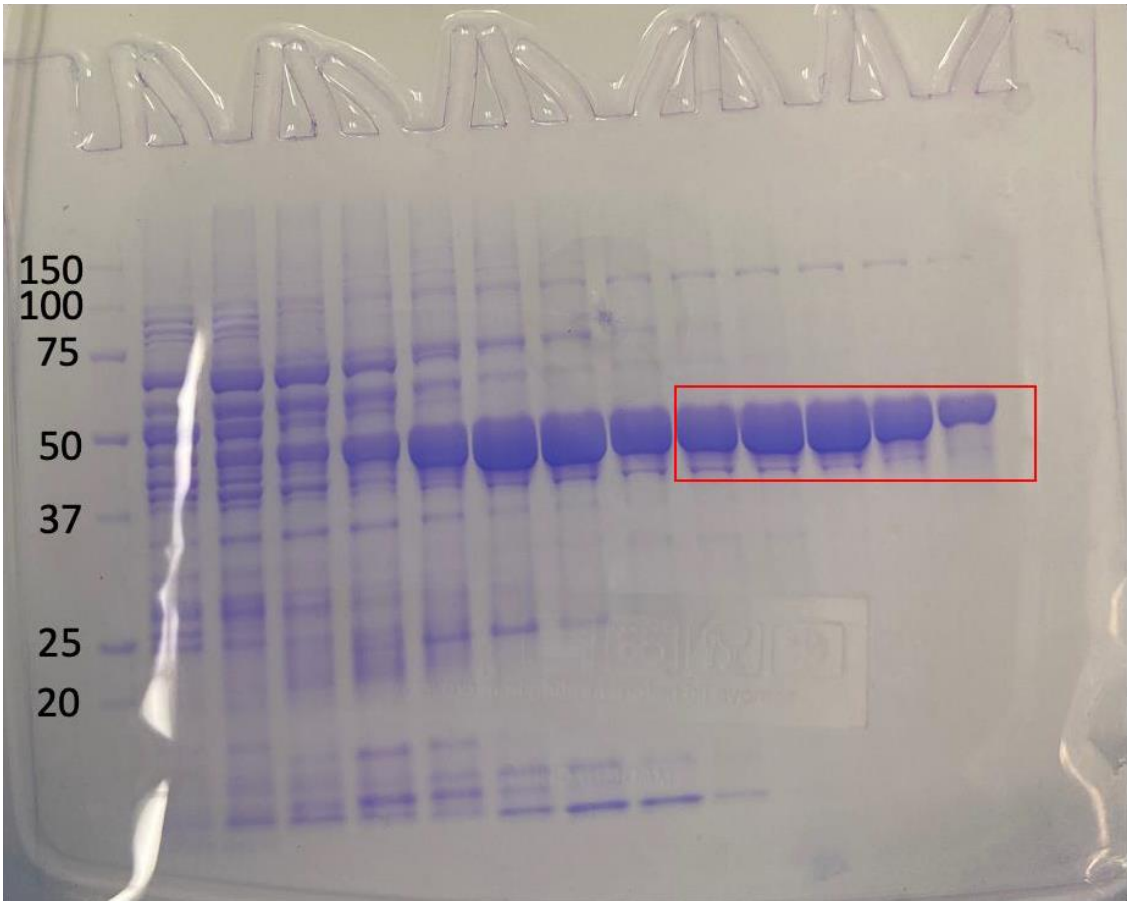

Figure 2.8. SDS-PAGE gel of TrzN shows the monomer at ~51kDa after IMAC purification.

The His_6 tag was removed by treating His_6-tagged TrzN with His_6-tagged TEV protease (EC 3.4.22.44) for 36 h at 4°C in TEV treatment buffer (50 mM Tris HCl, 1.5 mM TCEP, 0.5 mM ethylenediaminetetraacetic acid tetrasodium salt dihydrate (EDTA), and 20% glycerol, pH 7.5).[20] Cleaved protein was concentrated to 3 mL with an Amicon Ultra-15 centrifugal filter device with a molecular weight cutoff (MWCO) of 30,000 (Millipore). The concentrated sample was loaded on IMAC to remove the remaining cleaved His_6 tag, uncut protein, and the His_6-tagged TEV. The flow through that contained TrzN was collected, concentrated with an Amicon Ultra-15 centrifugal filter device with a molecular weight cutoff (MWCO) of 30,000 (Millipore), and washed with 50 mM HEPES buffer pH 7.0. Purified sample was reanalyzed by SDS-PAGE as described above. The protein concentration was determined as described above.[10,12,19]

2.5.3 Kinetic Assay

The enzyme was assayed for the catalytic activity as previously described using atrazine as the substrate in 0.1 M sodium phosphate buffer, pH 7.0.[10,19] The hydrolysis of atrazine was quantified spectrophotometrically by continuously monitoring the decrease in absorbance at 264 nm (ε_{264} = 3.5 $mM^{-1}cm^{-1}$) that accompanies atrazine dechlorination, as previously reported.[16] This region contains no detectable product formation. Assays were performed using 0.05 mg/mL TrzN within a 1 mL quartz cuvette in triplicate on a temperature-controlled Agilent 8453 UV-Vis spectrophotometer. Data analysis was performed using OriginPro 9.0 (OriginLab, Northampton, MA). Plots of the initial rate of hydrolysis of various concentrations of atrazine were fit to the Michaelis-Menten equation to find V_{max} and K_m. V_{max} values were converted to k_{cat} using the

molar mass of TrzN. One unit of enzyme activity was defined as the amount of enzyme that catalyzed the hydrolysis of 1 μmol of atrazine per minute at 25°C.

2.5.4 pH Profiles

The enzymatic activities of TrzN at pH values between 4.0 and 10.0 were measured using atrazine as the substrate. The concentration of each buffer used was 0.1 M, and the following buffers were used: sodium tetraborate (9.20-10.00), sodium phosphate (5.8-8.0), sodium acetate (4.0-5.5), and sodium citrate (3.0-6.2). The kinetic parameters k_{cat}, K_m, and k_{cat}/K_m were determined using nine different substrate concentrations ranging from 0-150 μM at each pH studied. Kinetic parameters and fits to the kinetic curves were obtained using the Visual Enzymatics 2010 plugin for Igor Pro 9 (Wavemetrics, Lake Oswego, Oregon). When transitioning between buffers, experiments were run at identical pH values but in different buffers with no observed effect on kinetic parameters.[21]

2.5.5 Solvent Isotope Effect Profiles

All buffers were prepared with 18.2 MΩ•cm filtered Millipore nanopure water. The buffers used in the preparation of all deuterated buffers were in their anhydrous form. The pH of each buffer used was adjusted by the addition of NaOD or DCl (both 99% + deuterium content; Cambridge Isotope Laboratories Inc., Andover, MA) and corrected for deuteration by adding 0.4 to the reading of the pH electrode.[20–22] The 5 mM atrazine stock used during the assays was made from deuterated methanol (99%+, Cambridge Isotope Laboratories Inc., Andover, MA)

2.5.6 Temperature Profiles

The enzymatic activities of TrzN at temperature values between 5°C and 80°C were measured using atrazine as the substrate in 0.1 M sodium phosphate buffer, pH 7.0. Assays were done as described above with the temperature-controlled Agilent 8453 UV-Vis spectrophotometer set to the desired temperature. The enzyme sample and buffer were incubated for 30 minutes in a water bath at the desired temperature and stored in the water bath for the duration of the experiment to ensure temperature equilibrium.

2.6 References

(1) Shapir, N.; Rosendahl, C.; Johnson, G.; Andreina, M.; Sadowsky, M. J.; Wackett, L. P. Substrate Specificity and Colorimetric Assay for Recombinant TrzN Derived from Arthrobacter Aurescens TC1. *Appl. Environ. Microbiol.* **2005**, *71* (5), 2214–2220. https://doi.org/10.1128/AEM.71.5.2214-2220.2005.

(2) de Albuquerque, F. P.; de Oliveira, J. L.; Moschini-Carlos, V.; Fraceto, L. F. An Overview of the Potential Impacts of Atrazine in Aquatic Environments: Perspectives for Tailored Solutions Based on Nanotechnology. *Sci. Total Environ.* **2020**, *700*. https://doi.org/10.1016/j.scitotenv.2019.134868.

(3) Solomon, K. R.; Baker, D. B.; Richards, R. P.; Dixon, K. R.; Klaine, S. J.; Point, T. W. La; Kendall, R. J.; Eeisskopf, C. P.; Giddings, J. M.; Giesy, J. P.; Lenwood W. Hall, J.; Williams, W. M. Ecological Risk Assessment of Atrazine In. *Environ. Toxicol.* **1996**, *15* (1), 31–76.

(4) Beaulieu, M.; Cabana, H.; Taranu, Z.; Huot, Y. Predicting Atrazine Concentrations in Waterbodies across the Contiguous United States: The Importance of Land Use, Hydrology, and Water Physicochemistry. *Limnol. Oceanogr.* **2020**, 2966–2983. https://doi.org/10.1002/lno.11568.

(5) Hayes, T. B.; Khoury, V.; Narayan, A.; Nazir, M.; Parka, A.; Brown, T.; Adame, L.; Chan, E.; Buchholz, D.; Stueve, T.; Gallipeau, S. Atrazine Induces Complete Feminization and Chemical Castration in Male African Clawed Frogs (Xenopus Laevis). *Proc. Natl. Acad. Sci. U. S. A.* **2010**, *107* (10), 4612–4617. https://doi.org/10.1073/pnas.0909519107.

(6) Liu, Z.; Wang, Y.; Zhu, Z.; Yang, E.; Feng, X.; Fu, Z.; Jin, Y. Atrazine and Its Main Metabolites Alter the Locomotor Activity of Larval Zebrafish (Danio Rerio). *Chemosphere* **2016**, *148*, 163–170. https://doi.org/10.1016/j.chemosphere.2016.01.007.

(7) Pathak, R. K.; Dikshit, A. K. Atrazine and Human Health. *Int. J. Ecosyst.* **2012**, *1* (1), 14–23. https://doi.org/10.5923/j.ije.20110101.03.

(8) Rostami, S.; Jafari, S.; Moeini, Z.; Jaskulak, M.; Keshtgar, L.; Badeenezhad, A.; Azhdarpoor, A.; Rostami, M.; Zorena, K.; Dehghani, M. Current Methods and Technologies for Degradation of Atrazine in Contaminated Soil and Water: A Review. *Environ. Technol. Innov.* **2021**, *24*, 102019. https://doi.org/10.1016/j.eti.2021.102019.

(9) Li, Q.; Li, Y.; Zhu, X.; Cai, B. Isolation and Characterization of Atrazine-Degrading Arthrobacter Sp. AD26 and Use of This Strain in Bioremediation of Contaminated Soil. *J. Environ. Sci.* **2008**, *20* (10), 1226–1230. https://doi.org/10.1016/S1001-0742(08)62213-5.

(10) Diviesti, K.; Holz, R. C. Catalytic Biomaterials for Atrazine Degradation. *Catalysts* **2023**, *13* (1). https://doi.org/10.3390/catal13010140.

(11) Diviesti, K.; Russell-parks, G. A.; Trewyn, B. G.; Holz, R. C. Atrazine Degradation Using Immobilized Triazine Hydrolase from Arthrobacter Aurescens TC1 in Mesoporous Silica Nanomaterials. **2023**. https://doi.org/10.1021/acsenvironau.3c00036.

(12) Shapir, N.; Pedersen, C.; Gil, O.; Strong, L.; Seffernick, J.; Sadowsky, M. J.; Wackett, L. P. TrzN from Arthrobacter Aurescens TC1 Is a Zinc Amidohydrolase. *J. Bacteriol.* **2006**, *188* (16), 5859–5864. https://doi.org/10.1128/JB.00517-06.

(13) Tang, J.; Yao, J.; Pan, D.; Huang, J.; Wang, J.; Li, Q. X.; Dong, F.; Wu, X. Characterization and Catalytic Mechanism of a Direct Demethylsulfide Hydrolase for Catabolism of the Methylthiol-s-Triazine Prometryn. *J. Hazard. Mater.* **2023**, *446* (October 2022), 130708. https://doi.org/10.1016/j.jhazmat.2022.130708.

(14) Seffernick, J. L.; Reynolds, E.; Fedorov, A. A.; Fedorov, E.; Almo, S. C.; Sadowsky, M. J.; Wackett, L. P. X-Ray Structure and Mutational Analysis of the Atrazine Chlorohydrolase TrzN. *J. Biol. Chem.* **2010**, *285* (40), 30606–30614. https://doi.org/10.1074/jbc.M110.138677.

(15) Topp, E.; Mulbry, W. M.; Zhu, H.; Nour, S. M.; Cuppels, D. Characterization of S-Triazine Herbicide Metabolism by a Nocardioides Sp. Isolated from Agricultural Soils. *Appl. Environ. Microbiol.* **2000**, *66* (8), 3134–3141. https://doi.org/10.1128/AEM.66.8.3134-3141.2000.

(16) Seffernick, J. L.; Reynolds, E.; Fedorov, A. A.; Fedorov, E.; Almo, S. C.; Sadowsky, M. J.; Wackett, L. P. X-Ray Structure and Mutational Analysis of the Atrazine Chlorohydrolase TrzN. *J. Biol. Chem.* **2010**, *285* (40), 30606–30614. https://doi.org/10.1074/jbc.M110.138677.

(17) Meyer, A. H.; Penning, H.; Elsner, M. C and N Isotope Fractionation Suggests Similar Mechanisms of Microbial Atrazine Transformation despite Involvement of Different Enzymes (AtzA and TrzN). *Environ. Sci. Technol.* **2009**, *43* (21), 8079–8085. https://doi.org/10.1021/es9013618.

(18) Schürner, H. K. V.; Seffernick, J. L.; Grzybkowska, A.; Dybala-Defratyka, A.; Wackett, L. P.; Elsner, M. Characteristic Isotope Fractionation Patterns in S -Triazine Degradation Have Their Origin in Multiple Protonation Options in the S -Triazine Hydrolase Trzn. *Environ. Sci. Technol.* **2015**, *49* (6), 3490–3498. https://doi.org/10.1021/es5055385.

(19) Jackson, C. J.; Coppin, C. W.; Carr, P. D.; Aleksandrov, A.; Wilding, M.; Sugrue, E.; Ubels, J.; Paks, M.; Newman, J.; Peat, T. S.; Russell, R. J.; Field, M.; Weik, M.; Oakeshott, J. G.; Scott, C. 300-Fold Increase in Production of the Zn2+-Dependent Dechlorinase TrzN in Soluble Form via Apoenzyme Stabilization. *Appl. Environ. Microbiol.* **2014**, *80* (13), 4003–4011. https://doi.org/10.1128/AEM.00916-14.

(20) Yang, X.; Bennett, B.; Holz, R. C. Insights into the Catalytic Mechanism of a Bacterial Hydrolytic Dehalogenase That Degrades the Fungicide Chlorothalonil. *J. Biol. Chem.* **2019**, *294* (36), 13411–13420. https://doi.org/10.1074/jbc.RA119.009094.

(21) Rao, S.; Holz, R. C. Analyzing the Catalytic Mechanism of the Fe-Type Nitrile Hydratase from Comamonas Testosteroni Ni1. *Biochemistry* **2008**, *47* (46), 12057–12064. https://doi.org/10.1021/bi801623t.

(22) Salomaa, P.; Schaleger, L. L.; Long, F. A. Solvent Deuterium Isotope Effects on Acid-Base Equilibria. *Phys. Inorg. Chem.* **1964**, *86* (1).

(23) Bornhorst, A. J.; Falke, J. J. Purification of Proteins Using Plyhistidine Affintity Tags. *Methods Enzymol.* **2000**, *326*, 245–254.

(24) Segel, I. *Enzyme Kinetics. Behavior and Analysis of Rapid Equilibrium and Steady-State Enzyme Systems*; John Wiley & Sons, Ltd, 1993.

(25) Bzymek, K. P.; Holz, R. C. The Catalytic Role of Glutamate 151 in the Leucine Aminopeptidase from Aeromonas Proteolytica. *J. Biol. Chem.* **2004**, *279* (30), 31018–31025. https://doi.org/10.1074/jbc.M404035200.

(26) Venkatasubban, K. S.; Schowen, R. L. The Proton Inventory Technique. *Crit. Rev. Biochem. Mol. Biol.* **1984**, *17* (1), 1–44. https://doi.org/10.3109/10409238409110268.

(27) Elrod, J. P.; Hogg, J. L.; Quinn, D. M.; Venkatasubban, K. S.; Schowen, R. L. Protonic Reorganization and Substrate Structure in Catalysis by Serine Proteases. **1980**, *929* (1979), 3917–3922.

(28) J. Christensen, J.; D. Hansen, L.; M. Izatt, R. *Handbook of Proton Ionization Heats and Realted Thermodynamic Quantities*; Wiley, 1976.

(29) L. Stein, R. Transition-State Structural Features for the of Thermolysin-Catalyzed Hydrolysis N - (3-[2-Furyl]Acryloyl) -Gly-LeuNH2. *ACS* **1988**, No. 110.

(30) Izquierdo, M. C.; Stein, R. L. Mechanistic Studies of Thermolysin. *J. Am. Chem. Soc.* **1990**, *112* (16), 6054–6062. https://doi.org/10.1021/ja00172a023.

(31) Reactions, E.; Fernandez, P. L.; Murkin, A. S. Inverse Solvent Isotope Effects in Enzyme-Catalyzed Reactions. **2020**, No. 1, 1–18.

(32) Helmreich, E.; Cori, C. F. The Effects of Ph and Temperature on the Kinetics of the Phosphorylase. *Proc. Natl. Acad. Sci. United States* **1964**, *52*, 647–654. https://doi.org/10.1073/pnas.52.3.647.

(33) Davoodi, J.; Wakarchuk, W. W.; Campbell, R. L.; Carey, P. R.; Surewicz, W. K. Abnormally High PKa of an Active-Site Glutamic Acid Residue in Bacillus Circulans Xylanase: The Role of Electrostatic Interactions. *Eur. J. Biochem.* **1995**, *232* (3), 839–843. https://doi.org/10.1111/j.1432-1033.1995.0839a.x.

(34) Zhai, X.; Reinhardt, C. J.; Malabanan, M. M.; Amyes, T. L.; Richard, J. P. Enzyme Architecture: Amino Acid Side-Chains That Function to Optimize the Basicity of the Active Site Glutamate of Triosephosphate Isomerase. *J. Am. Chem. Soc.* **2018**, *140* (26), 8277–8286. https://doi.org/10.1021/jacs.8b04367.

(35) Dawson, R. M. C.; Elliott, D. C.; Elliott, W. H.; Jones, K. M. Data for Biochemical Research. No. BOOK, 654p. : ill.

(36) Holliday, G. L.; Mitchell, J. B. O.; Thornton, J. M. Understanding the Functional Roles of Amino Acid Residues in Enzyme Catalysis. *J. Mol. Biol.* **2009**, *390* (3), 560–577. https://doi.org/10.1016/j.jmb.2009.05.015.

(37) Fisher, Z.; Hernandez Prada, J. A.; Tu, C.; Duda, D.; Yoshioka, C.; An, H.; Govindasamy, L.; Silverman, D. N.; McKenna, R. Structural and Kinetic Characterization of Active-Site Histidine as a Proton Shuttle in Catalysis by Human Carbonic Anhydrase II. *Biochemistry* **2005**, *44* (4), 1097–1105. https://doi.org/10.1021/bi0480279.

(38) Edgcomb, S. P.; Murphy, K. P. Variability in the PKa of Histidine Side-Chains Correlates with Burial within Proteins. *Proteins Struct. Funct. Genet.* **2002**, *49* (1), 1–6. https://doi.org/10.1002/prot.10177.

(39) Perutz, M. F.; Gronenborn, A. M.; Clore, G. M.; Fogg, J. H.; Shih, D. T. b. The PKa Values of Two Histidine Residues in Human Haemoglobin, the Bohr Effect, and the Dipole Moments of α-Helices. *J. Mol. Biol.* **1985**, *183* (3), 491–498. https://doi.org/10.1016/0022-2836(85)90016-6.

(40) Riccardi, D.; Cui, Q. PKa Analysis for the Zinc-Bound Water in Human Carbonic Anhydrase II: Benchmark for "Multiscale" QM/MM Simulations and Mechanistic Implications. *J. Phys. Chem. A* **2007**, *111* (26), 5703–5711. https://doi.org/10.1021/jp070699w.

(41) Cleland, W. W. Use of Isotope Effects to Elucidate Enzyme Mechanisms. *CRC Crit. Rev. Biochem.* **1982**, *13* (4), 385–428. https://doi.org/10.3109/10409238209108715.

(42) Welsh, K. M.; Creighton, D. J.; Klinman, J. P. Transition-State Structure in the Yeast Alcohol Dehydrogenase Reaction: The Magnitude of Solvent and Secondary Hydrogen Isotope Effects1. *Biochemistry* **1980**, *19*.

(43) Yang, X.; Diviesti, K.; Miller, C.; Bennett, B.; Holz, R. C. Insights into the Catalytic Mechanism of the Chlorothalonil Dehalogenase from Pseudomonas Sp. CTN-3. *Front. Chem. Biol.* **2023**, *2* (February), 1–10. https://doi.org/10.3389/fchbi.2023.1105607.

(44) Nojima, H.; Ikai, A.; Oshima, T.; Noda, H. Reversible Thermal Unfolding of Thermostable Phosphoglycerate Kinase. Thermostability Associated with Mean Zero Enthalpy Change. *J. Mol. Biol.* **1977**, *116* (3), 429–442. https://doi.org/10.1016/0022-2836(77)90078-X.

(45) Razavi, B. S.; Blagodatskaya, E.; Kuzyakov, Y. Nonlinear Temperature Sensitivity of Enzyme Kinetics Explains Canceling Effect-A Case Study on Loamy Haplic Luvisol. *Front. Microbiol.* **2015**, *6* (OCT), 1–13. https://doi.org/10.3389/fmicb.2015.01126.

(46) Scopes, R. K. The Effect of Temperature on Enzymes Used in Diagnostics. *Clin. Chim. Acta* **1995**, *237* (1–2), 17–23. https://doi.org/10.1016/0009-8981(95)06060-Q.

CHAPTER 3

CATALYTIC BIOMATERIALS FOR ATRAZINE DEGRADATION†

Based on a paper published in *Catalyst*

Karla Diviesti [a] and Richard C. Holz [a,b]

3.1 Abstract

Triazine hydrolase from *Arthrobacter aurescens* TC1 (TrzN) was successfully immobilized in alginate beads (TrzN:alginate), alginate beads coated in chitosan (TrzN:chitosan) and tetramethylorthosilicate (TMOS) gels using the sol-gel method (TrzN:sol-gel) for the first time. TrzN:alginate and TrzN:chitosan hydrolyzed 50 µM of atrazine in 6 hours with negligible protein loss with an ~80% conversion rate. On the other hand, the TrzN:sol-gel biomaterial converted >95% of a 50 µM atrazine solution in an hour with negligible protein loss. Treatment of each of these biomaterials with trypsin confirmed the catalytic activity is due to the encapsulated enzyme and not surface bound TrzN. All three of the biomaterials showed potential for long-term storage and reuse with the only limitation arising from the loss of protein in storage buffer for the TrzN:alginate and TrzN:chitosan biomaterials, not denaturation of the encapsulated TrzN. TrzN:sol-gel stood out with ~100% activity being retained after 10 consecutive reactions. Additionally, the materials stayed active in methanol concentrations <10%, suggesting the ability to increase the solubility of atrazine with organic solvents. The structural integrity of the TrzN:alginate and TrzN:chitosan materials became limiting in extreme pH conditions while

---

[a]Department of Chemistry, Colorado School of Mines, Golden, CO 80401 U.S.A

[b]Quantitative Biosciences and Engineering Program, Colorado School of Mines, Golden, CO 80401 U.S.A

† This work was supported by the National Science Foundation (CHE-200241, RCH).

* See appendix A for permission and citation

TrzN:sol-gel outperformed WT TrzN. Overall, the TrzN:sol-gel biomaterial proved to serve as the best atrazine dichlorination biocatalyst. As sol-gels can be cast into any shape desired including pellets, which can be used in columns, the TrzN:sol-gel biomaterial provides a new avenue to design bioremediation methodologies for the removal of atrazine from the environment.

3.2 Introduction

Atrazine (2-chloro-4-ethylamino-6-isopropylamino-s-triazine) is a water-soluble herbicide that inhibits photosynthesis in targeted plants [1,2]. Originally patented in 1958, commercial use in the United States began in 1959 and today it's the second most used herbicide, with roughly 30,000 tons applied annually to sorghum, sugarcane, and corn crops [2-4]. Atrazine is persistent and mobile in aquatic environments, primarily through surface runoff where it enters groundwater via leaching [2,5]. Once in the watershed, atrazine has the potential to travel miles as it has a half-life of six months to several years, which is troublesome considering the potential downstream effects [2,6,7]. Atrazine toxicity impacts eukaryotes including, but not limited to, crustaceans, insects, mollusk, fish, amphibians, and reptiles [2,8-10]. The effects observed in aquatic eukaryotes after atrazine exposure raises concerns for the possible effects atrazine presents to humans, such as, lung and kidney diseases, cardiovascular damage, retinal degeneration, and cancer, which is why in 2003 the European union banned atrazine [1]. In the US, the EPA Endocrine Disruptor Testing Advisory committee recognized atrazine as an endocrine toxin in humans in 2000 and shortly thereafter, the agency for Toxic substances and Disease Registry (ATSDR) warned people in rural communities, near agricultural lands, are at an increased risk of atrazine exposure primarily through their drinking water [11].

Given the widespread use of atrazine and its toxicity to both aquatic environments and humans, its biodegradation and environmental clean-up has become a topic of significant importance [12].

Triazine hydrolase from *Arthrobacter aurescens* TC1 (TrzN, EC 3.8.1.8) has great potential as a biocatalyst for the bioremediation of atrazine because it irreversibly catalyzes the dichlorination of atrazine to its less toxic derivative hydroxyatrazine under physiological conditions (Figure 1) [13,14]. However, when utilizing enzymes for remediation purposes a major concern arises in one's ability to separate the enzyme from the reaction mixture [15]. A related issue involves aprotic solvent contaminants typically used for extraction, which degrades bacterial cells and decreases most free enzymes activity significantly. One way to overcome these challenges is through the immobilization of enzymes in optically transparent and sufficiently porous materials that permit small substrates access to the entrapped enzyme. Recent studies have demonstrated that encapsulated proteins retain their solution structure and native function while residing in a material, and nanoscopic confinement within materials stabilizes proteins against thermal and proteolytic degradation [16,17].

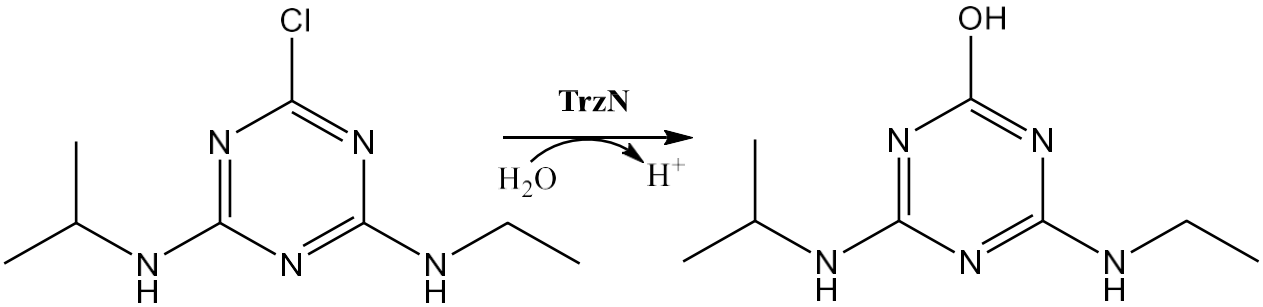

Figure 3.1. Hydrolysis of atrazine to hydroxyatrazine and chloride by TrzN.

Bioremediation methods utilizing TrzN have been limited to whole cells that naturally express TrzN or in one case, simply adding pure TrzN to a contaminated drainage ditch [12,18]. While these were somewhat successful in degrading atrazine, purified TrzN encapsulated in a material is necessary as a major issue is the difficulty in recovering whole cells or free enzymes from the environment as well as thermal and proteolytic degradation. Side reactions within a cell also pose problems. Herein we report the immobilization of purified TrzN within an alginate matrix in the absence and presence of a chitosan outer layer and also within silica glasses derived through the sol-gel process [16]. These novel biocatalytic materials are capable of the hydrolytic dichlorination of atrazine into its less toxic derivative hydroxyatrazine under mild conditions.

3.3 Results and Discussion

3.3.1 Encapsulation of TrzN

Wild-type (WT) TrzN was obtained by overexpression of the gene from *Arthrobacter aurescens* TC1 with an engineered N-terminal hexa-histidine (His_6) affinity tag in *E. coli* that was synthesized with optimized *E. coli* codon usage. Per liter of culture, ~9 mg of pure TrzN was obtained after a single purification step utilizing immobilized metal affinity chromatography (IMAC). SDS gel page reveals a single polypeptide band at ~51 kDa, consistent with previous studies. Purified TrzN was found to catalyze the hydrolysis of atrazine with a k_{cat} value of 4.0 ± 0.1 s^{-1} and a K_m value of 43 ± 3 μM in 50 mM HEPES buffer at pH 7.0 and 25°C using a continuous spectrophotometric assay that monitors atrazine degradation at 264 nm (ε_{264} = 3.5 $mM^{-1}cm^{-1}$). These values are consistent with those previously reported [19].

Having pure, catalytically active TrzN in hand allowed for its encapsulation into alginate beads (TrzN:alginate), TrzN:alginate coated with chitosan (TrzN:chitosan), and

tetramethylorthosilicate (TMOS) gels using the sol-gel method (TrzN:sol-gel). Analysis of both the buffer in which the biomaterials were stored and the buffer from all the washing steps using the Bradford assay indicated that on average >99 % of the TrzN present is encapsulated within the materials as < 0.5% of the TrzN used was present in either the wash or the storage buffer. Quantitating the reaction of atrazine with each of the TrzN biomaterials is difficult as the exact quantity of encapsulated enzyme is not known; however, assuming that ~99 % of the enzyme used was encapsulated ~99% of the solution activity was retained for TrzN:sol-gel at 25 ºC while TrzN:alginate and TrzN:chitosan retained approximately 28% and 30% respectively. Interestingly, the TrzN:alginate, TrzN:chitosan, and TrzN:sol-gel biomaterials readily react with atrazine (Figure 3.2) at 25 °C in 50 mM HEPES buffer, pH 7 with ~80 % and ~95%conversion of atrazine to the non-toxic hydroxyatrazine product over a 6-hr reaction period for TrzN:alginate and TrzN:chitosan respectively. While 100% degradation of atrazine by TrzN:sol-gel was observed after only 1-hr, a six-fold improvement compared to the alginate biomaterials. These data indicates that each of these biomolecular nanocomposites display the expected enzymatic properties including substrate recognition as TrzN in solution.

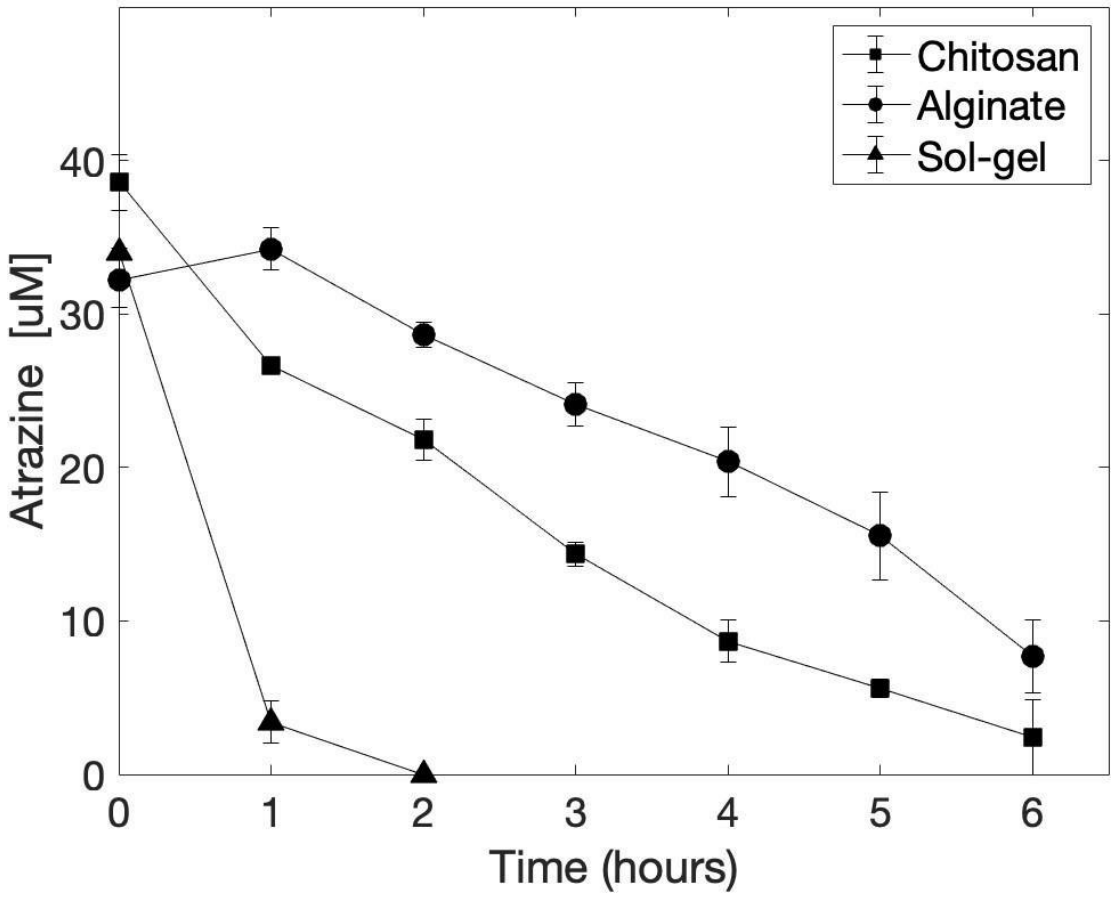

Figure 3.2. Time course for the hydrolysis of atrazine using TrzN:alginate, TrzN:chitosan, and TrzN:sol–gel.

Scanning electron microscope (SEM) images of each of these biomaterials reveal the size of the TrzN:alginate and TrzN:chitosan beads as well as the porous nature of the surfaces, confirming solution and substrate access to the encapsulated enzyme (Figure 3). The SEM data of TrzN:alginate (Figure 3A) and TrzN:chitosan (Figure 3B) reveal that the average bead size ranged from 1 to 2 mm in diameter. The chitosan coating is clearly visible in the SEM (Figure 3B) as TrzN:chitosan shows up as dark in color when the data are collected with an electron detector, which detects back-scattered electrons. Conversely, the TrzN:alginate, which has higher atomic number atoms such as Ca^{2+} on its surface, appear lighter in color in the SEM. Zooming in by 500X on the TrzN:chitosan and TrzN:sol-gel biomaterials reveal the porous nature of these materials consistent in the observed kinetics of substrate turnover for the TrzN:alginate, TrzN:chitosan, and TrzN:sol-gel biomaterials, which appear to be governed by mass transport of the substrate through the porous materials to the enzyme active site and product release.

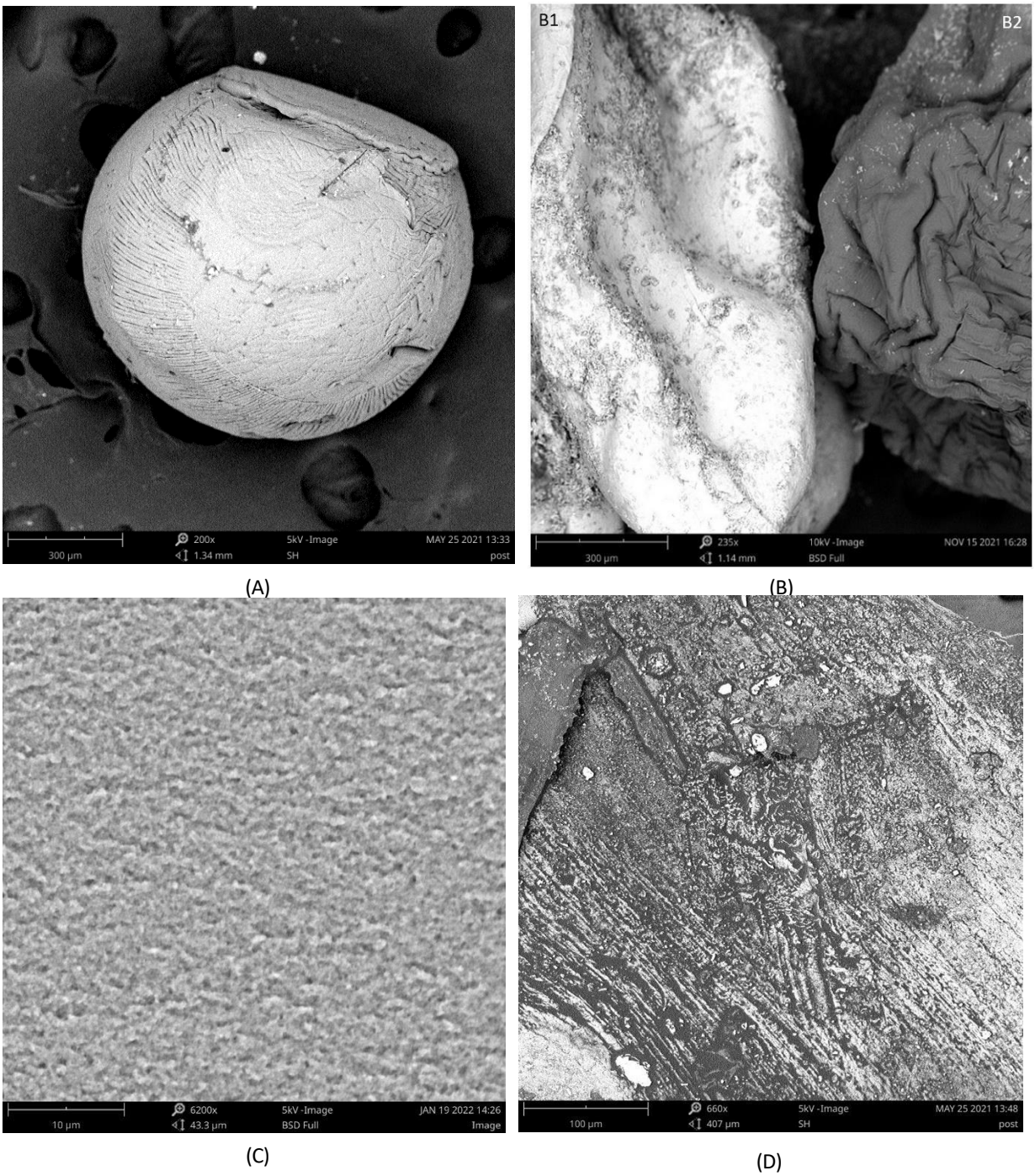

(A) (B)

(C) (D)

Figure 3.3. (A) SEM image of TrzN:alginate biomaterial at 200× magnification. The scale bar is 300 µm. (B) SEM images of TrzN:alginate (left, B1) and TrzN:chitosan (right, B2) biomaterials at 235× magnification. The scale bar is 300 µm. TrzN:alginate and TrzN:chitosan averaged between 1 and 2 mm in diameter. (C) SEM image of the TrzN:sol–gel biomaterial at 510× magnification. The scale bar is 100 µm. (D) SEM image of a cross-sectional view of the dried TrzN:alginate biomaterial at 660× magnification. The scale bar is 100 µm.

3.3.2 Proteolytic Digestion of WT TrzN and the TrzN:alginate, TrzN:chitosan, and TrzN:sol-gel Biomaterials

To ensure that the substrate has access to the fully immobilized enzyme and not enzyme that is simply adhered to the surface, each of the biomaterials were treated with trypsin to proteolytically digest all surface accessible protein (Figure 4). TrzN:alginate and TrzN:chitosan was digested with trypsin for 30 min at 35 °C with constant shaking. The TrzN:alginate and TrzN:chitosan biomaterials retained 75 and 80 ± 5% of their original activity compared to a TrzN enzyme solution sample, which retained 55 ± 5% of its activity. On the other hand, the TrzN:sol-gel biomaterial retained 85 ± 5% of its activity even after 18-hrs in the presence of trypsin at 35 °C compared to a TrzN enzyme control sample, which only retained 45 ± 5% of its activity over the same time period, while the TrzN:alginate and TrzN:chitosan biomaterials exhibited no detectable activity at 18-hrs. These data indicate that substrate has access to the TrzN enzyme entrapped in the interior of each biomaterial, which is an active catalyst but protected from proteolytic digestion. Even though the TrzN:sol-gel and TrzN:chitosan provided comparable protection against proteolytic cleavage over 30 min, the TrzN:sol-gel biomaterial was much more robust as it retained its activity after 18 hrs while TrzN:chitosan. These data also indicate that surface bound enzyme is hydrolyzed, but interior TrzN is protected resulting in a catalyst that is more robust that the free enzyme.

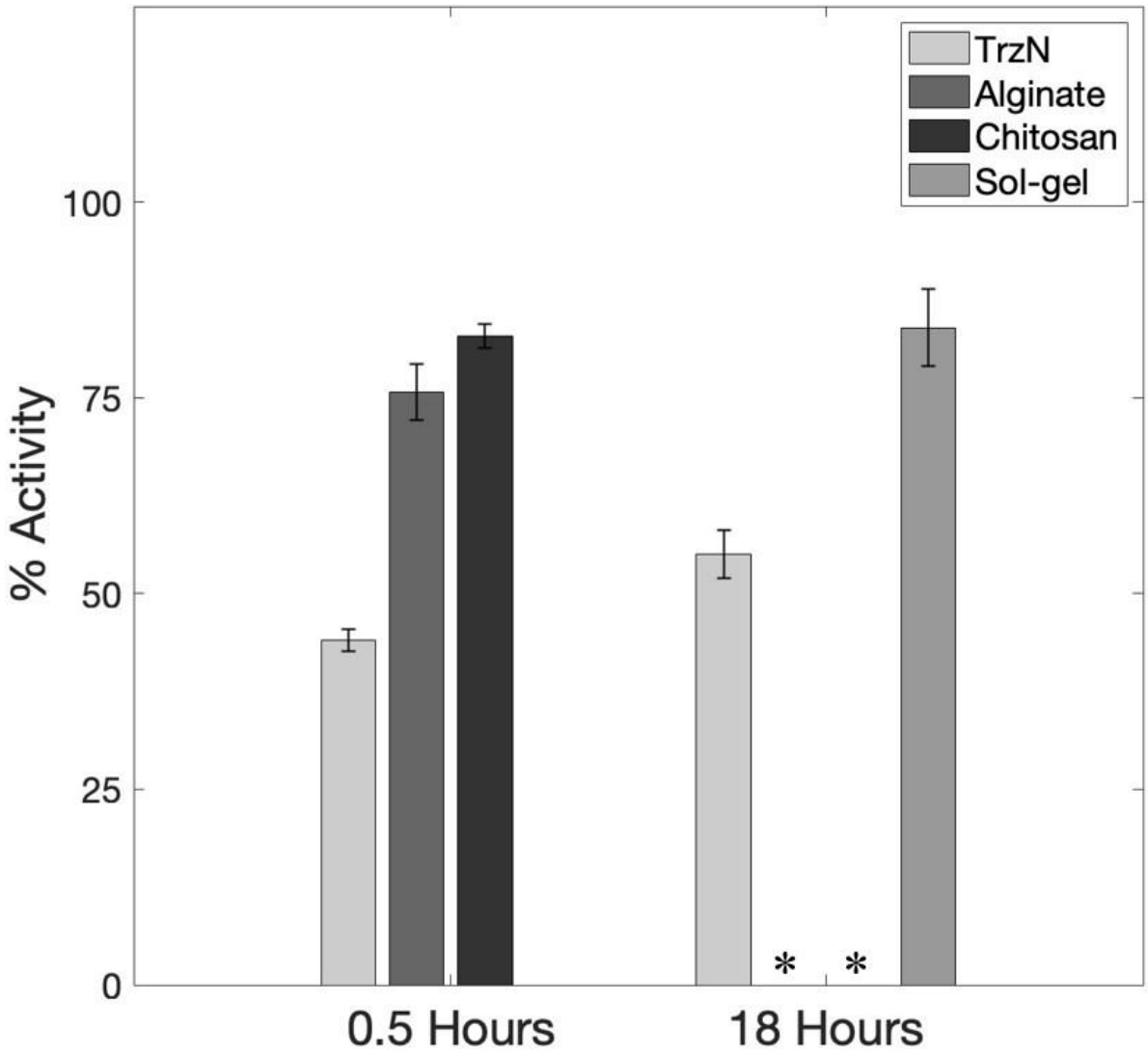

Figure 3.4. Residual activity of soluble TrzN, TrzN:sol–gel, TrzN:alginate, and TrzN:chitosan biomaterials proteolytically digested with trypsin. The soluble TrzN and the biomaterials were incubated at a 2:1 ratio of trypsin:TrzN at 35 °C. TrzN:alginate and TrzN:chitosan were digested for 30 min, while TrzN:sol–gel was digested for 18 h. A soluble TrzN control was digested for both 0.5 and 18 h, as 18 h is the recommended digestion time for complete protein degradation by trypsin digestion. * indicates that there was no detectable activity.

3.3.3 Thermostability of WT TrzN and the TrzN:alginate, TrzN:chitosan, and TrzN:sol-gel Biomaterials

The thermostability of WT TrzN and the TrzN:sol-gel, TrzN:alginate, and TrzN:chitosan biomaterials, was evaluated over a temperature range of 50 – 80 °C (Figure 5). Both WT TrzN and each of the TrzN biomaterials are very thermally stable at 50 °C over a 30 min incubation time with WT TrzN exhibiting a k_{cat} of 3.8 ± 0.1 s^{-1}, which is identical to that observed at 25 °C. As the temperature was increased to 80 °C, the k_{cat} value for WT TrzN increased to 5.0 ± 0.2 s^{-1} while the TrzN:alginate and TrzN:sol-gel biomaterials were inactive. On the other hand, the TrzN:chitosan biomaterial retained ~30% of its original activity at 80 °C. ICP-AES analysis of the reaction buffers showed a significantly higher concentration of Ca^{2+} ions in the TrzN:alginate reaction buffer compared to those of TrzN:chitosan. These data suggest the polymer structure of the alginate tightened [20], resulting in less substrate accessibility to the encapsulated enzyme. Little or no Ca^{2+} ions in the chitosan reaction buffer indicates the chitosan was continuing to act as a barrier to protect the alginate matrix, resulting in increased activity in the chitosan coated biomaterial vs the alginate [21]. Temperature has a direct relationship to internal pore structure of alginate beads and previous work reported a significant loss of moisture occurring during heat shock of alginate beads which created a dense porous structure [20]. Therefore, the addition of a chitosan coating around the alginate matrix retains the integrity of the alginate material, resulting in increased thermostability [21].

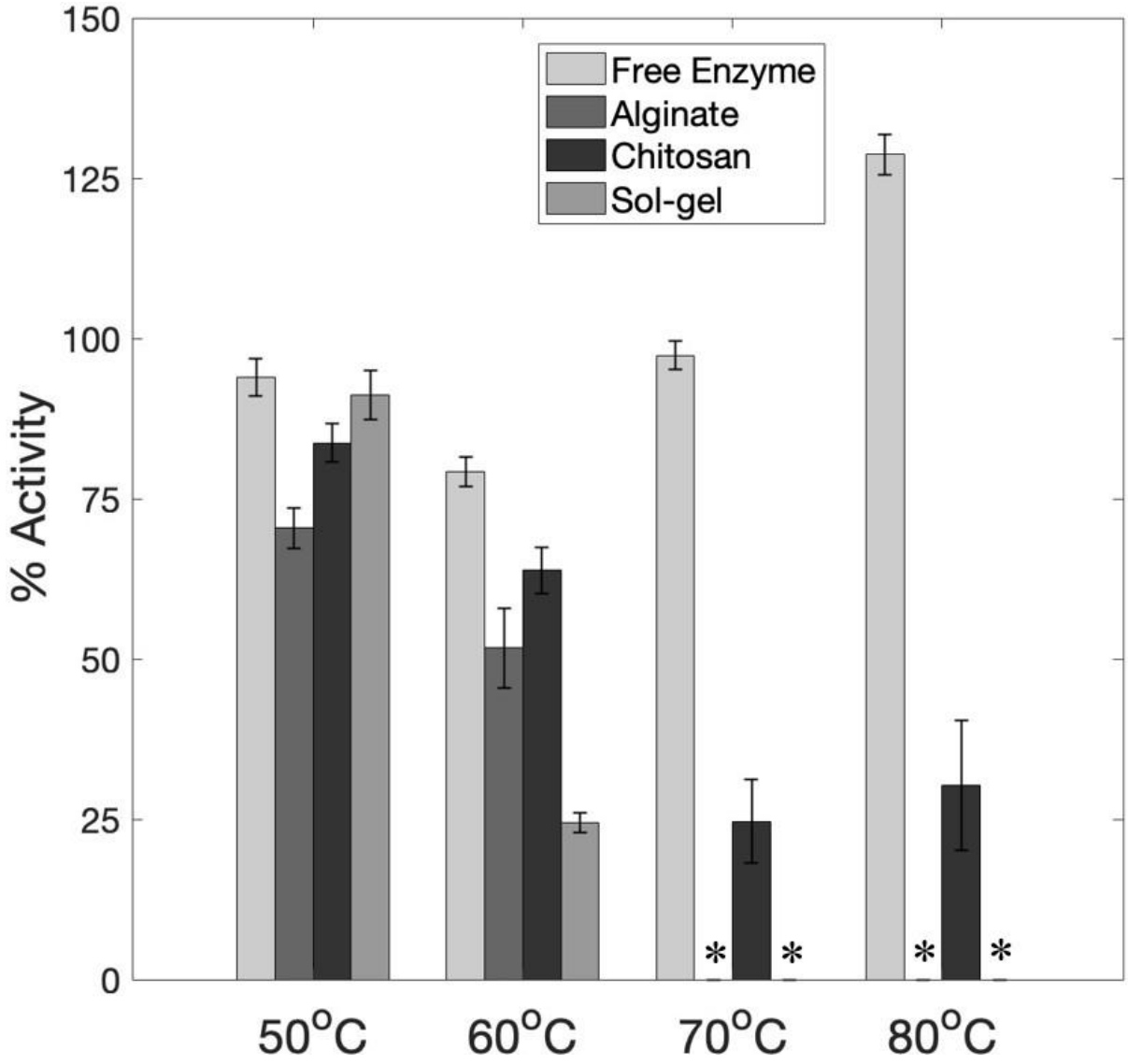

Figure 3.5. Thermostabilities of soluble TrzN, TrzN:alginate, and TrzN:chitosan biomaterials. The residual activities of the soluble enzyme and each biomaterial were recorded after a 30 min heat shock in a 50, 60, 70, and 80 °C water bath followed by measuring the dichlorination of atrazine at 25 °C for 6 h. * indicates that there was no detectable activity

3.3.4 Reusability And Long-Term Stability Of The Trzn:biomaterials

For commercial applications, a biocatalyst must be reusable and have long-term stability. With this is mind, we sought to investigate whether each of the biomaterials could be recycled in subsequent reactions (Figure 6). After every use, each of the TrzN biomaterials were thoroughly washed with HEPES buffer, pH 7.0 to remove residual atrazine and hydroxyatrazine then stored in buffer until they were submitted to the same reaction conditions. The conversion of atrazine to hydroxyatrazine decreases over a six-week period for each of the TrzN biomaterials with ~65% of the initial activity remaining for TrzN:sol-gel but <20% for TrzN:chitosan and no observable activity for the TrzN:alginate biomaterial. Remarkably, soluble TrzN can also be stored at 4 °C in buffer over a six-week period without significant loss of activity (Figure 6). The observed loss in activity for the TrzN:alginate biomaterial compared to WT TrzN, which lost ~70% of its original activity is due to enzyme loss during extended storage in an aqueous solution. Similarly, the TrzN:chitosan biomaterial lost ~55%. As previously reported, alginate beads tend to be "leaky" and while chitosan coating helps to decrease enzyme loss it does not eliminate it [22]. The TrzN:sol-gel biomaterial also lost enzyme over the course of the six-week experiment but to a significantly lesser extent than either the TrzN:alginate or TrzN:chitosan biomaterials. These data indicates that the enzyme that remained in the biomaterials stayed active and the loss in activity is due to the loss of immobilized enzyme not enzymatic denaturation within the matrix or product build up within the matrix hindering the diffusivity of the substrate to the enzyme [23]. The cyclical reusability of TrzN:sol-gel over ten reactions revealed no loss in activity adding to the conclusion that enzyme loss in extended storage was the cause of activity loss. Overall, the TrzN:sol-gel biomaterial performed the best and encapsulation of TrzN in a sol-gel

provides a matrix for the storage of TrzN that can be recycled, stored, and reused for extended periods of time.

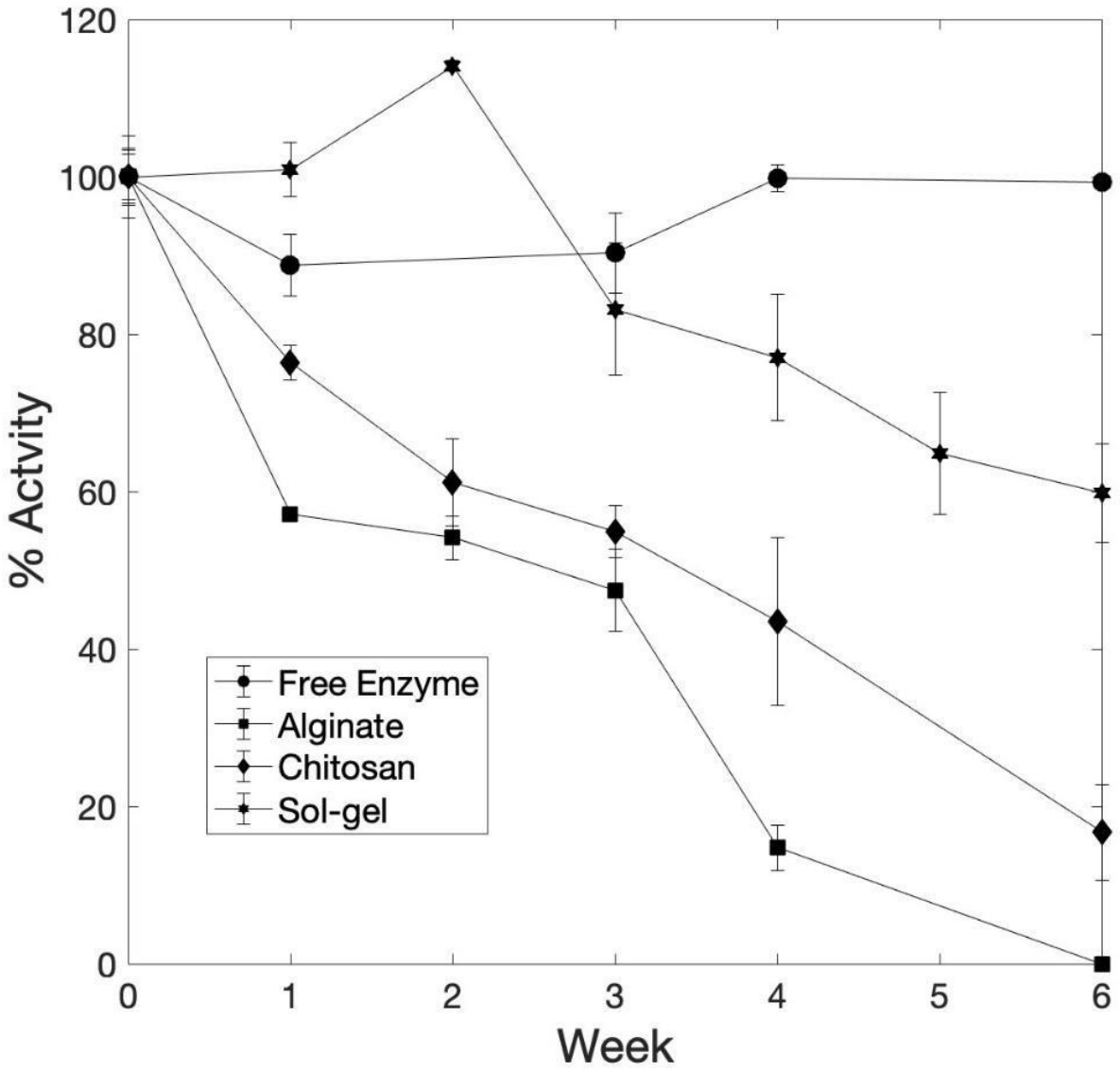

Figure 3.6. Long-term stabilities of soluble TrzN, TrzN:alginate, TrzN:chitosan, and TrzN:sol–gel calculated over the 6-week experiment. The k_{cat} value of soluble TrzN was evaluated with 150 μM atrazine at 25 °C stored in 0.1 M sodium phosphate buffer pH 7.0 at 4 °C until the following week. The TrzN:alginate, TrzN:chitosan, and TrzN:sol–gel biomaterials were evaluated weekly for the degradation of 50 mM atrazine in 50 mM HEPES, pH 7.0. The biomaterials were washed and stored at 4 °C in 50 mM HEPES pH 7.0 for 1 week before repeating the experiment.

3.3.5 Stability Of The WT Trzn And Trzn:Biomaterials In An Organic Co-Solvent

Atrazine presents itself traditionally in watersheds containing negligible amounts of organic solvents [24]; however, at higher concentrations atrazine solubility becomes problematic and requires organic solvents. Thus, understanding the biomaterial's function in solutions with organic solvents is important in exploring their potential as bioremediation catalysts as enzymes typically denature when exposed to organic solvents [16]. The activity of the TrzN:alginate, TrzN:chitosan, and TrzN:sol-gel biomaterials were examined in 5:95, 10:90, and 20:80 MeOH:water solvent mixtures (Figure 7). At 5:95 and 10:90 MeOH:water solution, each of the biomaterials retained at least 70% of the WT TrzN enzyme but all exhibited a significant decrease in activity at a MeOH:water mixture of 20:80 with the TrzN:alginate biomaterial performing the worst with only 10% residual activity. At higher methanol concentrations, both the TrzN:alginate and TrzN:chitosan biomaterials lost all activity, however, the TrzN:sol-gel biomaterial retained ~5% of its residual activity in a 70:30 MeOH:water solution. For comparison purposes, WT TrzN exhibits ~75% of its native enzyme's activity in 20:80 MeOH:water mixtures. The poorer performance in organic solvents for the TrzN:alginate and TrzN:chitosan biomaterials is due to increased Ca^{2+} ion concentration in the reaction solution, determined via ICP-AES. Previously, it was reported that ethanol in concentrations >15% reduces the hydrodynamic volume of alginate beads resulting in a tightening of the polymer chains, which restricts substrate access to an encapsulated enzyme [25]. Therefore, of the three biomaterials tested, sol-gel encapsulation clearly performs the best in stabilizing against increasing protic solvents.

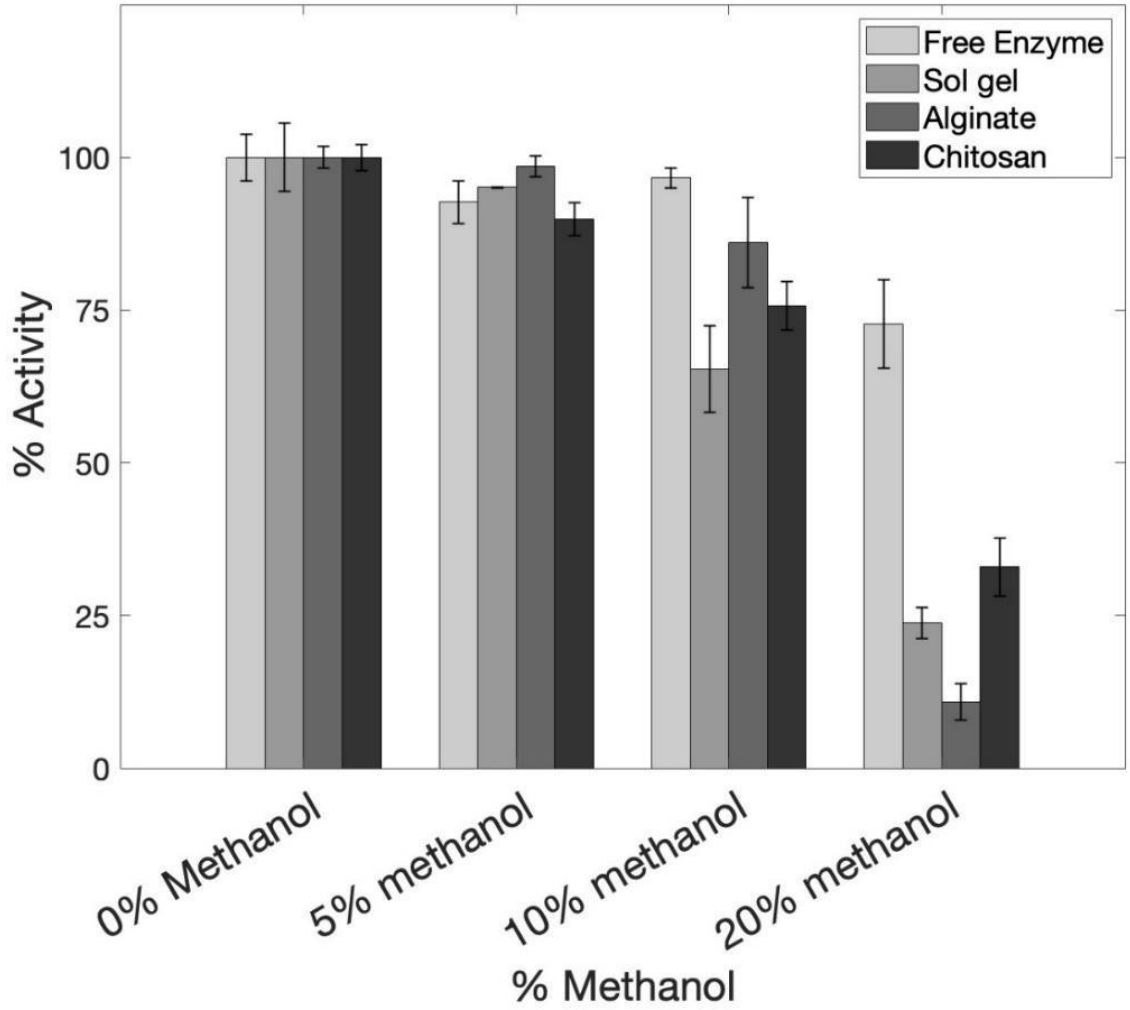

Figure 3.7. Activities of soluble TrzN, TrzN:alginate, TrzN:chitosan, and TrzN:sol–gel for the conversion of 50 mM atrazine to hydroxyaztraine in 5:95, 10:90, and 20:80 MeOH:water (*v*/*v*) co-solvent solutions.

3.3.6 Stability of the WT TrzN and TrzN:biomaterials at Nonphysiological pH Values

Typically, when using biomaterials in aqueous bioremediation strategies, the engineered material is expected to perform in native watershed conditions. Although watersheds typically present a pH at ~7, outside influences such as polluted runoff can cause the pH to fluctuate outside of the neutral range [26]. With this in mind, it is important to investigate the activity of TrzN:alginate, TrzN:chitosan, and TrzN:sol-gel biomaterials in pH conditions at both higher (pH

9.0) and lower (pH 4.0) values than physiological pH (Figure 8). At pH 4.0, (50 mM citric acid buffer), both the TrzN:alginate and TrzN:chitosan biomaterials exhibited no detectable activity while the TrzN:sol-gel biomaterial exhibited ~45% of its residual activity. At pH 9.0, (50 mM glycine buffer) TrzN:alginate again exhibited no detectable activity while the TrzN:chitosan and TrzN:sol-gel biomaterials retained ~20 and ~95% of their residual activities, respectively. For comparison purposes, WT TrzN exhibits ~25 and ~45% of its residual activities at pH 4.0 and 9.0, respectively. Therefore, sol-gel encapsulation clearly affords significant stabilization against both increased and decreased proton ion concentrations likely due to the strong electrostatic interaction between the silica sol and TrzN [27,28]

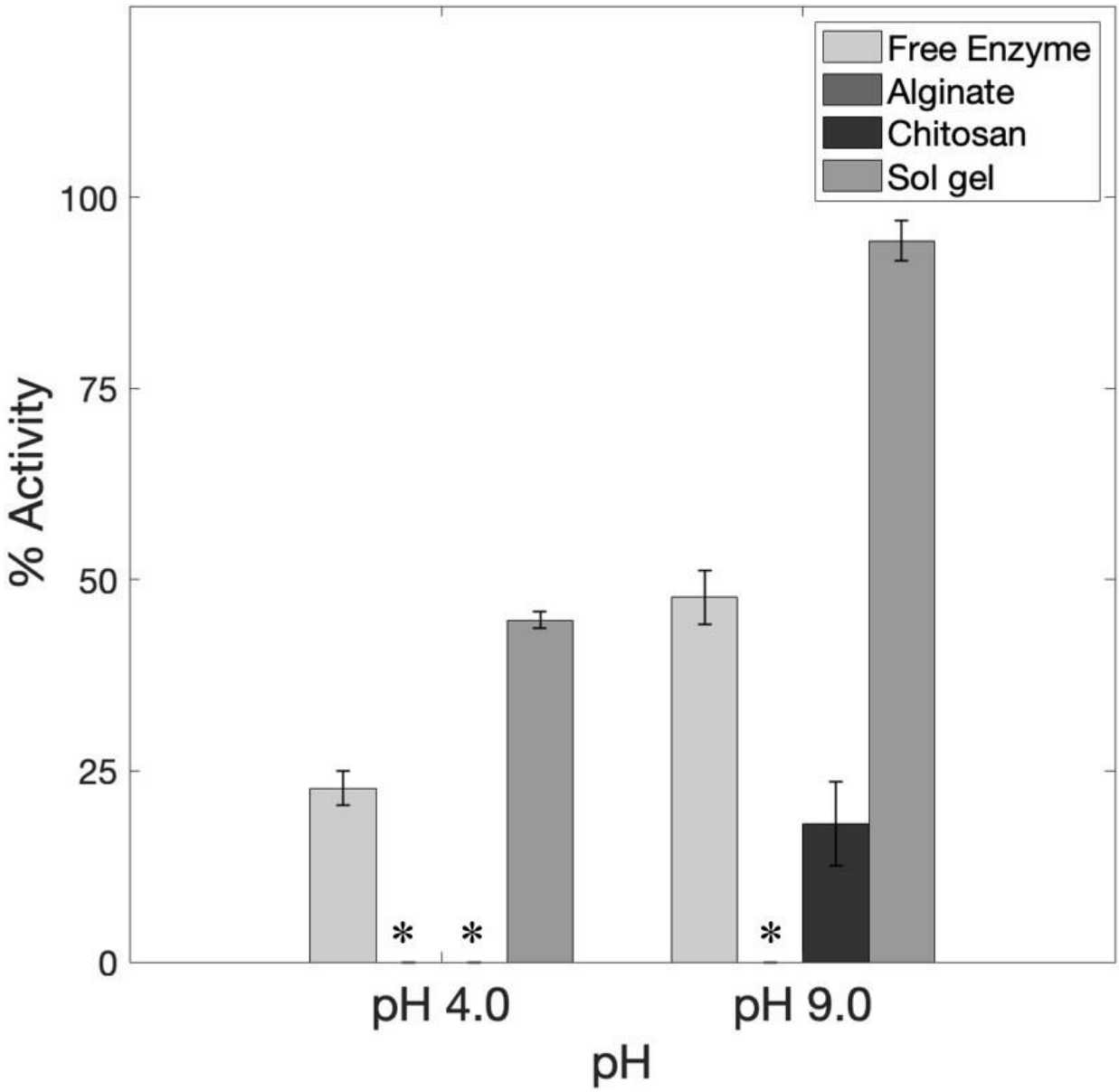

Figure 3.8. Activities of soluble TrzN, TrzN:alginate, and TrzN:chitosan for the conversion of 50 mM atrazine to hydroxyatrazine in 50 mM citric acid pH 4.0 buffer and 50 mM glycine buffer pH 9.0. * indicates that there was no detectable activity.

3.4 Materials and Methods

3.4.1 Materials

Sodium alginate was purchased from Spectrum Chemical MFG corp. Chitosan, Atrazine, Tetramethyl orthosilicate (TMOS, ≥ 99%), and Type I Trypsin from bovine pancreas were both purchased from Sigma-Aldrich. All reagents were of the highest purity available and received without further purification.

3.4.2 Expression And Purification Of Trzn

The gene from *Arthrobacter aurescens* TC1 that encodes for TrzN with the D38N, L131P, and A159V mutations was synthesized with optimized *E. coli* codon usage that includes a polyhistidine (His_6) affinity tag engineered onto the N-terminus between NdeI and XhoI restriction site of the kanamycin resistant pET28a(+) to create the TrzN/pET28a(+) plasmid. The TrzN/pET28a(+) plasmid was transformed into *E. coli* BL21(DE3) competent cells (Stratagene) for expression. A 100 mL LB-Miller starter culture was inoculated from a single colony with 50 µg/mL of kanamycin. A 9 L culture was inoculated from this starter culture using 10 mL/liter supplemented with 5 µM isopropyl ß-d-1-thiogalactopyranoside (IPTG) and grown at 37°C for 48 h [19]. Cells were harvested by centrifugation at 7000 rpm 4°C, for 15 min. The cells were resuspended at 2 mL per gram of buffer A (50 mM NaH_2PO_4, 500 mM NaCl, 10 mM imidazole, pH 7.5) then lysed by sonication on ice in three 10 min (30s on, 45s off) intervals using a 21W Misonex sonicator 3000. Cell debris was removed by centrifugation at 17,500 rpm, 4°C, for 40 min. The protein was purified by immobilized metal affinity chromatography (IMAC) using Ni-NTA (nickel-nitrilotriacetic acid) Superflow Cartridges (Qiagen). The column was equilibrated with buffer A and the crude protein extract was loaded onto the IMAC column. Unbound protein

was eluted with 15 column volumes (CV) of buffer A at a flow rate of 2 mL/min. Elution of TrzN was initiated with 15 CV of 3% buffer B (buffer A with 500 mM imidazole). Elution finished with a linear gradient (3-100%) of buffer B over 20 CVs at a flow rate of 2 mL/min. Peak fractions were pooled and resuspended in 50 mM HEPES pH 7.5 and concentrated with an Amicon Ultra-15 centrifugal filter device with a molecular weight cutoff (MWCO) of 30,000 (Millipore). SDS gel page reveals a single polypeptide band at ~51 kDa, consistent with previous studies. The protein concentration was determined by UV-Vis absorbance at 280 nm (61,670 Molar Absorptivity) and with a Coomassie (Bradford) Protein Assay Kit (Thermo Scientific). Expression of TrzN and purification using immobilized metal affinity chromatography (IMAC) resulted in ~10 mg/L of soluble TrzN enzyme [19,13].

3.4.3 Kinetic Activity Assay

Hydrolysis of atrazine by TrzN was quantified spectrophotometrically by continuously monitoring the decrease in absorbance at 264 nm (ε_{264} = 3.5 $mM^{-1}cm^{-1}$) that accompanies atrazine dichlorination [29]. This region contains no detectable product absorption. The activity of purified TrzN was determined by measuring the hydrolysis of a 150 µM atrazine solution in 0.1 M sodium phosphate buffer, pH 7.0 [19]. Assays were performed in a 1 mL quartz cuvette in triplicate on an Agilent 8453 UV-visible spectrophotometer. One unit of enzyme activity was defined as the amount of enzyme that catalyzed the hydrolysis of 1 µmol of atrazine per minute at 35°C. Plots of the initial rate of hydrolysis of various concentrations of atrazine were fit to the Michaelis-Menten equation, which provided a k_{cat} of 3.97± 0.14 s^{-1} and a k_m value of 43.1 ± 2.9 µM, similar to those previously reported [19].

3.4.4 Immobilization Of Trzn In A Sol-Gel And Alginate Beads In The Absence And Presence Of A Chitosan Coating

Sodium alginate powder was added to 50 mM sodium phosphate buffer to 1% (w/v) and heated to 50 °C with vigorous shaking. TrzN (5 mg) was added to 4.5 mL of the cooled alginate solution with gentle stirring and transferred to a 5 mL syringe with a 16 G needle. The TrzN:alginate mixture was dripped into 50 mL of a 1 M $CaCl_2$ solution with stirring (200 rpm) at 4°C. After ~2 hrs, a 1 mL sample was removed and a Coomassie (Bradford) Protein Assay Kit (Thermo Scientific) was used to determine the amount of TrzN encapsulated into alginate beads. Next, 150 mL of nanopure water was added and the beads were stirred for another 30 minutes to stop the gelation process. The resulting beads were then filtered and washed three times with 20 mL of nanopure water. The beads air dried for ~30 minutes and then stored overnight at 4°C in 5 mL of 50 mM HEPES buffer, pH 7.0.

TrzN:alginate beads were also coated in chitosan using a previously published procedure [30]. Briefly, a chitosan solution was prepared by dissolving 0.8 g of chitosan (Sigma-Aldrich) in 90 mL of nanopure water after which 200 µl of glacial acetic acid (Fisher) was added to facilitate the dissolution. The solution was filtered, and the volume increased to 100 mL with nanopure water providing a final concentration of 0.8% (w/v). The pH was adjusted to 5.6 and TrzN:alginate beads were placed in 50 mL of this chitosan solution and stirred at 200 rpm for ~45 minutes. After the coating process, the TrzN:chitosan beads were washed three times with 20 ml of nanopure water and dried in air for 30 minutes. The beads were stored overnight at 4°C in 5 mL of 50 mM HEPES buffer, pH 7.

The sol consisted of 1.57 mL of TMOS, 0.350 mL nanopure (18 Ω) H_2O, and 0.011 mL of 0.040 M HCl as previously described [16]. The mixture was sonicated on ice for 30 minute,

and then left on ice for ~1 hour prior to the addition of TrzN. An equal volume of TMOS sol (0.100 mL) was mixed with an equal volume of TrzN (2.5 mg) in 50 mM Tris-HCl, pH 7.5. The mixture was left on ice until gelation occurred creating TrzN:sol-gel monoliths. The monoliths were washed three times with 0.400 mL of 50 mM Tris-HCl, pH 7.5 (sol-gel buffer) and stored at 4°C in 0.400 mL of the same buffer. The next day, the aged monoliths were crushed with a metal spatula to produce a heterogenous material and then washed three times with 0.400 mL of the sol-gel buffer. The wash and storage buffers were collected and tested for protein loss using the Coomassie (Bradford) Protein Assay kit.

3.4.5 Kinetic Characterization Of The Trzn:Alginate, Trzn:Chitosan, And Trzn:Sol-Gel Biomaterials

The activity of the TrzN:alginate, TrzN:chitosan, and TrzN:sol-gel biomaterials was determined by measuring the hydrolysis of atrazine by continuously monitoring the decrease in absorbance at 264 nm (ε_{264} = 3.5 $mM^{-1}cm^{-1}$) that accompanies atrazine dichlorination [29]. A solution of 50 µM atrazine in 50 mM HEPES pH 7.0 at 25 or 35 °C was reacted with TrzN:alginate, TrzN:chitosan, and TrzN:sol-gel with constant stirring at 200 rpm. Aliquots of the reaction mixture (0.3 mL) were taken at fixed time intervals and the hydrolysis of atrazine analyzed. The specific activity (U/mg) of each biomaterial was calculated from the reaction rate (µmol/L/min), the amount of TrzN immobilized, and the volume of the reaction. The concentration of atrazine produced was determined using standard curves of absorbance versus known atrazine concentrations.

3.4.6 Proteolytic Digestion Of Soluble Trzn, Trzn:Alginate, Trzn:Chitosan, And Trzn:Sol- Gel

Trypsin digestion of soluble TrzN (0.007 mg), TrzN:alginate beads (5 mg of TrzN), TrzN:chitosan beads (5 mg TrzN), and TrzN:sol-gel (2.5 mg TrzN) was performed at a ratio of 2:1 trypsin to TrzN in 50 mM Tris-HCl and 1 mM $CaCl_2$ pH 7.6 (trypsin reaction buffer). TrzN:alginate and TrzN:chitosan was reacted for 30 min at 25°C with constant stirring at 200 rpm while TrzN:sol-gel was reacted for 18 hours at 35°C with constant stirring at 200 rpm. Along with the digested biomaterial samples, a control utilizing TrzN in trypsin reaction buffer was also incubated in an identical fashion. Following digestion, TrzN:alginate and TrzN:chitosan samples were filtered and washed three times with 20 mL of nanopure water while TrzN:sol-gel samples were filtered and washed three times with 0.4 mL sol-gel buffer to remove trypsin and digestion products. The biomaterials and digested TrzN were assayed for catalytic activity using standard assay conditions.

3.4.7 Recycling Experiments For Trzn:Alginate, Trzn:Chitosan And Trzn:Sol-Gel

A 20 mL solution of 50 µM atrazine in 50 mM HEPES, pH 7.0 at 25 °C and reacted with TrzN:alginate or TrzN:chitosan for 6 hrs after which an aliquot (0.3 mL) was removed and the amount of atrazine dichlorination determined. The product mixture was then decanted, and the resulting biomaterial washed with 20 mL nanopure water. A 1 mL aliquot was taken of the reaction buffer to test for protein loss from the biomaterial using the Coomassie (Bradford) Protein Assay Kit (Thermo Scientific). The TrzN:alginate and TrzN:chitosan beads were stored at 4 °C in 5 mL of 50 mM HEPES pH 7.0 and reused on a weekly basis for six weeks.

A 5 mL solution of 50 µM atrazine in 50 mM HEPES pH 7.0 at 35°C was reacted with TrzN:sol-gel for 1 hour after which the solution was centrifuged at 4000 rpm for 5 minutes. An aliquot (0.3 mL) of the supernatant was removed and the amount of atrazine dichlorination determined. A 1 mL aliquot of the supernatant was also taken to test for protein loss from the biomaterial using the Coomassie (Bradford) Protein Assay Kit (Thermo Scientific). The TrzN:sol-gel biomaterial was washed three times with 0.4 mL of sol-gel buffer and stored at 4°C in 0.4 mL of sol-gel buffer and reused on a weekly basis for six weeks. The reaction was also repeated on a different TrzN:sol-gel biomaterial 10 times over a 1 Hr time period as described above resulting in 10 separate cycles with the same sample of TrzN:sol-gel biomaterial.

3.4.8 Activity Of Soluble And Immobilized Trzn In Organic Co-Solvents

The activity of soluble TrzN with 5, 10, and 20% (v/v) methanol as the organic co-solvent toward atrazine was measured spectrophotometrically at 25°C as described above. Each measurement was taken in triplicate. The degradation of atrazine using TrzN:Alginate, TrzN:Chitosan, and TrzN:sol-gel with organic co-solvents at 5, 10, and 20% (v/v) was carried out in their respective reaction conditions described previously. Aliquots, 1 mL, were taken at the start and end of the reaction and analyzed spectrophotometrically as described above.

3.4.9 Activity Of Soluble And Immobilized Trzn At Varying Ph Values

The activity of soluble and encapsulated TrzN in 50 mM citric acid, pH 4.0 and 50 mM glycine buffer, pH 9.0, towards atrazine was measured spectrophotometrically as described above. Each measurement was taken in triplicate. Samples, 1.5 mL, were taken at the end of the

reactions and tested for protein loss using Coomassie (Bradford) Protein Assay Kit (Thermo Scientific) and sent for ICP-MS analysis.

3.4.10 Thermostability Of Soluble And Immobilized Trzn

The thermostability of TrzN, TrzN:alginate, and TrzN:chitosan was determined incubating each for 30 min at 50, 60, 70, and 80 °C. TrzN:alginate and TrzN:chitosan materials were suspended in 5 mL of 50 mM HEPES pH 7.0 and after the incubation period, a 1.5mL sample was collected for ICP-MS and protein analysis using the Coomassie (Bradford) Protein Assay Kit (Thermo Scientific). Residual activity of the free enzyme and encapsulated TrzN was determined spectrophotometrically. The thermostability of the TrzN:sol-gel biomaterial was evaluated over a temperature range of 50-80°C with incubation times of 0, 30, 60, 180, 300, 420, and 600 minutes. After the incubation period was complete, the residual activity was determined spectrophotometrically.

3.5 Conclusions

In summary, this work presents the first immobilization of TrzN in any biomaterial. Alginate beads and sol-gels was chosen as the first biomaterials to test due to their well-documented properties. Table 1 summarizes the results of the biomaterials tested. Chitosan coated alginate was also tested as a potential solution to the material limitations that can accompany alginate matrices. The resulting biomaterials (TrzN:alginate, TrzN:chitosan, and TrzN:sol-gel) all exhibited catalytic activity toward atrazine protected and the WT enzyme from proteolytic digestion. When evaluating reusability, the TrzN:sol-gel material remained active for a full 6 weeks and was clearly superior to the other biomaterials tested. Moreover, the TrzN:sol-

gel could be reused multiple times making it a good candidate for bioremediation strategies. Similarly, the TrzN:sol-gel was the superior biomaterial for use in organic solvents and non-physiological pH values as it retained ~25% activity in a 20:80 MeOH:Water mixture and was the only biomaterial to retain significant activity at both high and low pH values. Therefore, the TrzN:sol-gel biomaterial proved to exhibit the best overall profile making it the most effective biocatalyst for the dichlorination of atrazine into its less toxic derivative hydroxyartrazine. The beauty of the TrzN:sol-gel biocatalytic material as a bioremediation tool resides in the fact that the TrzN:sol-gel materials can be cast into any shape desired including pellets, which can be used in columns, providing a new avenue to design bioremediation methodologies for the removal of atrazine from the environment.

Table 3.1. Summary of the activities of TrzN:alginate, TrzN:chitosan, and TrzN:sol–gel.

			Percent Residual Activity				
Material	**Reaction Time**	**Trypsin Digestion**	**6 week storage**	**Thermostability**	**Organic co-solvent**	**pH 4.0**	**pH 9.0**
TrzN:Alginate	6 hours	75%	0%	52% at 60°C	10% in 20:80 MeOH:water	0%	0%
TrzN:Chitosan	6 hours	80%	20%	30% at 80°C	33% in 20:80 MeOH:water	0%	18%
TrzN:Sol-gel	1 hour	85%	65%	24% at 60°C	24% in 20:80 MeOH:water	45%	94%

3.6 References

(1) Pathak, R. K.; Dikshit, A. K. Atrazine and Human Health. *Int. J. Ecosyst.* **2012**, *1* (1), 14–23. https://doi.org/10.5923/j.ije.20110101.03.

(2) de Albuquerque, F. P.; de Oliveira, J. L.; Moschini-Carlos, V.; Fraceto, L. F. An Overview of the Potential Impacts of Atrazine in Aquatic Environments: Perspectives for Tailored Solutions Based on Nanotechnology. *Sci. Total Environ.* **2020**, *700*. https://doi.org/10.1016/j.scitotenv.2019.134868.

(3) Solomon, K. R.; Baker, D. B.; Richards, R. P.; Dixon, K. R.; Klaine, S. J.; Point, T. W. La; Kendall, R. J.; Weisskopf, C. P.; Giddings, J. M.; Giesy, J. P.; Lenwood W. Hall, J.; Williams, W. M. Ecological Risk Assessment Of Atrazine In. *Environ. Toxicol.* **1996**, *15* (1), 31–76.

(4) Beaulieu, M.; Cabana, H.; Taranu, Z.; Huot, Y. Predicting Atrazine Concentrations in Waterbodies across the Contiguous United States: The Importance of Land Use, Hydrology, and Water Physicochemistry. *Limnol. Oceanogr.* **2020**, 2966–2983. https://doi.org/10.1002/lno.11568.

(5) Graymore, M.; Stagnitti, F.; Allinson, G. Impacts of Atrazine in Aquatic Ecosystems. *Environ. Int.* **2001**, *26* (7–8), 483–495. https://doi.org/10.1016/S0160-4120(01)00031-9.

(6) Mudhoo, A.; Garg, V. K. Sorption, Transport and Transformation of Atrazine in Soils, Minerals and Composts: A Review. *Pedosphere* **2011**, *21* (1), 11–25. https://doi.org/10.1016/S1002-0160(10)60074-4.

(7) Chernyak, S. M.; Rice, C. P.; McConnell, L. L. Evidence of Currently-Used Pesticides in Air, Ice, Fog, Seawater and Surface Microlayer in the Bering and Chukchi Seas. *Mar. Pollut. Bull.* **1996**, *32* (5), 410–419. https://doi.org/10.1016/0025-326X(95)00216-A.

(8) Ocking, D. A. J. H.; Abbitt, K. I. J. B. Amphibian Contributions To Ecosystem Services. *Herpetol. Conserv. Biol.* **2014**, *9*, 1–17.

(9) Hayes, T. B.; Khoury, V.; Narayan, A.; Nazir, M.; Parka, A.; Brown, T.; Adame, L.; Chan, E.; Buchholz, D.; Stueve, T.; Gallipeau, S. Atrazine Induces Complete Feminization and Chemical Castration in Male African Clawed Frogs (Xenopus Laevis). *Proc. Natl. Acad. Sci. U. S. A.* **2010**, *107* (10), 4612–4617. https://doi.org/10.1073/pnas.0909519107.

(10) Liu, Z.; Wang, Y.; Zhu, Z.; Yang, E.; Feng, X.; Fu, Z.; Jin, Y. Atrazine and Its Main Metabolites Alter the Locomotor Activity of Larval Zebrafish (Danio Rerio). *Chemosphere* **2016**, *148*, 163–170. https://doi.org/10.1016/j.chemosphere.2016.01.007.

(11) ATSDR. Public Health Statement Atrazine. *Agency Toxic Subst. Regist.* **2015**, No.

September, 5–8.

(12) Rostami, S.; Jafari, S.; Moeini, Z.; Jaskulak, M.; Keshtgar, L.; Badeenezhad, A.; Azhdarpoor, A.; Rostami, M.; Zorena, K.; Dehghani, M. Current Methods and Technologies for Degradation of Atrazine in Contaminated Soil and Water: A Review. *Environ. Technol. Innov.* **2021**, *24*, 102019. https://doi.org/10.1016/j.eti.2021.102019.

(13) Shapir, N.; Pedersen, C.; Gil, O.; Strong, L.; Seffernick, J.; Sadowsky, M. J.; Wackett, L. P. TrzN from Arthrobacter Aurescens TC1 Is a Zinc Amidohydrolase. *J. Bacteriol.* **2006**, *188* (16), 5859–5864. https://doi.org/10.1128/JB.00517-06.

(14) Mu, Y.; Zhan, G.; Huang, C.; Wang, X.; Ai, Z.; Zou, J.; Luo, S.; Zhang, L. Dechlorination-Hydroxylation of Atrazine to Hydroxyatrazine with Thiosulfate: A Detoxification Strategy in Seconds. *Environ. Sci. Technol.* **2019**, *53* (6), 3208–3216. https://doi.org/10.1021/acs.est.8b06351.

(15) Sheldon, R. A. Enzyme Immobilization: The Quest for Optimum Performance. *Adv. Synth. Catal.* **2007**, *349* (8–9), 1289–1307. https://doi.org/10.1002/adsc.200700082.

(16) Martinez, S.; Kuhn, M. L.; Russell, J. T.; Holz, R. C.; Elgren, T. E. Acrylamide Production Using Encapsulated Nitrile Hydratase from Pseudonocardia Thermophila in a Sol-Gel Matrix. *J. Mol. Catal. B Enzym.* **2014**, *100*, 19–24. https://doi.org/10.1016/j.molcatb.2013.11.014.

(17) Zhang, Y.; Dong, X.; Jiang, Z.; Cao, B.; Ge, S.; Hu, M. Assessment of the Ecological Security of Immobilized Enzyme Remediation Process with Biological Indicators of Soil Health. *Environ. Sci. Pollut. Res.* **2013**, *20* (8), 5773–5780. https://doi.org/10.1007/s11356-012-1455-2.

(18) LI, Q.; LI, Y.; ZHU, X.; CAI, B. Isolation and Characterization of Atrazine-Degrading Arthrobacter Sp. AD26 and Use of This Strain in Bioremediation of Contaminated Soil. *J. Environ. Sci.* **2008**, *20* (10), 1226–1230. https://doi.org/10.1016/S1001-0742(08)62213-5.

(19) Jackson, C. J.; Coppin, C. W.; Carr, P. D.; Aleksandrov, A.; Wilding, M.; Sugrue, E.; Ubels, J.; Paks, M.; Newman, J.; Peat, T. S.; Russell, R. J.; Field, M.; Weik, M.; Oakeshott, J. G.; Scott, C. 300-Fold Increase in Production of the Zn2+-Dependent Dechlorinase TrzN in Soluble Form via Apoenzyme Stabilization. *Appl. Environ. Microbiol.* **2014**, *80* (13), 4003–4011. https://doi.org/10.1128/AEM.00916-14.

(20) Kim, S.; Jeong, C.; Cho, S.; Kim, S. B. Effects of Thermal Treatment on the Physical Properties of Edible Calcium Alginate Gel Beads: Response Surface Methodological Approach. *Foods* **2019**, *8* (11). https://doi.org/10.3390/foods8110578.

(21) Fareez, I. M.; Lim, S. M.; Mishra, R. K.; Ramasamy, K. Chitosan Coated Alginate-Xanthan Gum Bead Enhanced PH and Thermotolerance of Lactobacillus Plantarum LAB12. *Int. J. Biol. Macromol.* **2015**, *72*, 1419–1428. https://doi.org/10.1016/j.ijbiomac.2014.10.054.

(22) Won, K.; Kim, S.; Kim, K. J.; Park, H. W.; Moon, S. J. Optimization of Lipase Entrapment in Ca-Alginate Gel Beads. *Process Biochem.* **2005**, *40* (6), 2149–2154. https://doi.org/10.1016/j.procbio.2004.08.014.

(23) Bedade, D. K.; Sutar, Y. B.; Singhal, R. S. Chitosan Coated Calcium Alginate Beads for Covalent Immobilization of Acrylamidase: Process Parameters and Removal of Acrylamide from Coffee. *Food Chem.* **2019**, *275* (June 2018), 95–104. https://doi.org/10.1016/j.foodchem.2018.09.090.

(24) Im, J. K.; Cho, Y. C.; Noh, H. R.; Yu, S. J. Geographical Distribution and Risk Assessment of Volatile Organic Compounds in Tributaries of the Han River Watershed. *Agronomy* **2021**, *11* (5). https://doi.org/10.3390/agronomy11050956.

(25) Hermansson, E.; Schuster, E.; Lindgren, L.; Altskär, A.; Ström, A. Impact of Solvent Quality on the Network Strength and Structure of Alginate Gels. *Carbohydr. Polym.* **2016**, *144*, 289–296. https://doi.org/10.1016/j.carbpol.2016.02.069.

(26) Baker, J. P.; Bernard, D. P.; Christensen, S. W.; Sale, M. J.; Freda, J.; Heltcher, K.; Marmorek, D.; Rowe, L.; Scanlon, P.; Suter, G.; Warren-Hicks, W. J.; Welbourn, P. M. Biological Effects of Changes in Surface Water Acid-Base Chemistry. *Acidic Depos. State Sci. Technol.* **1990**.

(27) Li, F. Y.; Xing, Y. J.; Ding, X. Immobilization of Papain on Cotton Fabric by Sol-Gel Method. *Enzyme Microb. Technol.* **2007**, *40* (7), 1692–1697. https://doi.org/10.1016/j.enzmictec.2006.09.007.

(28) Náray-Szabó, G. Electrostatic Effects in Proteins. *Period. Biol.* **1999**, *101* (4), 325–331. https://doi.org/10.1146/annurev.biophys.14.1.387.

(29) Seffernick, J. L.; Reynolds, E.; Fedorov, A. A.; Fedorov, E.; Almo, S. C.; Sadowsky, M. J.; Wackett, L. P. X-Ray Structure and Mutational Analysis of the Atrazine Chlorohydrolase TrzN. *J. Biol. Chem.* **2010**, *285* (40), 30606–30614. https://doi.org/10.1074/jbc.M110.138677.

(30) DeGroot, A. R.; Neufeld, R. J. Encapsulation of Urease in Alginate Beads and Protection from α-Chymotrypsin with Chitosan Membranes. *Enzyme Microb. Technol.* **2001**, *29* (6–7), 321–327. https://doi.org/10.1016/S0141-0229(01)00393-3.

CHAPTER 4

ATRAZINE DEGRADATION USING IMMOBILIZED TRIAZINE HYDROLASE FROM *ARTHROBACTER AURESCENS* TC1 IN MESOPOROUS SILICA NANOMATERIALS†

Based on a paper published in *ACS Environmental Au**

Karla Diviesti,[b,‡] Glory A. Russell-Parks,[a,c,‡] Brian G. Trewyn[a,c,d,*] and Richard C. Holz[a,b]

4.1 Abstract

Triazine hydrolase from *Arthrobacter aurescens* TC1 (TrzN) was successfully immobilized on mesoporous silica nanomaterials (MSN), for the first time. For both non-functionalized MSNs and MSNs functionalized with Zn(II), three pore sizes were evaluated for their ability to immobilize wild-type (WT) TrzN; MCM-41 (small, 3 nm pores), MSN-10 (medium, 6-12 nm pores), and pore expanded PEMSN-10 (large, 15-30 nm pores). Of these six TrzN:MSN biomaterials, it was shown that TrzN:MSN-10 was the most active ($3.8 \pm 0.4 \times 10^{-5}$ U/mg) towards the hydrolysis of a 50 µM atrazine solution at 25°C. The TrzN:MSN-10 biomaterial was then coated in chitosan (TrzN:MSN-10:Chit), as chitosan has been shown to increase stability in extreme conditions such as low/high pH, heat shock, and the presence of

---

[a]Department of Chemistry, Colorado School of Mines, Golden, CO 80401 U.S.A
[b]Quantitative Biosciences and Engineering Program, Colorado School of Mines, Golden, CO 80401 U.S.A
[c]National Renewable Energy Laboratory, Golden, CO 80401 U.S.A
[d]Materials Science Program, Colorado School of Mines, , Golden, CO 80401U.S
†This work was supported by the National Science Foundation (CHE-200241, RCH) and the National Institution of Health (1R15CA271365, BGT).
‡ Represents co-first authorship, K.D and G.R.P contributed equally to this paper
* See Appendix A for permission and citation
Supplementary material can be found in Appendix B

organic solvents. TrzN:MSN-10:Chit was shown to be a superior TrzN biomaterial to TrzN:MSN-10, as it exhibited higher activity under all storage conditions, in the presence of 20% MeOH, at low and high pH values, and elevated temperatures up to 80 ºC. Finally, the TrzN:MSN-10:Chit biomaterial was shown to be fully active in river water, which establishes it as a functional biomaterial under actual field conditions. Combination of these data indicate that the TrzN:MSN-10:Chit biomaterial exhibited the best overall catalytic profile making it a promising biocatalyst for the bioremediation of atrazine.

4.2 Introduction

Originally patented in 1958 in Switzerland, atrazine (2-chloro-4-ethylamino-6-isopropylamino-s-triazine) has been used commercially in the United States since 1959 and today is the second most applied herbicide, with ~30,000 tons annually to sorghum, sugarcane, and corn crops.[1–3] Atrazine is water-soluble and functions to inhibit photosynthesis in targeted plants but is an environmental contaminant of streams, rivers, and groundwater. It is persistent and mobile in aquatic environments, primarily through surface runoff where it gets into groundwater via leaching. Its ability to enter and move through these environments after application is troublesome due to the potential downstream effects, particularly given its half-life of six months to several years and its toxicity to many eukaryotes such as crustaceans, insects, mollusks, fish, amphibians, and reptiles.[1,4–6] The documented effects of atrazine on lower order eukaryotes raises concerns for possible toxicity to humans. Links have been shown between atrazine exposure and lung and kidney diseases, cardiovascular damage, retinal degeneration, and cancer, which is why in 2003 the European Union banned atrazine.[7] In the US, the EPA recognized atrazine as an endocrine toxin in humans. Given the widespread use of atrazine in the

US and its toxicity to both aquatic environments and humans, its biodegradation and environmental remediation has become a topic of significant importance.[8]

Triazine hydrolase from *Arthrobacter aurescens* TC1 (TrzN, EC 3.8.1.8) is a Zn(II)-dependent hydrolytic dehalogenase that catalyzes the conversion of atrazine to its less toxic derivative hydroxyatrazine, under physiological conditions. Converting atrazine to hydroxyatrazine is considered the most efficient way to decrease atrazine contamination in the environment; therefore, TrzN is the biocatalyst of choice for the production of biomaterials that can be used in the bioremediation of atrazine contamination. Bioremediation methods utilizing TrzN, to date, have been limited to whole cells that naturally express TrzN or in one case, simply adding pure TrzN to a contaminated drainage ditch.[8,9] While these were somewhat successful in atrazine bioremediation, purified TrzN immobilized on a support material is necessary as a major challenge is the recovery of whole cells or free enzymes from the environment. In addition, within a cell, side reactions pose challenges with competing metabolic pathways and toxicity of the substrate and/or products.[10] Recently, some of us demonstrated that TrzN could be successfully immobilized within alginate and tetramethylorthosilicate (TMOS) sol-gels, that function as effective biocatalysts for atrazine degradation.[11] Although effective, the response of sol-gel biocatalysts tends to be limited/slow due to diffusion limitations. In addition, depending on the procedure used to prepare these systems there can be gradual leaching over time.[12]

Mesoporous silica nanomaterials (MSNs) provide a promising platform for the entrapment of enzymes, offering enhanced stability, improved catalytic activity, and protection against harsh environmental conditions.[13] These unique materials possess an ordered pore structure with well-defined pore sizes and high surface areas, which is ideal for immobilizing enzymes. Not only does the porous nature of mesoporous silica facilitates the diffusion of

substrates and products, allowing efficient enzyme-substrate interactions, these materials are highly tunable so they can accommodate various enzymes as well as substrates.[14,15] Moreover, the surface chemistry of these nanomaterials can be easily modified, enabling tailored immobilization strategies and enhanced enzyme loading. For example, various metal ions are commonly incorporated within MSNs which promotes a covalent interaction to occur between the metal ion and a protein tag. Although metal ions such as Cu^{2+}, Ni^{2+}, and Co^{2+} can be utilized there is a tradeoff between the specificity and affinity of the interaction between the metal ion selected and the protein tag.[16] For this work, we functionalized our material(s) with Zn^{2+} ions to covalently tether TrzN through its N-terminus histidine (His) tag allowing for increased stability in comparison to the non-covalent protein loaded materials. The Zn^{2+}/His-tag chelation is a highly used bioconjugation as there is a strong affinity for the imidazole group within the His-tag.[17] Therefore, TrzN was immobilized within MSNs (non-covalently and covalently) providing a novel biocatalytic nanomaterial that is capable of the hydrolytic degradation of atrazine under mild conditions.

4.3 Results and Discussion

4.3.1 Material Characterization

The physical properties of the mesoporous silica nanomaterials (MSNs) were examined by a series of characterization techniques. The calculated Brunauer−Emmett−Teller (BET) surface areas and Barrett− Joyner−Halenda (BJH) pore diameters from nitrogen sorption analysis are shown in Table 4.1. These data demonstrate the successful synthesis of three different pore sized MSN materials. The physical properties of the non-functionalized MSN materials are characteristic of these types of MSNs and are consistent with previous reports.[19] After

functionalizing with Zn(II), a decrease in surface area was observed, indicating the incorporation of Zn(II). A decrease in surface area and pore volume was also observed for the MSN-10 coated with chitosan suggesting the coating procedure was successful. Type IV isotherms, which are characteristic of mesoporous materials, were maintained after Zn(II) functionalization and chitosan coating (Figure B.1-B.4,). The steep slope at low P/P_0 observed with the mobile composition of matter No. 41 (MCM-41) sample is indicative of micropore filling caused by the presence of enhanced adsorbent-adsorptive interactions.[29]

Table 4.1. Properties of synthesized mesoporous silica nanomaterials (MSNs).

Sample	**BET Surface Area (m^2/g)**	**Pore Diameter (nm)**	**Pore Volume (cm^3/g)**
MCM-41	968	3	1.26
MSN-10	397	9	1.14
PEMSN-10	321	21	2.46
Zn@MCM-41	736	2.5	0.857
Zn@MSN-10	358	9	1.14
Zn@PEMSN-10	293	15	1.52
Chitosan MSN-10	225	9	0.685

TEM analysis of MSN-10 shows the hexagonal particle morphology and ordered pore distribution of the unmodified material (Figure 4.1A). Elemental mapping reveals the presence

and uniform dispersion of Zn(II) throughout the nanoparticle after functionalization (Figure 4.1B, 4.1C, 4.1D). STEM images of MCM-41 show the particles are uniform in shape and size (Figure S5, Supporting Information) while STEM images of pore expanded MSN-10 (PEMSN-10) show porous, non-uniform particles. This material was deemed acceptable for this study as the desired pore properties were achieved (Figure B.6). Elemental mapping of MCM-41 and PEMSN-10 materials also show the dispersion and presence of Zn(II) (Figure B.5-B.6)These findings suggest that TrzN could be covalently tethered throughout the material (surface and pores, size permitting). The amount of Zn(II) incorporated into the materials was quantified by ICP-AES after digesting the solid materials in HF and aqua regia and diluting with 5 wt. % HCl (Table B.1), further confirming the successful addition of Zn(II). The 100-peak observed at 2θ of 0.7° for the unfunctionalized MSN-10 in the low angle pXRD analysis indicates ordered pores, which can also be observed in the STEM images (Figure B.7). After the addition of the chitosan coating, SEM images show that there are no changes to particle morphology (Figure B.8). TGA analysis was also performed, which revealed a mass loss at 180 °C in the presence of chitosan (Figure B.9).[30] The mass loss from the chitosan coating is low, which is expected as we expect the coating to be thin.

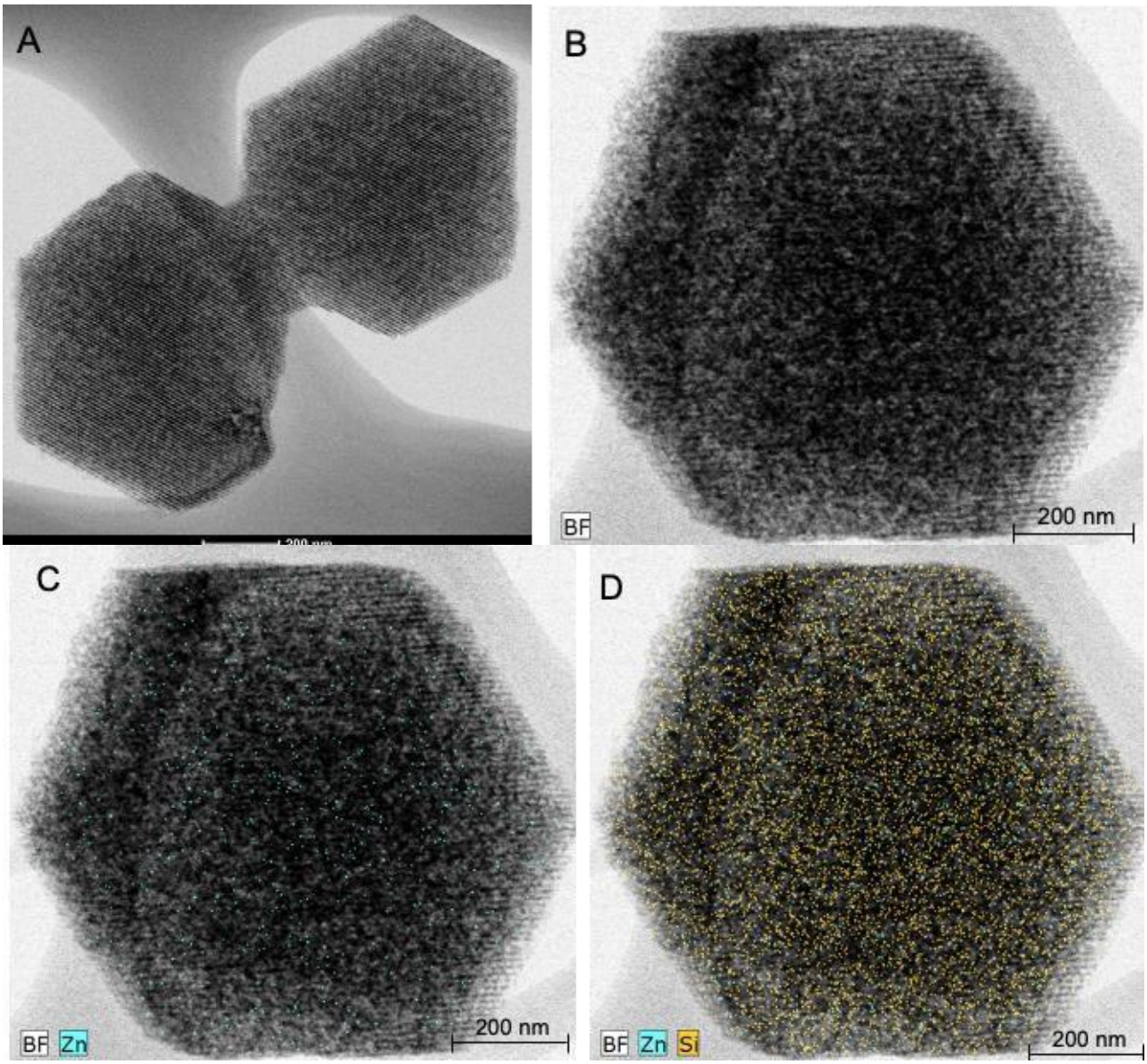

Figure 4.1. STEM images of unfunctionalized **(A)** and Zn(II) functionalized MSN-10 (B, C, D). Zn(II) is represented as blue and Si is represented as yellow. The scale bar is 200 nm.

4.3.2 Immobilization of TrzN.

Purified wild-type (WT) TrzN catalyzed the hydrolysis of atrazine and exhibited a k_{cat} value of 4.0 ± 0.1 s^{-1} and a K_m value of 43 ± 3 μM at 25°C in 50 mM HEPES buffer, pH 7.0, consistent with those previously reported.[23] TrzN was incorporated onto non-functionalized MSNs, which lacks direct, controlled chemical interactions for immobilizing enzymes within the pore framework as only of silica surface interactions with amino acids of TrzN exist. To provide further stability of TrzN, the bare MSNs were functionalized with Zn(II) to encourage a covalent bond between the N-terminal His_6 affinity tag on TrzN and the Zn(II) coated MSN surface. Transmission electron microscopy (TEM) images, (Figure 4.1B) in addition to ICP analysis (see Appendix B) demonstrates the successful incorporation of Zn(II) on the MSN surface.

For both functionalized and non-functionalized MSNs, three pore sizes were evaluated for their ability to immobilize 5 mg of catalytically active, pure TrzN; MCM-41 (small, 3 nm), MSN-10 (medium, 6-12 nm), and pore expanded PEMSN-10 (large, 15-30 nm) (Table 1**,** see Appendix B for N_2 sorption isotherms, XRD and ICP). For the small pore size, the non-functionalized MSN immobilized 37.1 ± 0.4% of the TrzN while the Zn(II) functionalized MSN immobilized 99.6 ± 0.2%. For the medium pore size, 24.2 ± 0.3% of the protein was immobilized while 98 ± 0.1% of protein was immobilized for the Zn(II) functionalized MSN. Lastly, the non-functionalized PEMSN-10 immobilized 36.7 ± 0.0% of the protein and the Zn(II) functionalized form immobilized 99.2 ± 0.1%. The protein loading was determined by calculating the change between the amount of protein in the loading buffer and the amount remaining after the immobilization step with a Coomassie (Bradford) Protein Assay Kit (Thermo Scientific).

Both the functionalized and non-functionalized Trzn:MSNs readily reacted with 50 μM atrazine at 25 °C in 50 mM HEPES buffer, pH 7.0 over a 1 hr. reaction period. The observed activities were evaluated over 5 cycles (Figure 4.2). Activity assays for the non-functionalized Trzn:MSNs revealed that the TrzN:MSN-10 biomaterial exhibited the highest specific activity at 3.8 E^{-05} ± 0.4 E^{-05} U/mg after 5 cycles, while the TrzN:MCM-14 biomaterial exhibited a specific activity of 3.0 E^{-05} ± 0.9 E^{-05} U/mg which was similar to the TrzN:PEMSN-10 biomaterials 3.1 E^{-05} ± 0.6 E^{-05} U/mg. The higher observed activity for the TrzN:MSN-10 biomaterial suggests 6-12 nm is the optimal pore size for TrzN immobilization. On the other hand, a clear trend emerged for the Zn(II) functionalized MSNs, regardless of pore size, as every TrzN:MSN biomaterial exhibited significantly lower activity than the corresponding non-functionalized TrzN:MSN biomaterial (Figure 4.2). These data are at first surprising considering increased activity is typically observed when enzymes are covalently attached, however after evaluating the electrostatic surface map of TrzN, a highly negative area was observed around the active site pocket (Figure SI10, supporting information) suggesting that the active site is blocked due to binding to the Zn(II) functionalized silica surface. Such a binding mode would be expected to inhibit substrate access to the TrzN active site.[31,32]

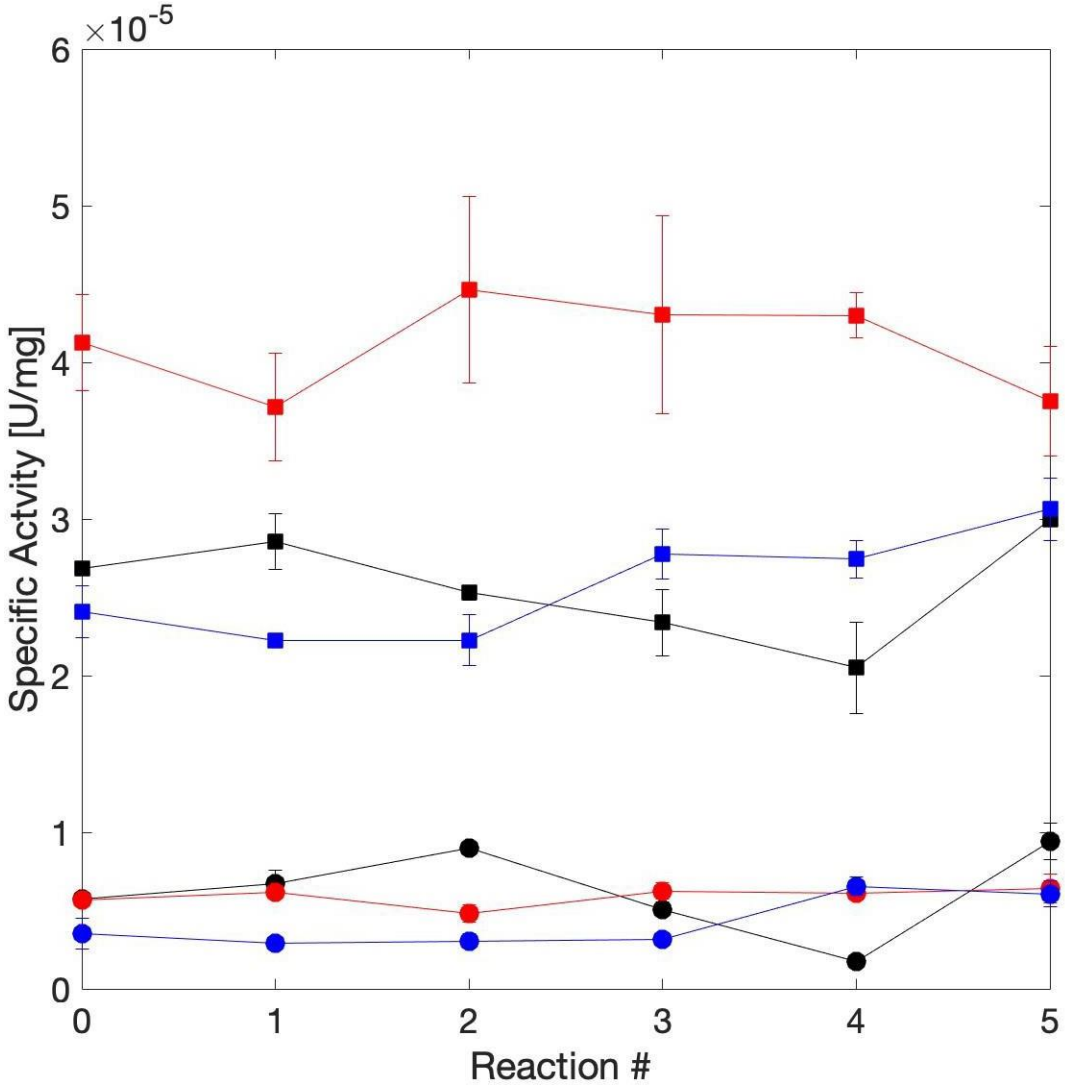

Figure 4.2. A five-cycle analysis, using specific activity U/mg, for the hydrolysis of 50 µM atrazine at 25 °C in 50 mM HEPES buffer, pH 7.0, for 1 hr. using TrzN loaded functionalized and non-functionalized MSNs; MCM-41 (small, 3-3.5 nm, black), MSN-10 (medium, 6-12 nm, red), and pore-expanded (PE) MSN-10 (large, ~15-30 nm, blue). The Zn(II) functionalized TrzN:MSNs are denoted as circles and the non-functionalized TrzN:MSNs are denoted as squares.

4.3.3 Immobilization Of Trzn On Msns With A Chitosan Coating

Chitosan is a derivative of chitin, the second most abundant cationic polymer in the world, and has a repeating structure of (1,4) linked ß-D-glucosamine.[33] When paired with biomaterials, chitosan has shown to increase stability in extreme condition such as low/high pH, heat shock, and the presence of organic solvents.[11,34,35] Specifically with MSN, chitosan has been used to enhance the efficacy of other catalysts used as delivery systems for drugs and therapeutics.[36,37] There is no or limited information available about studies using chitosan coated MSN for purposes beyond delivery such as environmental remediation. As chitosan is permeable to substrate, coating TrzN:MSN biomaterials with chitosan was hypothesized to provide additional protection for TrzN without inhibiting catalytic activity. Therefore, the TrzN:MSN-10 biomaterial was coated with chitosan (TrzN:MSN-10:Chit) and was shown to readily reacted with 50 μM atrazine at 25 °C in 50 mM HEPES buffer pH 7.0 over a 1 hr. reaction period with no detectable protein loss after the reaction (Figure 4.3). Compared to the TrzN:MSN-10 biomaterial, the TrzN:MSN-10:Chit biomaterial exhibited 94 ± 4% of the activity, suggesting the added coating had little to no effect on TrzNs ability to hydrolyze atrazine. These data indicates that both the TrzN:MSN-10 and TrzN:MSN-10:Chit biomaterials display the expected enzymatic properties, including substrate recognition, as WT TrzN in solution.

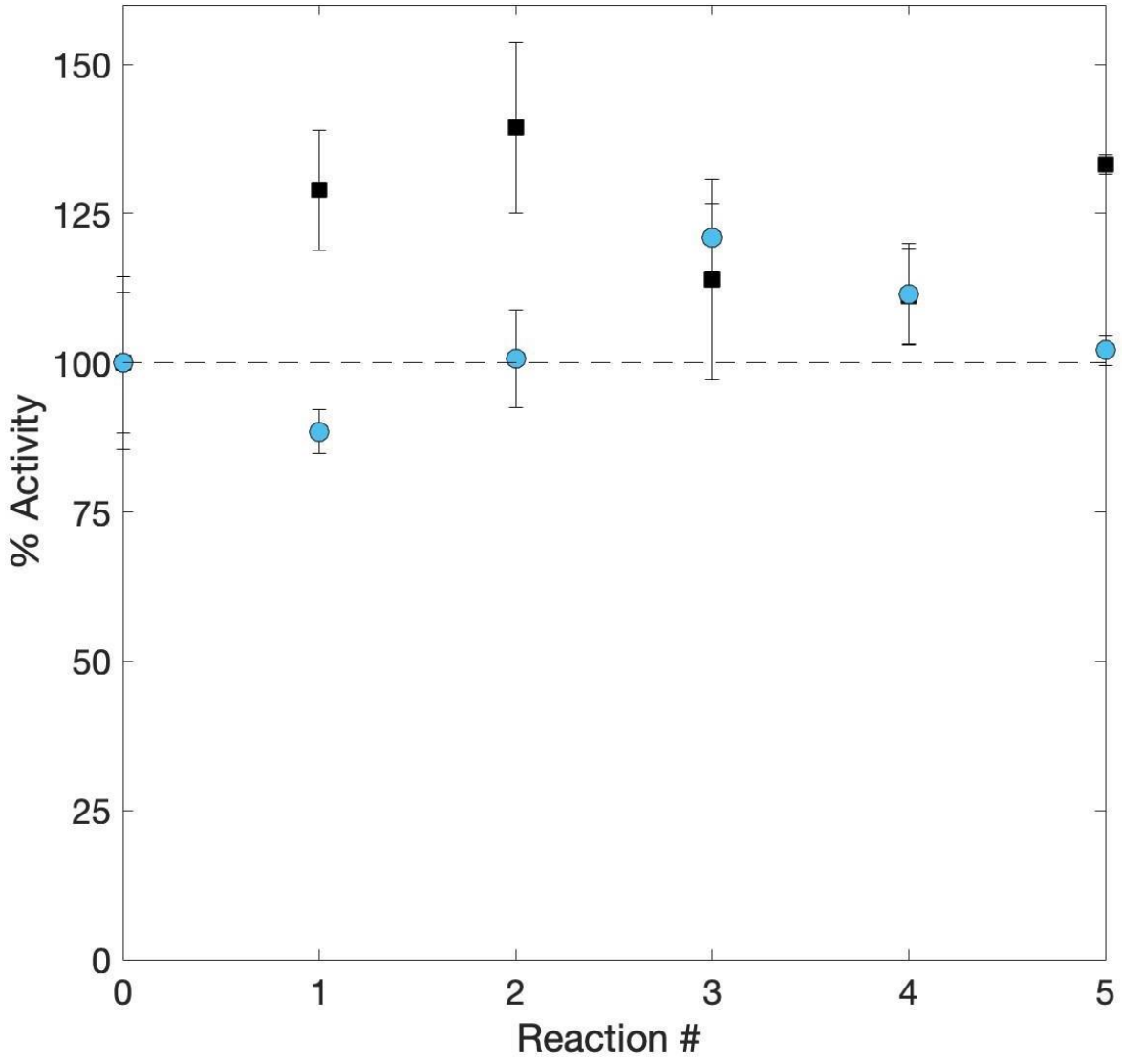

Figure 4.3. The cyclical reusability of TrzN:MSN-10 (black squares) and TrzN:MSN-10:Chit (light blue circles) evaluated over five cycles by monitoring the hydrolysis of 50 µM atrazine at 25 °C in 50 mM HEPES buffer, pH 7.0, for 1 hr. Each point represents five 1 hr. cycles with no wash step between cycles.

4.3.4 Reusability and recycling of TrzN:MSN biomaterials

For commercial applications, a biocatalyst must be reusable and have long-term stability. With this in mind, TrzN:MSN-10 and TrzN:MSN-10:Chit biomaterials were investigated under numerous reusability conditions. First, the biocatalysts were recycled multiple times in subsequent reactions (Figure 4.3). The materials were tested over five, 1 hr. cycles with no wash step in-between cycles. Both materials retained full activity over the five consecutive reactions with no quantifiable protein loss. Next, both biocatalysts were tested over a six-week period with three different storage conditions: dry (no buffer) at 4 °C, wet in 1 mL of 50 mM HEPES buffer pH 7.0 at 4 °C, and dry at -80 °C . A wash step with 50 mM HEPES buffer, pH 7.0 was essential after every reaction to remove residual atrazine and hydroxyatrazine. Over the six-week period, the TrzN:MSN-10:Chit biomaterial outperformed the TrzN:MSN-10 biomaterial in all three storage methods. In the dry storage method at 4 °C (Figure B.11A) TrzN:MSN-10 and TrzN:MSN-10:Chit retained 15 ± 11% and 59 ± 2% of their initial activity, respectively. In the -80 °C storage method (Figure B.11B), TrzN:MSN-10 retained 39 ± 7% while TrzN:MSN-10:Chit retained 73 ± 10% of their initial activity. Lastly, in the aqueous storage method (Figure 4.4), the TrzN:MSN-10 biomaterial retained 24 ± 7% while the TrzN:MSN-10:Chit biomaterial retained 78 ± 4% of their initial activity. During these experiments, there was no detectable protein loss. The chitosan coating increases the stability of the biocatalyst most likely by preventing denaturation of amino acids during the storage processes.[11,38] Remarkably, WT TrzN can also be stored at 4 °C in buffer over a six-week period without significant loss of activity.[11] However, comparison in activity between soluble and immobilized enzyme can be flawed due to potential distortion of the enzyme from multi-interactions between the enzyme and support.[31]

Overall, both biocatalysts showed strong retention of activity during cyclical use over a six-week period with the chitosan coating significantly improving activity retention of TrzN

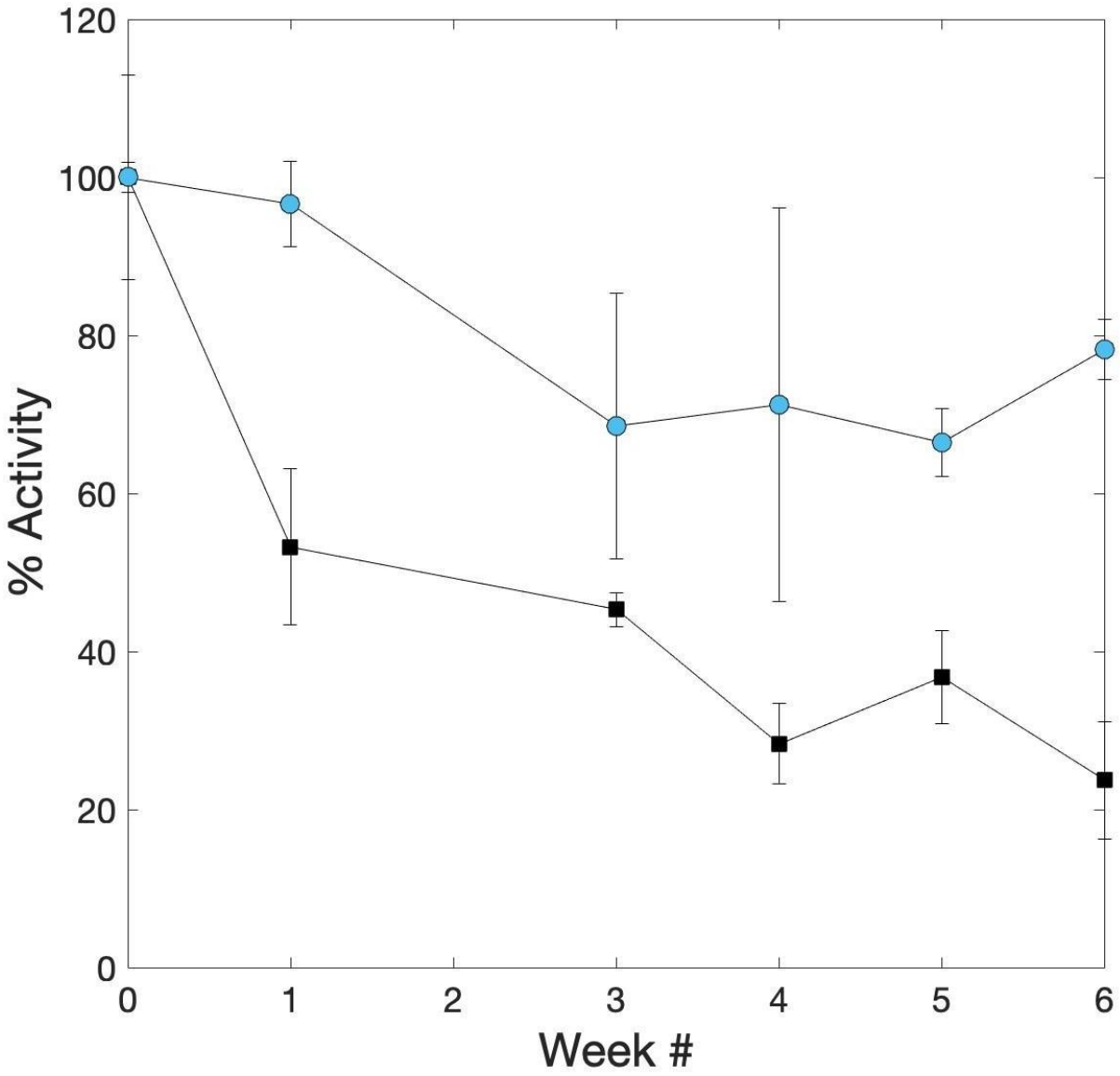

Figure 4.4. Long-term stability of TrzN:MSN-10 (black squares) and TrzN:MSN-10:Chit (light blue circles) measured over a six-week period. The hydrolysis of 50 µM atrazine at 25 °C in 50 mM HEPES buffer, pH 7.0, for 1 hr. Each biocatalyst was washed and stored at 4 °C in 1 mL of 50 mM HEPES buffer, pH 7.0 and weekly removed from the storage buffer, decanted and the experiment run.

4.3.5 Stability Of Trzn:MSN Biomaterials In Organic Co-Solvents.

Understanding the ability of the TrzN:MSN-10 biomaterial to function in organic solvents is important in exploring the nanoparticles overall potential as a bioremediation catalyst. Although atrazine presents itself typically in environments with little to no detectable organic solvents, at higher concentrations atrazine's solubility becomes problematic and requires the addition of organic solvents.[39] Additionally, enzymes typically denature when exposed to organic co-solvents.[28] Therefore, exploring the activity of the TrzN:MSN-10 and TrzN:MSN-10:Chit biomaterials in organic co-solvents is crucial for establishing them as potential bioremediation catalysts. The activity of TrzN:MSN-10 and TrzN:MSN-10:Chit was examined in MeOH:HEPES buffer, pH 7.0, ratios of 5:95, 10:90, 20:80, 50:50, 75:25, and 100:0 at 25 °C for 1 hr. (Figure 4.5). In 5% MeOH, TrzN:MSN-10 exhibited no loss in activity (110 ± 12%) while the TrzN:MSN-10:Chit biomaterial lost ~10% of its activity (89 ± 5%). Increasing the MeOH concentration to 10% resulted in a loss of ~25% of the observed activity for the TrzN:MSN-10 biomaterial while the TrzN:MSN-10:Chit biomaterial lost ~60% (39 ± 2%) of its initial activity. However, in 20% MeOH the TrzN:MSN-10 biomaterial retained only 3 ± 2% of its initial activity while the TrzN:MSN-10:Chit biomaterial retained 27 ± 3% of its initial activity. For comparison purposes, WT TrzN exhibits ~75% of its native activity in 20% MeOH.[11] It should be noted that enzyme immobilization typically involves new interactions between the enzyme and support, which may alter enzyme conformation, which likely explains the greater loss in activity for immobilized TrzN compared to WT TrzN.[31] This new conformation could help explain the higher inhibition of immobilized TrzN compared to soluble TrzN.[11] These data indicate that the TrzN:MSN-10:Chit biomaterial performs the best in the presence of MeOH.

Both the TrzN:MSN-10 and TrzN:MSN-10:Chit biomaterial could be partially reactivated after reaction in MeOH:HEPES co-solvent solutions by washing the biomaterials with 50 mM HEPES, pH 7.0 (Figure 4.5, insert). The washed biomaterials were reacted with 50 μM atrazine at 25 °C in 50 mM HEPES buffer, pH 7.0 for 1 hour revealing that up to 30% MeOH, both biomaterials could be almost fully reactivated. Even at 50:50 MeOH:HEPES both biomaterials could be reactivated to 47 ± 6% of their original activity. At higher MeOH concentrations, TrzN:MSN-10:Chit could still be reactivated but the uncoated TrzN:MSN-10 biomaterial could not. These suggest that TrzN is not being fully denatured by MeOH, likely due to stabilization of the protein structure by the biomaterial. Coating the TrzN:MSN-10 biomaterial with chitosan further stabilizes the enzyme structure by "locking" it in place and providing an extra barrier of protection from MeOH. Overall, the TrzN:MSN-10 and TrzN:MSN-10:Chit biomaterials are both active in organic co-solvents, an important finding for bioremediation processes that involve solvent extraction of atrazine from organic soil samples.

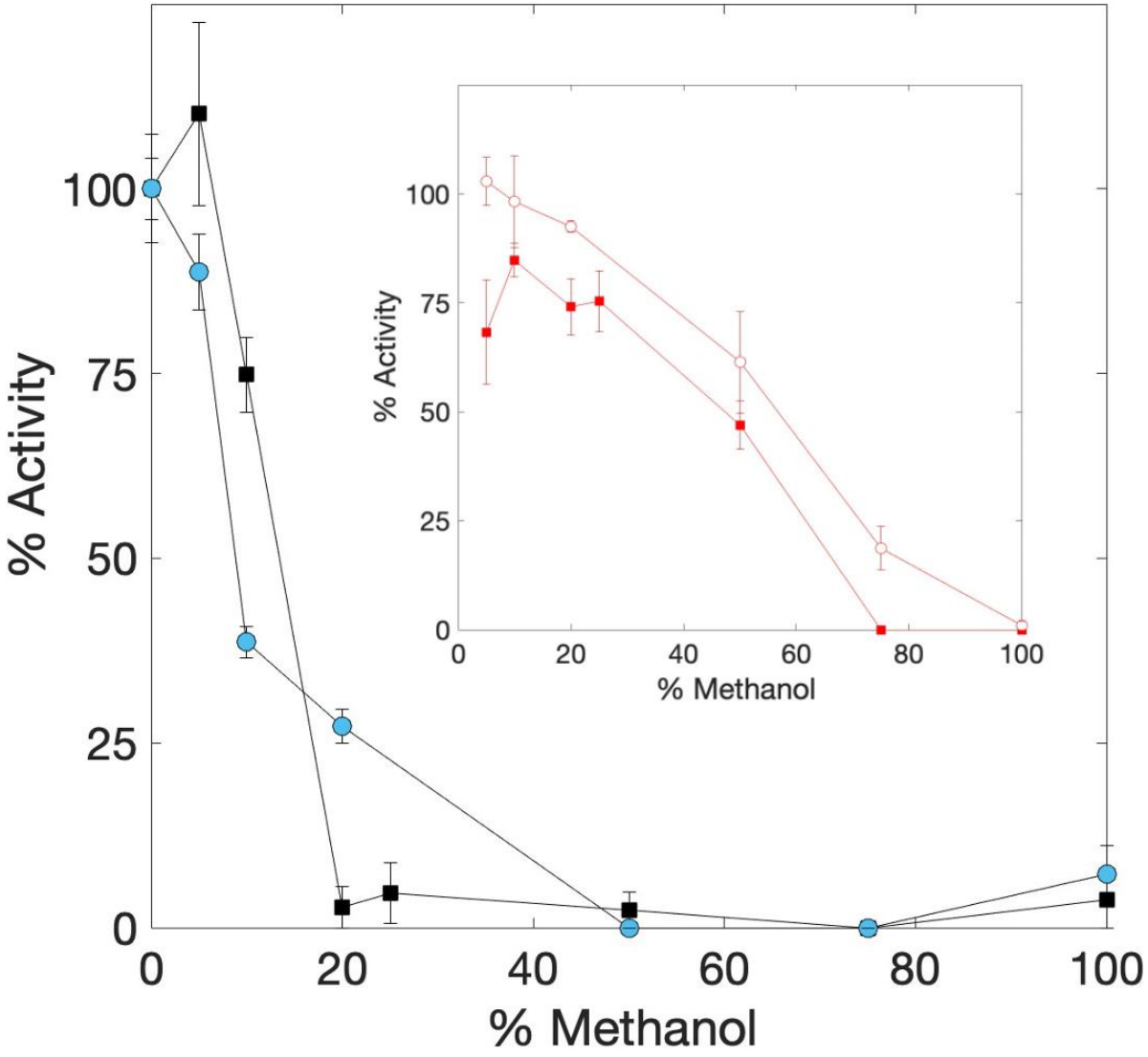

Figure 4.5. Activity of TrzN:MSN-10 (black squares) and TrzN:MSN-10:Chit (light blue circles) by monitoring the hydrolysis of 50 µM atrazine at 25 °C in 50 mM HEPES buffer, pH 7.0, for 1 hr. at varying MeOH concentrations (0-100%). **Insert:** After reacting with the respective MeOH concentration, TrzN:MSN-10 (red squares) and TrzN:MSN-10:Chit (red lined circles) were washed and reacted at standard conditions *i.e*. 25 °C with 50 µM atrazine in 50 mM HEPES buffer pH 7.0 for 1 hr.

4.3.6 Stability of TrzN:MSN-10 and TrzN:MSN-10:Chit biomaterials at non-physiological pH values.

When utilizing biocatalysts for water bioremediation purposes, the catalyst is expected to be used at the watersheds pH, which is typically around pH 7. However, outside influences such as polluted runoff can cause the pH to fluctuate outside of the neutral range.[40] With this in mind, it is important to investigate the activity of the TrzN:MSN-10 and TrzN:MSN-10:Chit biomaterials at lower (pH 4.0) and higher (pH 9.0) pH values (Figure 4.6). At a pH value of 4.0 (50 mM citric acid buffer) the TrzN:MSN-10 biomaterial had no detectable activity while the TrzN:MSN-10:Chit biomaterial exhibited 15 ± 1% of its activity at pH 7.0. For comparison purposes, WT TrzN exhibited 27 ± 3% activity at pH 4.0, a value that is quite similar to that of the TrzN:MSN-10:Chit biomaterial. At a pH value of 9.0 (50 mM glycine buffer) the TrzN:MSN-10 biomaterial exhibited 89 ± 10% of its activity at pH 7.0 while the TrzN:MSN-10:Chit biomaterial was fully active 111 ± 9%. At pH 9.0, both biomaterials outperformed WT TrzN which only exhibited 46 ± 2% of its activity at pH 7.0. Due to the higher maintained activity at both pH 4.0 and pH 9.0, it can be concluded that coating the TrzN:MSN-10 biomaterial with chitosan enhances stability of TrzN at pH values outside of the neutral range.

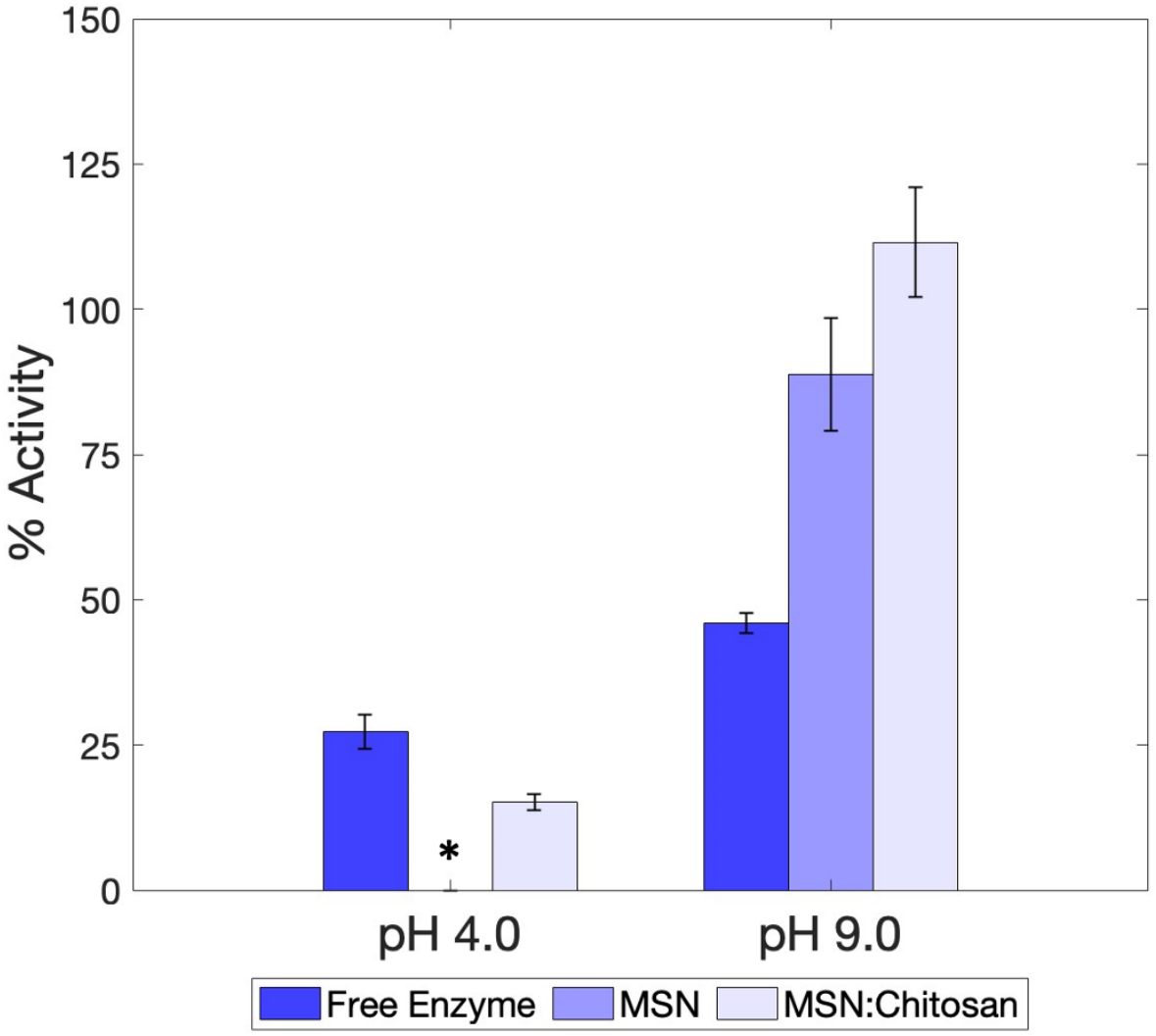

Figure 4.6. Hydrolysis of 50 µM atrazine by WT TrzN, TrzN:MSN-10 and TrzN:MSN-10:Chit at 25 °C in 50 mM citric acid buffer, pH 4.0, or 50 mM glycine buffer, pH 9.0 for 1 hr. An "*" indicates there was no detectable activity.

4.3.7 Thermostability Of TrzN:MSN-10 And Trzn:MSN-10:Chit Biomaterials.

The thermostability of the TrzN:MSN-10 and TrzN:MSN-10:Chit biomaterials was evaluated over a temperature range of 50-80 °C using a 30 min. heat shock (Figure 4.7). After heat shock treatment, the biocatalysts were tested using the standard assay procedure i.e. 50 μM atrazine at 25 °C in 50 mM HEPES buffer, pH 7.0. After the 50 °C heat shock, the TrzN:MSN-10 biomaterial retained 50 ± 1% and the TrzN:MSN-10:Chit biomaterial retained 60 ± 5% of its original activity. As the temperature was increased, the activities of both biomaterials continued to drop with TrzN:MSN-10 exhibiting 21 ± 6%, 7 ± 1% and 0% of its original activity at 60, 70, and 80 °C, respectively. The chitosan coating provided additional thermal protection for TrzN with the TrzN:MSN-10:Chit biomaterial exhibiting 43 ± 2%, 32 ± 3%, and 34 ± 6% of its original activity at 60, 70, and 80 °C. For comparison purposes, WT TrzN retains >80% of its original activity after a 50, 60, 70 and 80 °C heat shock. The decrease in activity in the biocatalysts compared to the soluble enzyme is likely due to the interactions that immobilize TrzN to the material, which restricts the essential motion of the folded state that are required for catalytic turnover.[41] This has been observed before in multipoint covalent immobilization methods. The chitosan coating stabilizes TrzN bound to the MSN-10 at higher temperatures, which is consistent previous studies where chitosan coating have been shown to increase the thermostability of immobilized enzymes.[11,35]

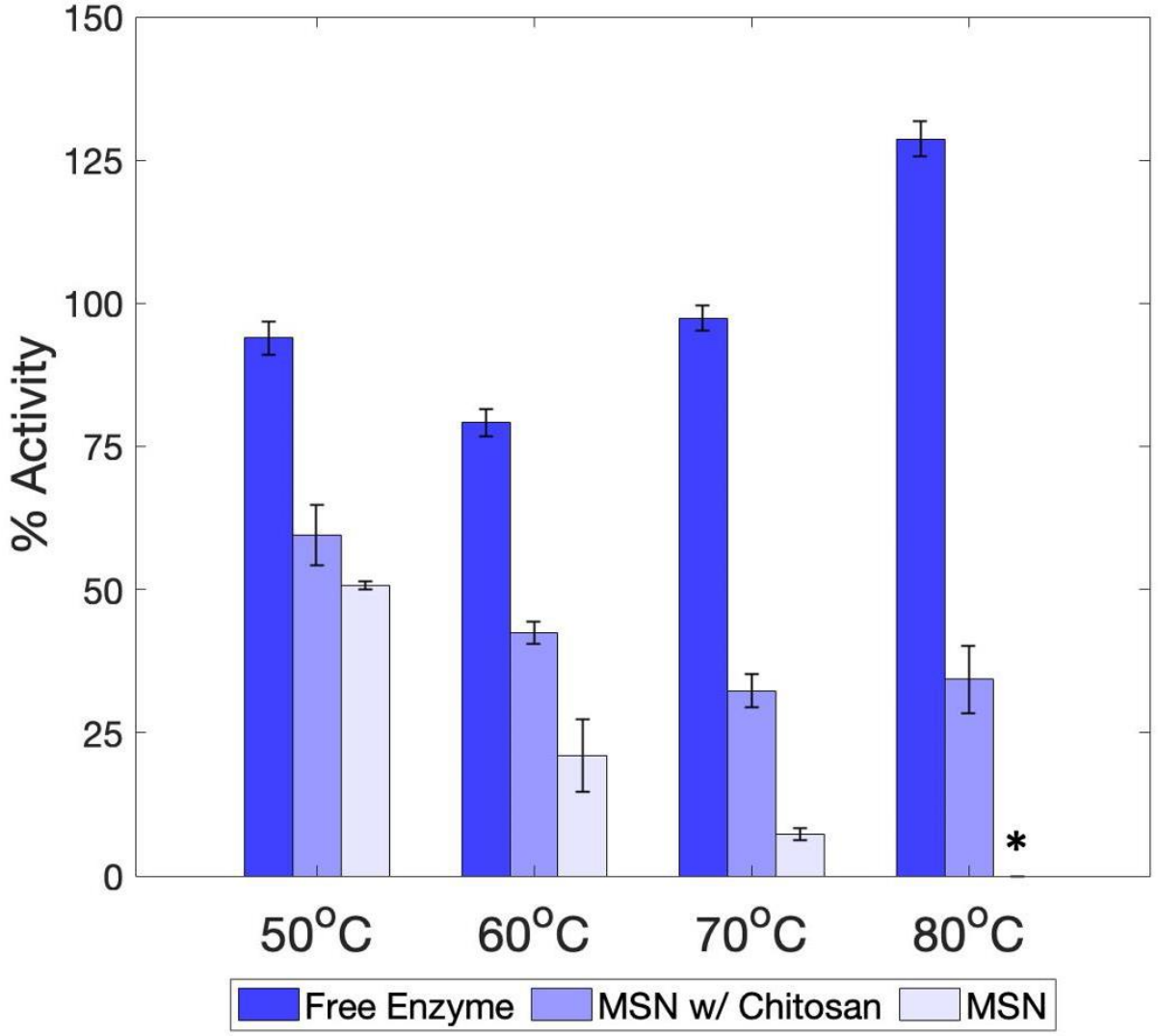

Figure 4.7. Thermostability of WT TrzN, TrzN:MSN-10 and TrzN:MSN-10:Chit. The specific activity, U/mg, for the hydrolysis of 50 µM atrazine at 25 °C in 50 mM HEPES buffer, pH 7.0, for 1 hr. was recorded after a 30 min. heat shock at 50, 60, 70, and 80 °C. An "*" indicates there was no detectable activity.

4.3.8 Activity Of TrzN:MSN-10 And TrzN:MSN-10:Chit Biomaterials In River Water.

The commercial bioremediation application of any biomaterial requires that they retain their desired catalytic activity in river or lake water. To replicate these conditions, water samples were collected from Clear Creek, in Golden, CO. There was no reported atrazine contamination in Clear Creek according to the most recent water quality report published by the city of Golden in 2022.[42] The sample had an initial temperature of 3 °C and a pH of 7.25. Two sample sets were prepared; first (group 1) was unmodified while the second (group 2) was autoclaved. Aliquots from group 1 were plated on agar plates and incubated at 37 °C. Bacterial growth was observed after 48 hours (SI12, Supporting information). Because atrazine is not present in Clear Creek, all samples were supplemented with 15 mM atrazine in 100% MeOH providing an atrazine concentration 50 µM and final MeOH concentrations of <1%. All samples were run at 25 °C at 200 rpm stirring for 1 hour. These data indicated that both the TrzN:MSN-10 and TrzN:MSN-10:Chit biomaterials retain full activity under field conditions. In addition to being fully functional, MSN-10 is a biocompatible material that is suitable for commercial bioremediation purposes.

4.4 Materials and Methods

4.4.1 Material

Chitosan, atrazine, type I Trypsin from bovine pancreas, and chymotrypsin were purchased from Sigma-Aldrich. Triblock copolymer Pluronic P104 ($PEO_{27}PPO_{61}PEO_{27}$) was received as a gift from BASF. Millipore nanopure water was filtered at 18.2 M Ohms. All reagents were of the highest purity available and were received without further purification.

4.4.2 Synthesis Of Mobil Composition Of Matter No. 41 (MCM-41; Pore Size Of ~3 Nm)

The commonly reported procedure was followed to synthesize MCM-41.[18] Briefly, 1.0 g of cetyltrimethylammonium bromide (CTAB) was added to 480 mL of nanopure water followed by the addition of 3 mL of NaOH (2.0 M). The mixture was stirred for 30 minutes at 80 °C and 4.6 g of tetraethylorthosilicate (TEOS) was then added dropwise and the mixture was allowed to stir for an additional 2 hrs. The opaque solution was then filtered and washed with nanopure water and ethanol three times each with the final wash being ethanol. The white material was dried overnight in air. The crude product was then dispersed in a methanol (25 mL) and a small volume of concentrated HCl was added (250 µL). This was stirred for 6 hrs. at 64 °C, which promoted the removal of the surfactant. The material was again filtered and washed with ethanol and dried overnight.

4.4.3 Synthesis of MSN-10 (pore size of 6-12 nm*)*

3.5 g of a nonionic surfactant, Pluronic P104, was dissolved in 1.6 M HCl at 55 °C for 1 hrs. 5.1 g of tetramethylorthosilicate (TMOS) was then added dropwise and the mixture was further stirred for 24 hrs. at 55 °C. During this time the solution changed from a clear, colorless solution to a white mixture. This mixture was transferred to a Teflon-lined autoclave and was hydrothermally treated at 150 °C for 24 hrs. Next, the mixture was cooled, filtered, and washed three times with both water and methanol with the final wash being methanol, leaving a white solid. Finally, the powder was dried overnight and then calcined at 550 °C for 6 hrs. to remove the surfactant.19

4.4.4 Synthesis of Pore Expanded MSN-10 (pore size of 15-30 nm)

The same procedure used to synthesize the MSN-10 material was followed except, 8.38 g of 1,2,4,5-Tetramethylbenzene was added dropwise to the solution to swell the pores after the P104 had dissolved. This mixture then stirred for an additional hour at 55 °C before TMOS was added. After hydrothermal treatment, washing and drying the material, an acid extraction was performed to remove the surfactant. Here, the crude pore expanded material was added to a solution consisting mainly of methanol (115 mL) and a small volume of concentrated HCl (2.3 mL), which was then refluxed for 6 hrs. The product was filtered and washed with water and methanol two times each and dried overnight in air.

4.4.5 Zn-functionalized of MSN-10

Zinc was incorporated within the MSN by following the published procedure.[20] A solution of the previously synthesized MSN-10 (1.0 g) dispersed in nanopure water (8.0 mL) was prepared along with a second solution consisting of $Zn(NO_3)_2$ (0.2 g) dissolved in nanopure water (2.0 mL). Initially, while raising the pH of the Zn-solution to 11, the addition of NH_4OH caused a precipitate to form; however, after further addition of NH_4OH, the solution returned to a clear and colorless solution. Once the pH of both solutions had been adjusted to 11, the Zn-solution was quickly added with stirring to the MSN-10 mixture. After stirring for 10 min, the solid material was separated via centrifugation (10 min.). Nanopure water (8 mL) was added to the solid material which was then allowed to stir for an additional 10 min. The material was then filtered and washed with water three times and dried overnight. Lastly, the material was calcined at 300 °C for 3 hrs.

4.4.6 Material Characterization

All MSN materials were characterized by the following techniques: nitrogen physisorption analysis at 77 K using a Micromeritics TriStar 3000. A 20 sec equilibration time was used to obtain the isotherms of each material. From these isotherms, the specific surface area and pore distribution of the samples were extracted through the Brunauer−Emmett−Teller (BET) equation and the Barrett− Joyner−Halenda (BJH) method; scanning transmission electron microscopy (STEM) images and the corresponding energy-dispersive X-ray spectroscopy (EDS) hypermaps were collected on a FEI Talos F200X operated at 200 kV. The samples were suspended in methanol and dropped onto a 300-mesh copper grid with lacey Formvar/ carbon (Ted Pella, 01883-F). Elemental EDS maps were both collected (acquisition time 5 min) and processed by standard methods using Bruker ESPRIT software; powder X-ray diffraction (pXRD) was performed on a Bruker D2 Phaser diffractometer with Cu Kα (λ = 1.54 Å) with a current of 10 mA and a voltage of 30 kV; inductively coupled plasma atomic emission spectroscopy (ICP-AES) analysis was performed on a Perkin Elmer Optima 8300, thermogravimetric analysis (TGA) using a TA Instruments TGA Q500 with the internal high-resolution programming ramping to 800 °C at a ramp rate of 10 °C min^{-1} in air; scanning electron microscopy (SEM) images were collecting on a SEMTech Solutions Refurbished Amray 3300 field emission scanning electron microscope with an accelerating voltage of 15 kV and a working distance between 10-15 mm.

4.4.7 Expression And Purification Of TrzN

The gene from *Arthrobacter aurescens* TC1 that encodes for TrzN with the D38N, L131P, and A159V mutations was expressed and purified as previously reported.[17] Briefly, A 100 mL LB-Miller starter culture was inoculated from a single colony with 50 µg/mL of

kanamycin. A 9 L culture was inoculated from this starter culture using 10 mL/liter supplemented with 5 µM isopropyl ß-d-1-thiogalactopyranoside (IPTG) and grown at 37°C for 48h.[23,11] Cells were harvested by centrifugation at 7000 rpm 4°C, for 15 min. The cells were resuspended at 2 mL per gram of buffer A (50 mM NaH_2PO_4, 500 mM NaCl, 10 mM imidazole, 1.5 mM tris(2-carboxyethyl)phosphine (TCEP), 10% glycerol, pH 8.0) then lysed by sonication on ice in three 10 min (30s on, 45s off) intervals using a 21W Misonex sonicator 3000. Cell debris was removed by centrifugation at 17,500 rpm, 4°C, for 40 min. The protein was purified by immobilized metal affinity chromatography (IMAC) using Ni-NTA (nickel-nitrilotriacetic acid) Superflow Cartridges (Qiagen). The column was equilibrated with buffer A and the crude protein extract was loaded onto the IMAC column. Unbound protein was eluted with 15 column volumes (CV) of buffer A at a flow rate of 2 mL/min. Elution of TrzN was initiated with 15 CV of 3% buffer B (buffer A with 500 mM imidazole). Elution finished with a linear gradient (3-100%) of buffer B over 20 CVs at a flow rate of 2 mL/min. Peak fractions were pooled and resuspended in 50 mM HEPES pH 7.5 and concentrated with an Amicon Ultra-15 centrifugal filter device with a molecular weight cutoff (MWCO) of 30,000 (Millipore). Sodium dodecyl sulfate-polyacrylamide gel electrophoresis (SDS-PAGE) reveals a single polypeptide band at ~51 kDa, consistent with previous studies (Figure B.13).[11,21,23] The protein concentration was determined by UV-Vis absorbance at 280 nm (ε_{280} = 61,670 $M^{-1}cm^{-1}$) and with a Coomassie (Bradford) Protein Assay Kit (Thermo Scientific). Expression of TrzN and purification using immobilized metal affinity chromatography (IMAC) resulted in ~10 mg/L of soluble TrzN enzyme.[11,21,23]

4.4.8 Kinetic Activity Assay

Hydrolysis of atrazine by TrzN was quantified spectrophotometrically by continuously monitoring the decrease in absorbance at 264 nm (ε_{264} = 3.5 $mM^{-1}cm^{-1}$) that accompanies atrazine dechlorination, as previously reported.[24] Briefly, the hydrolysis of a 150 µM atrazine solution in 0.1 M sodium phosphate buffer, pH 7.0 was monitored at 264 nm.[23] Assays were performed in a 1 mL quartz cuvette in triplicate on an Agilent 8453 UV-Vis spectrophotometer. One unit of enzyme activity was defined as the amount of enzyme that catalyzed the hydrolysis of 1 µmol of atrazine per minute at 25°C. Plots of the initial rate of hydrolysis of various concentrations of atrazine were fit to the Michaelis-Menten equation, which provided a k_{cat} of 4.0 ± 0.1 s^{-1} and a K_m value of 43 ± 3 µM, similar to those previously reported.[11,21,23]

4.4.9 Immobilization Of TrzN On MSNs In The Absence And Presence Of A Chitosan Coating

TrzN was adhered to MSNs (5 mg) in 50 mM HEPES buffer, pH 7.0 (1.0 mL) followed by the addition of 2.5 mg of TrzN in 250 µL of 50 mM HEPES buffer, pH 7.0. The TrzN:MSN mixture was placed on a shaker plate for 20 hrs. at room temperature (160 rpm). The TrzN:MSN biomaterial was then centrifuged (10 min.) and the supernatant was separated from the solid material and the amount of protein loaded was quantified using a Coomassie (Bradford) Protein Assay Kit (Thermo Scientific).[25] TrzN:MSN were also coated in chitosan by modifying and combining two previously published procedures.[11,26] A 0.5% w/v chitosan solution was used and prepared in a 2% acetic acid solution pH 6.0. The TrzN:MSN material (5 mg) was placed in 5 mL of the chitosan solution and stirred at 25°C at 200 rpm for 24 hrs. After the coating process, the TrzN:MSN-chitosan biomaterial was separated by centrifugation at 4,000 rpm 20°C, for 10

min. The samples were washed with 50 mM HEPES buffer, pH 7.0 and allowed to air dry for 30 minutes prior to being used.

4.4.10 Kinetic Characterization of the TrzN:MSN Biomaterials

Hydrolysis of atrazine by each TrzN:MSN biomaterial, was determined using a 50 µM atrazine solution in 50 mM HEPES pH 7.0 at 25°C with constant stirring (200 rpm).[11,27] Aliquots of the reaction mixture (0.3 mL) were taken at fixed time intervals and the hydrolysis of atrazine analyzed via the UV-Vis assay previously described for WT TrzN. The specific activity (U/mg) of each biomaterial was calculated from the reaction rate (µmol/L/min), the amount of TrzN immobilized, and the volume of the reaction.[11,28] Reaction buffer (1 mL) was collected at the end of each reaction for protein loss analysis using a Coomassie (Bradford) Protein Assay Kit (Thermo Scientific). The concentration of atrazine produced was determined using standard curves of absorbance versus known atrazine concentrations.

4.4.11 Recycling Experiments for TrzN:MSN Biomaterials

A 5 mL solution of 50 µM atrazine in 50 mM HEPES, pH 7.0 at 25 °C was reacted with each TrzN:MSN biomaterial for 1 hr. after which an aliquot (1 mL) was removed and the amount of atrazine dechlorination determined via the UV-Vis assay previously described for WT TrzN. The product mixture was then decanted, and The TrzN:MSN samples were stored in three post reaction storage conditions: no buffer stored at -80°C, no buffer stored at 4°C, and 1 mL of HEPES buffer pH 7.0 at 4°C and reused on a weekly basis for six weeks. The reaction buffer was tested for protein loss from the MSN using the Coomassie (Bradford) Protein Assay Kit (Thermo Scientific). The reaction was also repeated on a different TrzN:MSN sample group over 6 cycles

with each cycle using standard reaction times and the conditions described above. Sample of TrzN:MSN biomaterials used for each cycle with no wash step in between cycles and an aliquot (1 mL) of reaction buffer, were taken after each cycle to evaluate protein loss using the Coomassie (Bradford) Protein Assay Kit (Thermo Scientific).

4.4.12 Activity Of Soluble And Immobilized TrzN In Organic Co-Solvents

The activity of soluble TrzN with 5, 10, and 20% (v/v) methanol as the organic co-solvent toward atrazine was measured spectrophotometrically at 25°C as described above. Each measurement was taken in triplicate. The degradation of atrazine using each TrzN:MSN biomaterial with organic co-solvents at concentration ranging from 5-100% (v/v) was carried out in their respective reaction conditions described previously. Aliquots (1 mL) were taken at the start and end of the reaction and analyzed spectrophotometrically as described above. After reacting with the co-solvent, samples were washed with 5 mL of 50 mM HEPES buffer pH 7.0 and the same sample was reacted again at the standard reaction time and conditions described previously.

4.4.13 Activity Of Soluble And Immobilized TrzN At pH Values Of 4 And 9

The activity of soluble and immobilized TrzN in 50 mM citric acid, pH 4.0, and 50 mM glycine buffer, pH 9.0, towards atrazine was measured spectrophotometrically as described above. Each measurement was taken in triplicate. Aliquots (1 mL) were taken at the end of the reactions and tested for protein loss using Coomassie (Bradford) Protein Assay Kit (Thermo Scientific).

4.4.14 Thermostability of soluble and immobilized TrzN

The thermostability of soluble and immobilized TrzN was determined by incubating each for 30 min at 50, 60, 70, and 80 °C. Soluble TrzN was in 1 mL aliquots in 50 mM HEPES buffer pH 7.0 while TrzN:MSN biomaterials were not suspended in buffer. Residual activity of the free enzyme and encapsulated TrzN was determined spectrophotometrically.

4.4.15 Activity of TrzN:MSN in natural water samples

Water samples were collected on April 14th 2023 from Clear Creek in Golden, CO. Temperature, pH, and metal analysis (using inductively coupled plasma atomic emission spectroscopy (ICP-AES)) were collected the same day. Aliquots (100, 200, and 300 µL) were plated on agar plates and incubated for 48 hours to detect general bacterial growth. Two sets of sample groups were tested from the Clear Creek samples; one group used autoclaved water samples and the other did not. Autoclaved samples were done prior to the addition of biocatalyst to ensure there was no inactivation due to the autoclave process. Activity of the TrzN:MSN biomaterials was tested spectroscopically as described above. Aliquots (1 mL) were taken at the end of the reactions and tested for protein loss using Coomassie (Bradford) Protein Assay Kit (Thermo Scientific).

4.5 Conclusion

In summary, TrzN was immobilized on non-functionalized MSNs with different pore sizes: MCM-41 (small, 3 nm), MSN-10 (medium, 6-12 nm), and pore expanded PEMSN-10 (large, 15-30 nm) and functionalized Zn(II). Each of these MSNs bound TrzN and were capable

of catalytically hydrolyzing atrazine at pH 7 and 25 ºC. The MSN support system with the highest TrzN activity was MSN-10 (TrzN:MSN-10), which became the focus of this study with and without a protective chitosan coating (TrzN:MSN-10:Chit). Coating the TrzN:MSN-10 biomaterial with chitosan did not reduce the observed activity but was shown to provide enhanced stability of TrzN improving reusability, organic solvent, thermal and pH stability. Both TrzN:MSN-10 and TrzN:MSN-10:Chit could be cyclically reused over five consecutive cycles with several storage conditions remaining active for at least 6 weeks. TrzN:MSN-10:Chit was superior to TrzN:MSN-10 as it exhibited higher activity under all storage conditions with >60% activity retained. TrzN:MSN-10:Chit was superior to TrzN:MSN-10 in the presence of 20% MeOH, low (pH 4) and high (pH 9) values, and high temperatures up to 80 ºC. Therefore, the TrzN:MSN-10:Chit biomaterial exhibited the best overall profile making this TrzN biomaterial a promising biocatalysts for the bioremediation of atrazine by dechlorination. The fact that TrzN:MSN-10:Chit was fully active in a river water establishes it as a function biomaterial under actual field conditions.

4.6 References

(1) de Albuquerque, F. P.; de Oliveira, J. L.; Moschini-Carlos, V.; Fraceto, L. F. An Overview of the Potential Impacts of Atrazine in Aquatic Environments: Perspectives for Tailored Solutions Based on Nanotechnology. *Sci. Total Environ.* **2020**, *700*. https://doi.org/10.1016/j.scitotenv.2019.134868.

(2) Solomon, K. R.; Baker, D. B.; Richards, R. P.; Dixon, K. R.; Klaine, S. J.; Point, T. W. La; Kendall, R. J.; Weisskopf, C. P.; Giddings, J. M.; Giesy, J. P.; Lenwood W. Hall, J.; Williams, W. M. Ecological Risk Assessment of Atrazine In. *Environ. Toxicol.* **1996**, *15* (1), 31–76.

(3) Beaulieu, M.; Cabana, H.; Taranu, Z.; Huot, Y. Predicting Atrazine Concentrations in Waterbodies across the Contiguous United States: The Importance of Land Use, Hydrology, and Water Physicochemistry. *Limnol. Oceanogr.* **2020**, 2966–2983. https://doi.org/10.1002/lno.11568.

(4) Ocking, D. A. J. H.; Abbitt, K. I. J. B. Amphibian Contributions to Ecosystem Services. *Herpetol. Conserv. Biol.* **2014**, *9*, 1–17.

(5) Hayes, T. B.; Khoury, V.; Narayan, A.; Nazir, M.; Parka, A.; Brown, T.; Adame, L.; Chan, E.; Buchholz, D.; Stueve, T.; Gallipeau, S. Atrazine Induces Complete Feminization and Chemical Castration in Male African Clawed Frogs (Xenopus Laevis). *Proc. Natl. Acad. Sci. U. S. A.* **2010**, *107* (10), 4612–4617. https://doi.org/10.1073/pnas.0909519107.

(6) Liu, Z.; Wang, Y.; Zhu, Z.; Yang, E.; Feng, X.; Fu, Z.; Jin, Y. Atrazine and Its Main Metabolites Alter the Locomotor Activity of Larval Zebrafish (Danio Rerio). *Chemosphere* **2016**, *148*, 163–170. https://doi.org/10.1016/j.chemosphere.2016.01.007.

(7) Pathak, R. K.; Dikshit, A. K. Atrazine and Human Health. *Int. J. Ecosyst.* **2012**, *1* (1), 14–23. https://doi.org/10.5923/j.ije.20110101.03.

(8) Rostami, S.; Jafari, S.; Moeini, Z.; Jaskulak, M.; Keshtgar, L.; Badeenezhad, A.; Azhdarpoor, A.; Rostami, M.; Zorena, K.; Dehghani, M. Current Methods and Technologies for Degradation of Atrazine in Contaminated Soil and Water: A Review. *Environ. Technol. Innov.* **2021**, *24*, 102019. https://doi.org/10.1016/j.eti.2021.102019.

(9) Li, Q.; Li, Y.; Zhu, X.; Cai, B. Isolation and Characterization of Atrazine-Degrading Arthrobacter Sp. AD26 and Use of This Strain in Bioremediation of Contaminated Soil. *J. Environ. Sci.* **2008**, *20* (10), 1226–1230. https://doi.org/10.1016/S1001-0742(08)62213-5.

(10) Sheldon, R. A. Enzyme Immobilization: The Quest for Optimum Performance. *Adv. Synth. Catal.* **2007**, *349* (8–9), 1289–1307. https://doi.org/10.1002/adsc.200700082.

(11) Diviesti, K.; Holz, R. C. Catalytic Biomaterials for Atrazine Degradation. *Catalysts* **2023**, *13* (1). https://doi.org/10.3390/catal13010140.

(12) Lin, J.; Brown, C. W. Sol-Gel Glass as a Matrix for Chemical and Biochemical Sensing. *TrAC - Trends Anal. Chem.* **1997**, *16* (4), 200–211. https://doi.org/10.1016/S0165-9936(97)00021-6.

(13) Yang, B.; Tang, K.; Wei, S.; Zhai, X.; Nie, N. Preparation of Functionalized Mesoporous Silica as a Novel Carrier and Immobilization of Laccase. *Appl. Biochem. Biotechnol.* **2021**, *193* (8), 2547–2566. https://doi.org/10.1007/s12010-021-03556-2.

(14) Wang, Y.; Caruso, F. Mesoporous Silica Spheres as Supports for Enzyme Immobilization and Encapsulation. *Chem. Mater.* **2005**, *17* (5), 953–961. https://doi.org/10.1021/cm0483137.

(15) Narayan, R.; Nayak, U. Y.; Raichur, A. M.; Garg, S. Mesoporous Silica Nanoparticles: A Comprehensive Review on Synthesis and Recent Advances. *Pharmaceutics* **2018**, *10* (3), 1–49. https://doi.org/10.3390/pharmaceutics10030118.

(16) Pei, X.; Luo, Z.; Qiao, L.; Xiao, Q.; Zhang, P.; Wang, A.; Sheldon, R. A. Putting

Precision and Elegance in Enzyme Immobilisation with Bio-Orthogonal Chemistry. *Chem. Soc. Rev.* **2022**, *51* (16), 7281–7304. https://doi.org/10.1039/d1cs01004b.

(17) López-Laguna, H.; Sánchez, J. M.; Carratalá, J. V.; Rojas-Peña, M.; Sánchez-García, L.; Parladé, E.; Sánchez-Chardi, A.; Voltà-Durán, E.; Serna, N.; Cano-Garrido, O.; Flores, S.; Ferrer-Miralles, N.; Nolan, V.; de Marco, A.; Roher, N.; Unzueta, U.; Vazquez, E.; Villaverde, A. Biofabrication of Functional Protein Nanoparticles through Simple His-Tag Engineering. *ACS Sustain. Chem. Eng.* **2021**, *9* (36), 12341–12354. https://doi.org/10.1021/acssuschemeng.1c04256.

(18) Chen, C.-Y.; Li, H.-X.; Davis, M. E. Studies on Mesoporous Materials. *Microporous Mater.* **1993**, *2* (1), 17–26. https://doi.org/10.1016/0927-6513(93)80058-3.

(19) Valenstein, J. S.; Kandel, K.; Melcher, F.; Slowing, I. I.; Lin, V. S. Y.; Trewyn, B. G. Functional Mesoporous Silica Nanoparticles for the Selective Sequestration of Free Fatty Acids from Microalgal Oil. *ACS Appl. Mater. Interfaces* **2012**, *4* (2), 1003–1009. https://doi.org/10.1021/am201647t.

(20) Schweitzer, N. M.; Hu, B.; Das, U.; Kim, H.; Greeley, J.; Curtiss, L. A.; Stair, P. C.; Miller, J. T.; Hock, A. S. Propylene Hydrogenation and Propane Dehydrogenation by a Single-Site Zn2+ on Silica Catalyst. *ACS Catal.* **2014**, *4* (4), 1091–1098. https://doi.org/10.1021/cs401116p.

(21) Shapir, N.; Pedersen, C.; Gil, O.; Strong, L.; Seffernick, J.; Sadowsky, M. J.; Wackett, L. P. TrzN from Arthrobacter Aurescens TC1 Is a Zinc Amidohydrolase. *J. Bacteriol.* **2006**, *188* (16), 5859–5864. https://doi.org/10.1128/JB.00517-06.

(22) Mu, Y.; Zhan, G.; Huang, C.; Wang, X.; Ai, Z.; Zou, J.; Luo, S.; Zhang, L. Dechlorination-Hydroxylation of Atrazine to Hydroxyatrazine with Thiosulfate: A Detoxification Strategy in Seconds. *Environ. Sci. Technol.* **2019**, *53* (6), 3208–3216. https://doi.org/10.1021/acs.est.8b06351.

(23) Jackson, C. J.; Coppin, C. W.; Carr, P. D.; Aleksandrov, A.; Wilding, M.; Sugrue, E.; Ubels, J.; Paks, M.; Newman, J.; Peat, T. S.; Russell, R. J.; Field, M.; Weik, M.; Oakeshott, J. G.; Scott, C. 300-Fold Increase in Production of the Zn2+-Dependent Dechlorinase TrzN in Soluble Form via Apoenzyme Stabilization. *Appl. Environ. Microbiol.* **2014**, *80* (13), 4003–4011. https://doi.org/10.1128/AEM.00916-14.

(24) Seffernick, J. L.; Reynolds, E.; Fedorov, A. A.; Fedorov, E.; Almo, S. C.; Sadowsky, M. J.; Wackett, L. P. X-Ray Structure and Mutational Analysis of the Atrazine Chlorohydrolase TrzN. *J. Biol. Chem.* **2010**, *285* (40), 30606–30614. https://doi.org/10.1074/jbc.M110.138677.

(25) Gaffney, D. A.; O'Neill, S.; O'Loughlin, M. C.; Hanefeld, U.; Cooney, J. C.; Magner, E. Tailored Adsorption of His6-Tagged Protein onto Nickel(Ii)-Cyclam Grafted Mesoporous Silica. *Chem. Commun.* **2010**, *46* (7), 1124–1126. https://doi.org/10.1039/b915169a.

(26) Heidari, R.; Khosravian, P.; Mirzaei, S. A.; Elahian, F. SiRNA Delivery Using Intelligent

Chitosan-Capped Mesoporous Silica Nanoparticles for Overcoming Multidrug Resistance in Malignant Carcinoma Cells. *Sci. Rep.* **2021**, *11* (1), 1–14. https://doi.org/10.1038/s41598-021-00085-0.

(27) Seffernick, J. L.; Reynolds, E.; Fedorov, A. A.; Fedorov, E.; Almo, S. C.; Sadowsky, M. J.; Wackett, L. P. X-Ray Structure and Mutational Analysis of the Atrazine Chlorohydrolase TrzN. *J. Biol. Chem.* **2010**, *285* (40), 30606–30614. https://doi.org/10.1074/jbc.M110.138677.

(28) Martinez, S.; Kuhn, M. L.; Russell, J. T.; Holz, R. C.; Elgren, T. E. Acrylamide Production Using Encapsulated Nitrile Hydratase from Pseudonocardia Thermophila in a Sol-Gel Matrix. *J. Mol. Catal. B Enzym.* **2014**, *100*, 19–24. https://doi.org/10.1016/j.molcatb.2013.11.014.

(29) Thommes, M.; Kaneko, K.; Neimark, A. V.; Olivier, J. P.; Rodriguez-Reinoso, F.; Rouquerol, J.; Sing, K. S. W. Physisorption of Gases, with Special Reference to the Evaluation of Surface Area and Pore Size Distribution (IUPAC Technical Report). *Pure Appl. Chem.* **2015**, *87* (9–10), 1051–1069. https://doi.org/10.1515/pac-2014-1117.

(30) Szymańska, E.; Winnicka, K. Stability of Chitosan - A Challenge for Pharmaceutical and Biomedical Applications. *Mar. Drugs* **2015**, *13* (4), 1819–1846. https://doi.org/10.3390/md13041819.

(31) Garcia-Galan, C.; Berenguer-Murcia, Á.; Fernandez-Lafuente, R.; Rodrigues, R. C. Potential of Different Enzyme Immobilization Strategies to Improve Enzyme Performance. *Adv. Synth. Catal.* **2011**, *353* (16), 2885–2904. https://doi.org/10.1002/adsc.201100534.

(32) Darby, J. F.; Atobe, M.; Firth, J. D.; Bond, P.; Davies, G. J.; O'Brien, P.; Hubbard, R. E. Increase of Enzyme Activity through Specific Covalent Modification with Fragments. *Chem. Sci.* **2017**, *8* (11), 7772–7779. https://doi.org/10.1039/c7sc01966a.

(33) Lee, K. Y.; Mooney, D. J. Alginate: Properties and Biomedical Applications. *Prog. Polym. Sci.* **2012**, *37* (1), 106–126. https://doi.org/10.1016/j.progpolymsci.2011.06.003.

(34) Bedade, D. K.; Sutar, Y. B.; Singhal, R. S. Chitosan Coated Calcium Alginate Beads for Covalent Immobilization of Acrylamidase: Process Parameters and Removal of Acrylamide from Coffee. *Food Chem.* **2019**, *275* (June 2018), 95–104. https://doi.org/10.1016/j.foodchem.2018.09.090.

(35) Fareez, I. M.; Lim, S. M.; Mishra, R. K.; Ramasamy, K. Chitosan Coated Alginate-Xanthan Gum Bead Enhanced PH and Thermotolerance of Lactobacillus Plantarum LAB12. *Int. J. Biol. Macromol.* **2015**, *72*, 1419–1428. https://doi.org/10.1016/j.ijbiomac.2014.10.054.

(36) Lohiya, G.; Katti, D. S. Carboxylated Chitosan-Mediated Improved Efficacy of Mesoporous Silica Nanoparticle-Based Targeted Drug Delivery System for Breast Cancer Therapy. *Carbohydr. Polym.* **2022**, *277* (October 2021), 118822.

https://doi.org/10.1016/j.carbpol.2021.118822.

(37) Ning, C.; Jiajia, J.; Meng, L.; Hongfei, Q.; Xianglong, W.; Tingli, L. Electrophoretic Deposition of GHK-Cu Loaded MSN-Chitosan Coatings with PH-Responsive Release of Copper and Its Bioactivity. *Mater. Sci. Eng. C* **2019**, *104* (May), 109746. https://doi.org/10.1016/j.msec.2019.109746.

(38) Chiang, Y. W.; Wang, T. H.; Lee, W. C. Chitosan Coating for the Protection of Amino Acids That Were Entrapped within Hydrogenated Fat. *Food Hydrocoll.* **2009**, *23* (3), 1057–1061. https://doi.org/10.1016/j.foodhyd.2008.04.007.

(39) Im, J. K.; Cho, Y. C.; Noh, H. R.; Yu, S. J. Geographical Distribution and Risk Assessment of Volatile Organic Compounds in Tributaries of the Han River Watershed. *Agronomy* **2021**, *11* (5). https://doi.org/10.3390/agronomy11050956.

(40) Baker, J. P.; Bernard, D. P.; Christensen, S. W.; Sale, M. J.; Freda, J.; Heltcher, K.; Marmorek, D.; Rowe, L.; Scanlon, P.; Suter, G.; Warren-Hicks, W. J.; Welbourn, P. M. Biological Effects of Changes in Surface Water Acid-Base Chemistry. *Acidic Depos. State Sci. Technol.* **1990**.

(41) Weltz, J. S.; Kienle, D. F.; Schwartz, D. K.; Kaar, J. L. Reduced Enzyme Dynamics upon Multipoint Covalent Immobilization Leads to Stability-Activity Trade-Off. *J. Am. Chem. Soc.* **2020**, *142* (7), 3463–3471. https://doi.org/10.1021/jacs.9b11707.

(42) City of Golden Public Works Department, www.cityofgolden.net/DrinkingWater (accessed 2023-08-13), *2022 Water Quality Report*; Golden, 2022.

CHAPTER 5

CONCLUSIONS

The studies reported herein have provided important information in elucidating the potential of TrzN to be a biocatalyst for the degradation of atrazine. In chapter 2, kinetic studies assisted in providing insight into the previously unknown mechanism of TrzN from *Arthrobacter aurescens* TC1. At pH of 7.0 and 20°C, a k_{cat} value of 22.6 $\pm$ 2 s^{-1} and a K_m of 34.7 $\pm$ 4 μM were obtained. These values are significantly higher than what has been previously reported. These values were recorded in the absence of the His_6 tag essential for purification. Upon further inspection, the kinetic parameters with the His_6 tag were a k_{cat} value of 6.4 $\pm$ 1 s^{-1} and a K_m of 16.4 $\pm$ 5 μM. These data agree with what was previously published and suggest the polyhistidine tag has an effect on the protein folding, the Zn(II) mononuclear site, or both. The proposed mechanism starts with substrate recognition in a mixed hydrophobic/polar pocket adjacent to active site. Results from solvent isotope studies of TrzN indicated a two-proton transfer. The pH studies of the kinetic constants k_{cat}, K_m and k_{cat}/K_m provide two ionizable groups, one with $pK_a \approx 3.6$ and one with a $pK_a \approx 10.8$, which were assigned to the active site residues Glu241 and Thr325. A third pK_a at ≈ 7, that is enzyme centered, was assigned to His274. Solvent kinetic isotope effect studies indicate that two protons are transferred in the transition-state, likely due to the breaking of a Zn(II)-bound water O-H bond by His274 and the transfer of this proton to Glu274 which shuttles it to a triazole nitrogen of the substrate atrazine. Thermostability studies show a positive enthalpy which is indicative of a conformation change upon substrate binding. This change is likely due to the bond formation and breaking during the nucleophilic attack on the ortho carbon by the Zn(II)-bound hydroxide. K_m was unaffected by a change in temperature

suggesting that the formation of the enzyme substrate complex is proceeding in equilibrium. Overall, the results are in good alignment with the previously published TrzN mechanism with direct evidence for the catalytic roles of His271, Glu274, and Thr325 and the transfer of two proton in the transition-state.

In chapter 3, TrzN was immobilized in alginate beads, chitosan coated alginate beads, and sol-gels. This was the first published example of TrzN being immobilized within a biomaterial. It was shown that TrzN:alginate and TrzN:chitosan hydrolyzed 50 μM of atrazine in 6 h with negligible protein loss and an ~80% conversion rate. The TrzN:sol-gel biomaterial showed a six-fold improvement exhibiting an ~95% conversion rate in an hour with negligible protein loss. The significant increase in activity was likely a result of the variable diffusivity of the alginate due to overall bead size and the pore size being susceptible to environmental effects. All three materials showed potential for long-term storage and reusability. The addition of a chitosan coating (TrzN:chitosan) greatly improved the biocatalyst's (TrzN:alginate) stability in extreme conditions such as pH, temperature, and the presence of organic solvents. Overall, TrzN:sol-gel biomaterial proved to be the best atrazine dechlorination biocatalyst of the three tested in this chapter. This study was the first look into the potential of TrzN to be immobilized with a biomaterial and successfully degrade atrazine.

The work presented in chapter 4 builds off what was learned in chapter 3. In this chapter, TrzN was immobilized using functionalized and non-functionalized MSN. The functionalized MSN was coated in Zn(II). The hope was to create a covalent tethering system between the MSN's surface and the N-terminus His_6 tag engineering on to TrzN for IMAC purification. What was observed was a greater protein retention during immobilization but a significant decrease in activity compared to the non-functionalized MSN. This was likely a result of the negatively

charged active site pocket of TrzN creating a “suction cup” effect with the material which prevented substrate from entering the active site. Three pore sizes were also evaluated, a medium pore size (6-12nm) exhibited the highest activity (TrzN:MSN-10). From chapter 3, it was clear that chitosan had a significant impact on biocatalyst stability. Therefore TrzN:MSN-10 was coated in chitosan (TrzN:MSN-10:Chit). TrzN:MSN-10:Chit was shown to be a superior TrzN biomaterial compared to TrzN:MSN-10, it exhibited higher activity under storage conditions, in the presence of methanol, at low and high pH values, and elevated temperatures up to 80°C. On top of that, both TrzN:MSN-10 and TrzN:MSN-10:Chit were shown to be fully active in river water thus establishing these materials as functional under field conditions. This chapter established that TrzN:MSN-10:Chit exhibited the best overall catalytic profile making it a promising biocatalyst for the degradation of atrazine.

There are numerous paths forward based off the result presented. Given the informative results obtained from chapter 2, there still exist a lot of gaps that need to be filled in establishing a more conclusive reaction mechanism for TrzN. First, the His274 residue plays a clear role in the catalytic mechanism as a proton shuttler. Unlike Glu241, which has been mutated in previous work, mutagenesis work would be necessary to clarify the role of His274. For this I would suggest mutating this residue to an alanine (His274Ala) since alanine would prevent the proton transfer from the Zn(II) bound water moiety. Other residues that could provide insight as a mutate would be arginine or lysine because they can both function as an acid/base. More extensive mutagenesis work should also be done on Glu241. As mentioned above, a Glu241Gln mutant was made previously. I suggest mutating this residue to alanine and aspartic acid. It would be expected that the Glu241Ala mutant would be inactive given its proposed role in transferring a proton and forming a catalytically critical hydrogen bond to the triazine nitrogen

atom. For the mutants that exhibit catalytic activity, the determination of the kinetic parameters K_m, k_{cat}, *and* k_{cat}/K_m as well as the kinetic isotope effect and temperature dependence should be collected and compared to the data reported in chapter 2 for WT TrzN. Crystallographic work would also compliment the mutagenesis work as well. The mutants should be crystallized in the absence and presence of atrazine by co-crystallization and soaking already pre-formed crystals. Other studies could include inhibitor studies, active site metal substitutions, and investigating the role of second sphere residues. Overall, there are numerous roots to follow that would aid in the elucidation of the TrzN mechanism which would provide insight into why it is an exceptional biocatalyst for the degradation of atrazine.

With the results presented in chapters 3 and 4, the clear path forward is using TrzN:sol-gel and TrzN:MSN-10:Chit biomaterials for larger lab-scale remediation experiments. The TrzN:sol-gel biomaterial can be cast into a desirable shape and size. The results from chapter 3 were on irregularly crushed TrzN:sol-gel samples, the next step would be to engineer and test a variety of casted shapes and sizes for the TrzN:sol-gel biomaterial and evaluate the activity. Once shape and size are optimized, I suggest the construction of a continuous flow reactor using TrzN:sol-gel and TrzN:MSN-10:Chit biomaterials. Concurrently, with biocatalyst becoming more popular, new materials and methods for creating superior biomaterials are being published more than ever. I suggest continual education on the literature to find and test other biomaterials that may be a better fit for TrzN than what has been described in chapters 3 and 4.

In conclusion this thesis has provided data to support the investigation of the enzymatic mechanism of TrzN from *Arthrobacter aurescens* TC1 to highlight TrzN's potential as a biocatalyst for the degradation of atrazine.

APPENDIX A

COPYRIGHT PERMISSION FROM CO-AUTHORS

Re: Thesis Chapter Permission Request

GR **Glory Russell-Parks (Student) <grussellpark...** Thursday, October 12, 2023 at 1:27 PM

To: Karla Diviesti (Student)

I, Glory Russell-Parks, hereby authorize Karla Diviesti to use any part or all of the manuscript entitled "Atrazine Degradation Using Immobilized Triazine Hydrolase from *Arthrobacter Aurescens* TC1 in Mesoporous Silica Nanomaterials" within her thesis.

From: Brian Trewyn <btrewyn@mines.edu>
Sent: Thursday, October 12, 2023 1:43 PM
To: Karla Diviesti (Student) <kdiviesti@mines.edu>
Cc: Glory Russell-Parks (Student) <grussellparks@mines.edu>; Richard Holz <rholz@mines.edu>
Subject: Re: Thesis Chapter Permission Request

I, Brian Trewyn, hereby authorize Karla Diviesti to use any part or all of the manuscript entitled "Atrazine Degradation Using Immobilized Triazine Hydrolase from *Arthrobacter Aurescens* TC1 in Mesoporous Silica Nanomaterials" within her thesis.

_____

Brian Trewyn, PhD.
https://chemistry.mines.edu/trewyn-research/
Associate Professor

RE: Thesis Chapter Permission Request

RH **Richard Holz <rholz@mines.edu>** Thursday, October 12, 2023 at 1:59 PM

To: Brian Trewyn; Karla Diviesti (Student); **Cc:** Glory Russell-Parks (Student)

I approve too.

Take care, Rick.

Richard C. Holz, Ph.D.
Provost and Professor
Colorado School of Mines
Golden, CO 80401
303-273-3003
COLORADOSCHOOLOFMINES | mines.edu

APPENDIX B

SUPPLEMENTRY MATERIAL

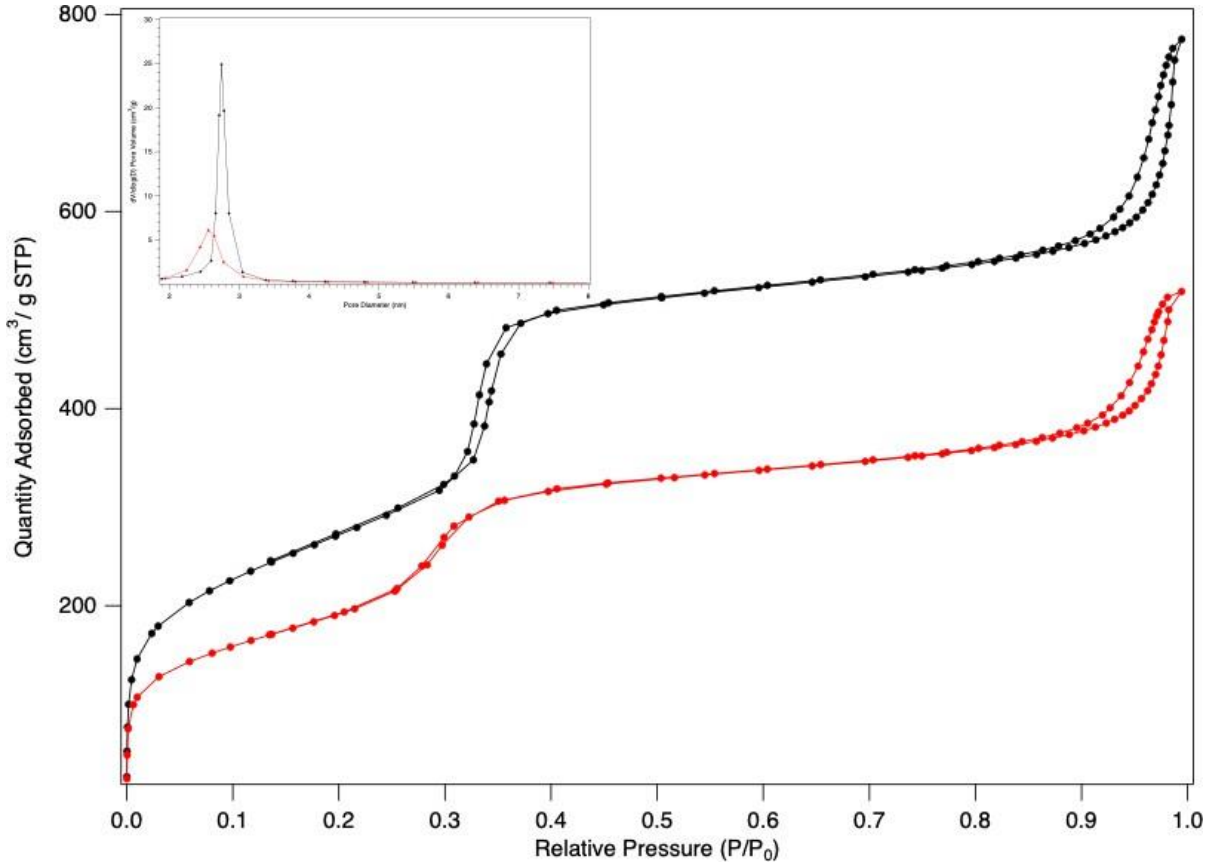

Figure B.1. Nitrogen sorption isotherms and pore size distributions (inset) of unfunctionalized MCM-41 (black) and Zn functionalized MCM-41 (red). The BET surface area of MCM-41 and Zn@MCM-41 was calculated as 968 m^2/g and 736 m^2/g, respectively.

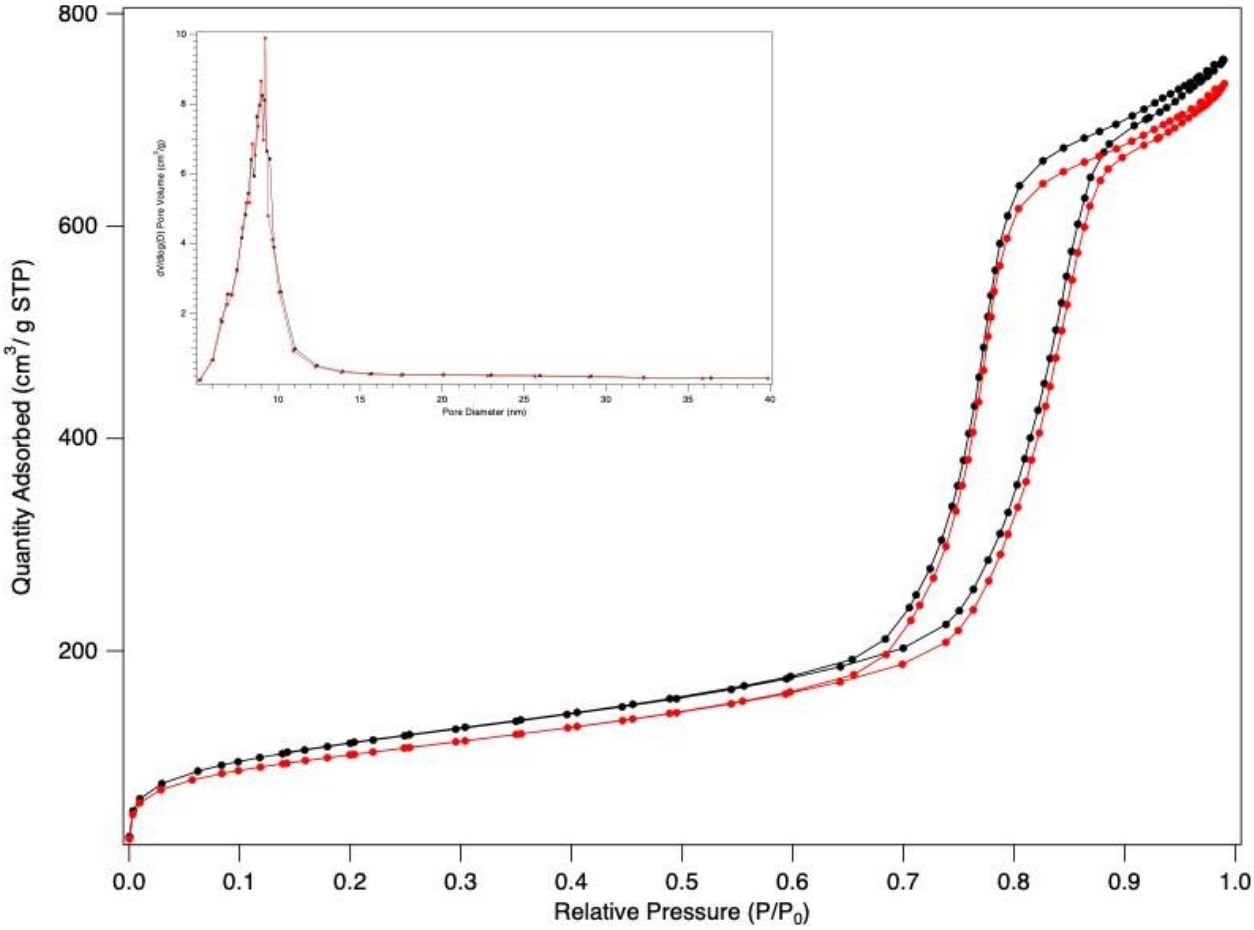

Figure B.2. Nitrogen sorption isotherms and pore size distributions (inset) of unfunctionalized MSN-10 (black) and Zn functionalized MSN-10(red). The BET surface area of MSN-10 and Zn@MSN-10 was calculated as 397 m^2/g and 358 m^2/g, respectively.

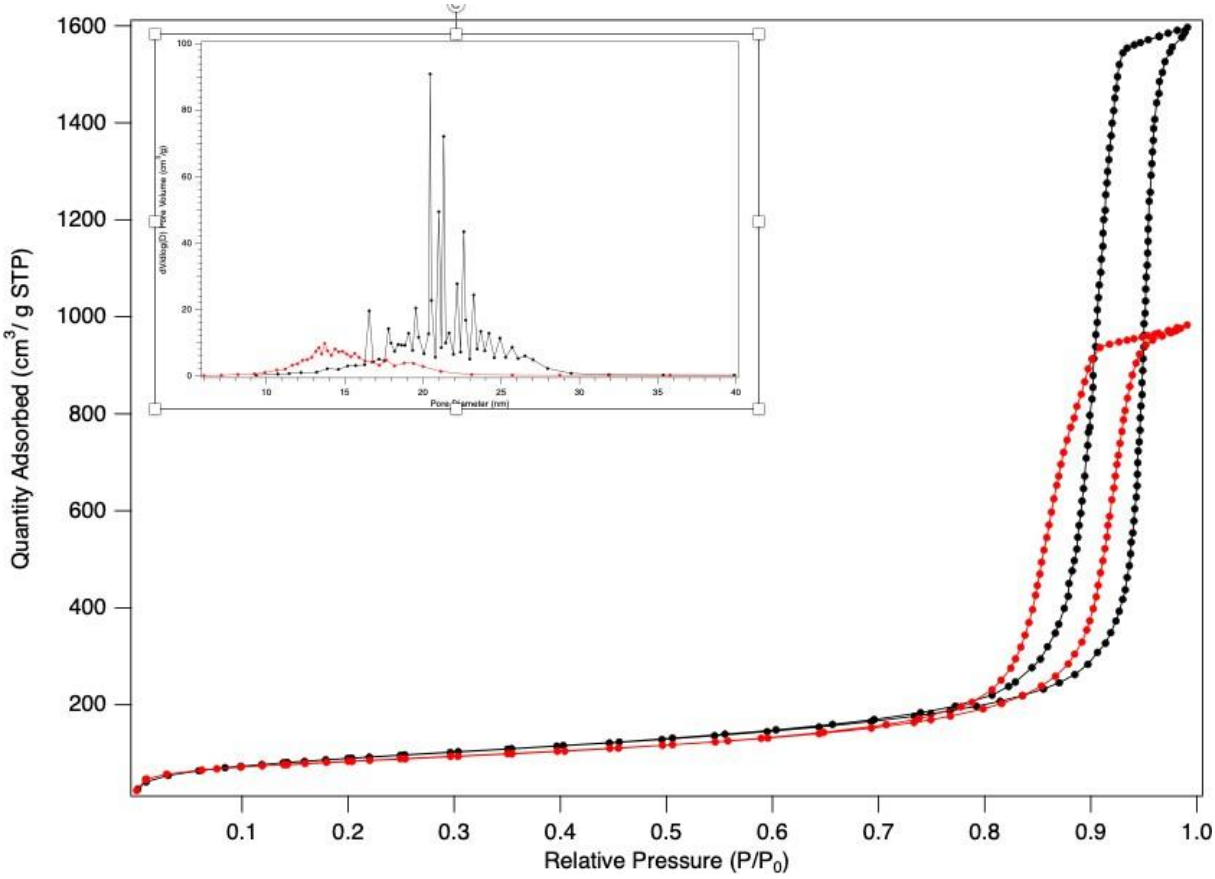

Figure B.3. Nitrogen sorption isotherms and pore size distributions (inset) of unfunctionalized PEMSN-10 (black) and Zn functionalized PEMSN-10 (red). The BET surface area of PEMSN-10 and Zn@PEMSN-10 was calculated as 321 m^2/g and 293 m^2/g, respectively.

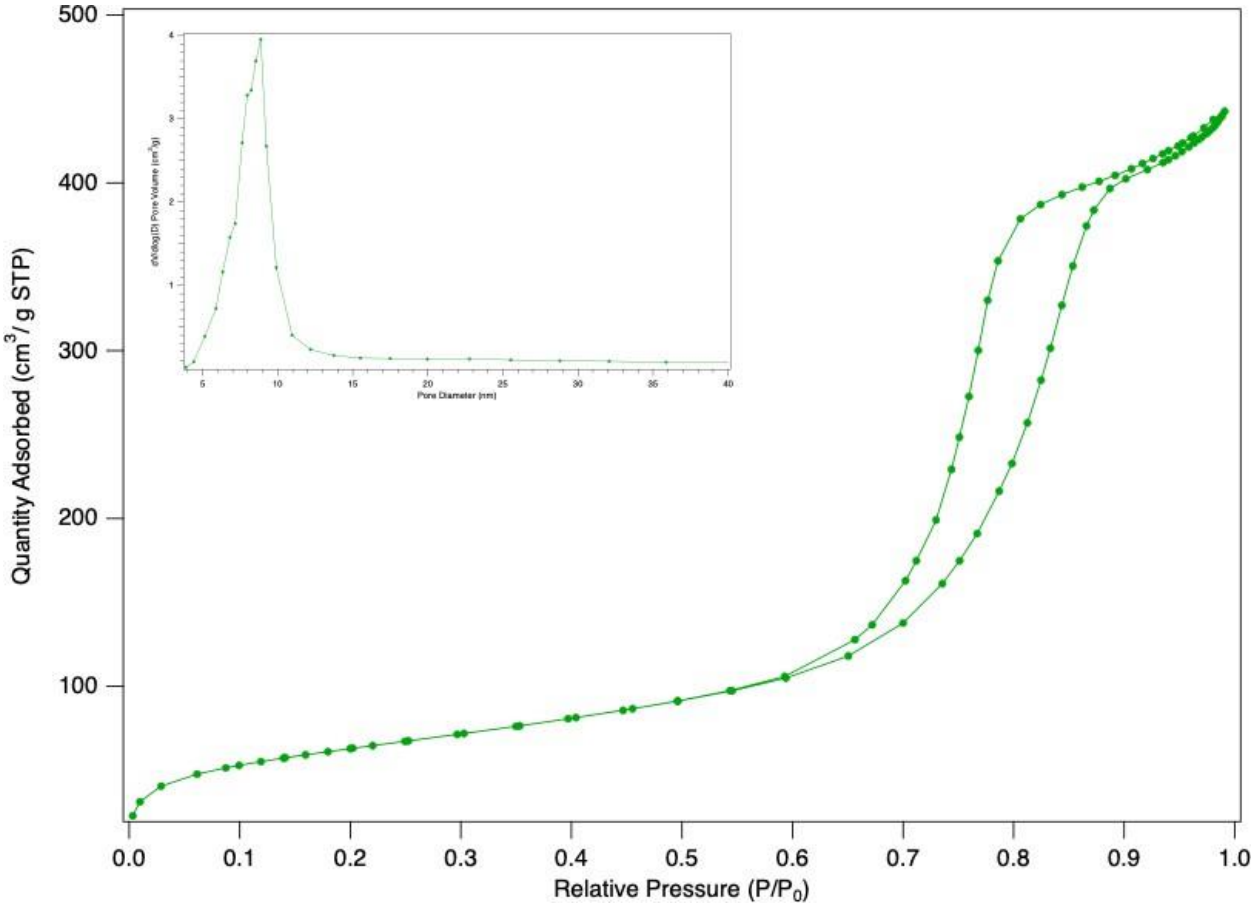

Figure B.4. Nitrogen sorption isotherms and pore size distributions (inset) of chitosan coated MSN-10. The BET surface area of chitosan coated MSN-10 was calculated as 225 m^2/g.

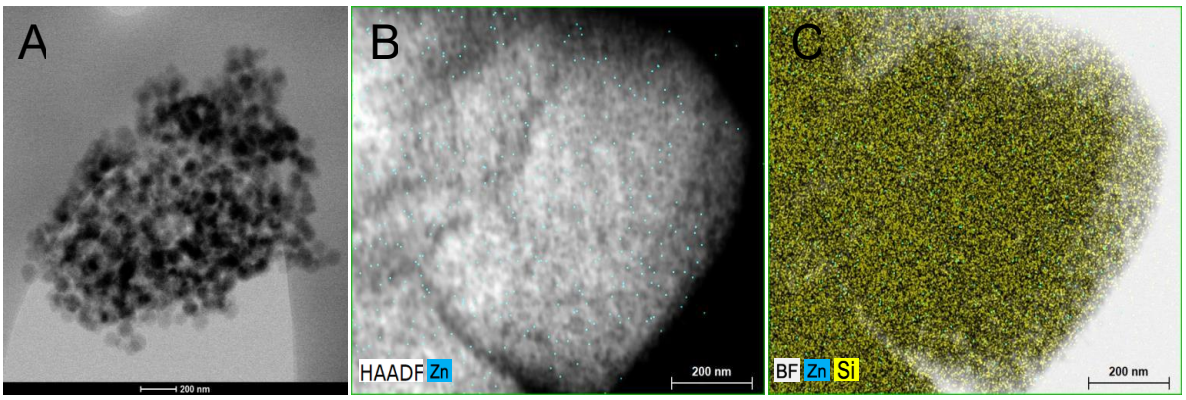

Figure B.5. Scanning transmission electron microscope (STEM) images of MCM-41 (A), elemental mapping of Zn on the MCM-41 support (B), elemental mapping of Zn and Si (C). Zn represented by blue and Si represented by yellow. All scale bars are 200 nm.

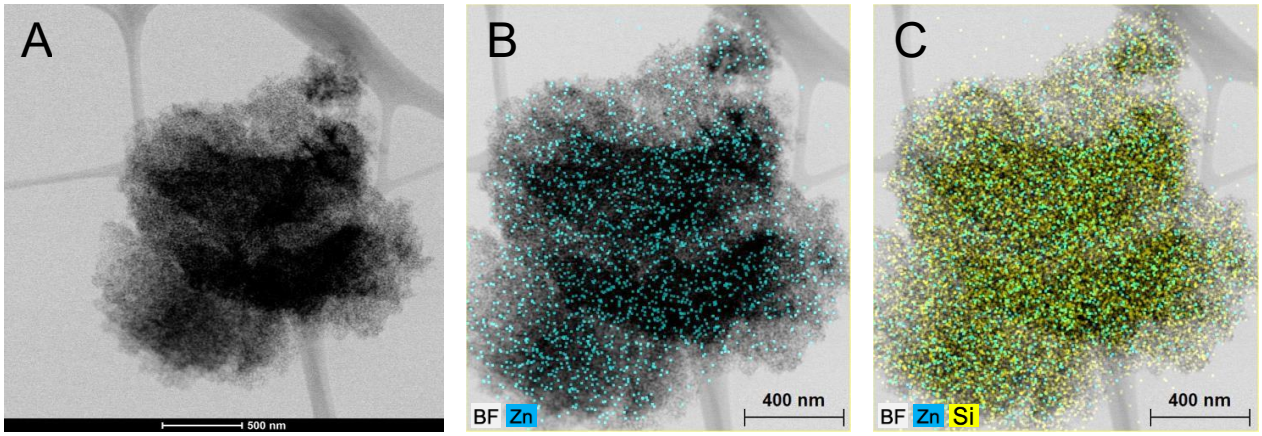

Figure B.6. Scanning transmission electron microscope (STEM) images of PEMSN-10 (A) scale bar is 500 nm, elemental mapping of Zn on the PEMSN-10 support (B) scale bar is 400 nm, elemental mapping of Zn and Si (C) scale bar is 400 nm. Zn represented by blue and Si represented by yellow.

Table B.1. Concentration of Zn loaded into each mesoporous silica nanomaterial determined by inductively coupled plasma atomic emission spectroscopy (ICP-AES)

Sample	Zn (ppm)
Zn@MCM-41	31.43
Zn@MSN-10	83.05
Zn@PEMSN-10	46.06

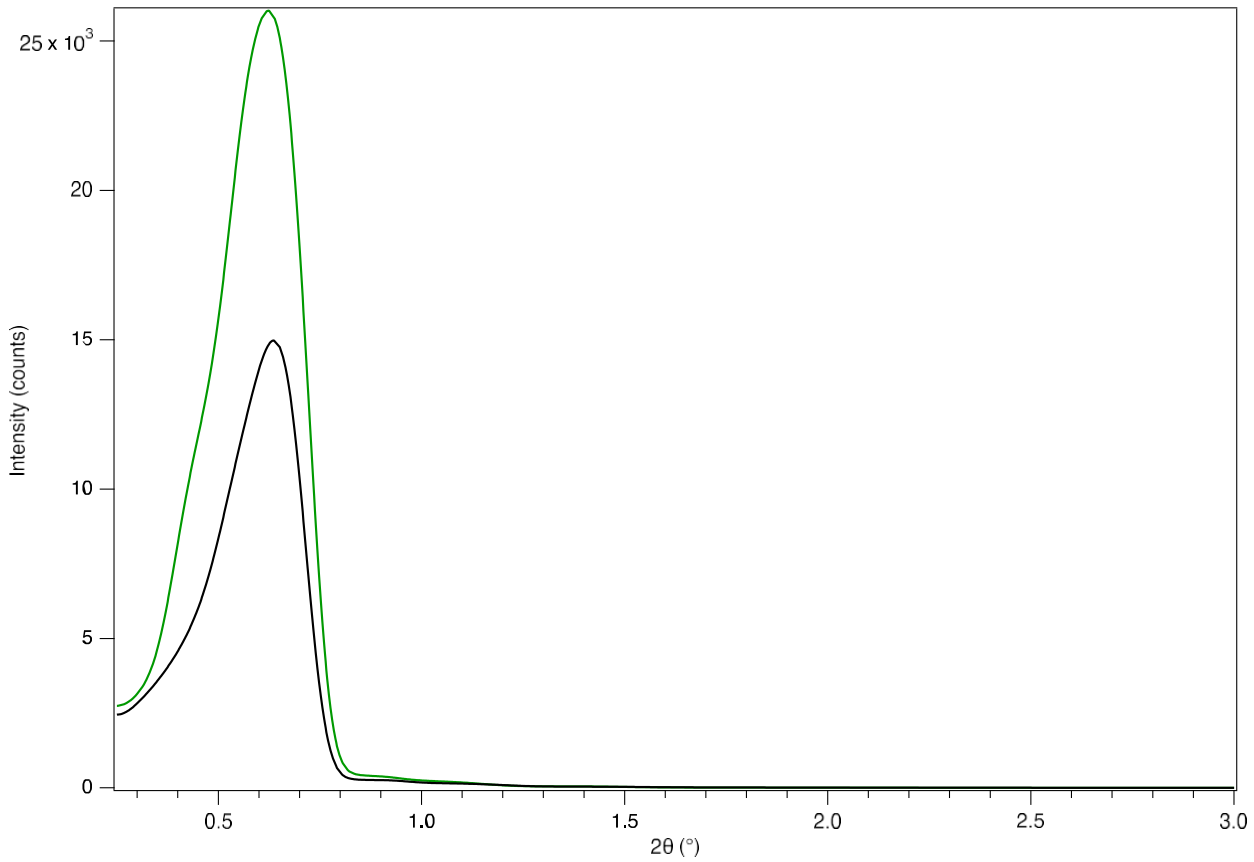

Figure B.7. Low angle powder X-ray diffraction patterns of MSN-10 (black) and chitosan coated MSN-10 (green).

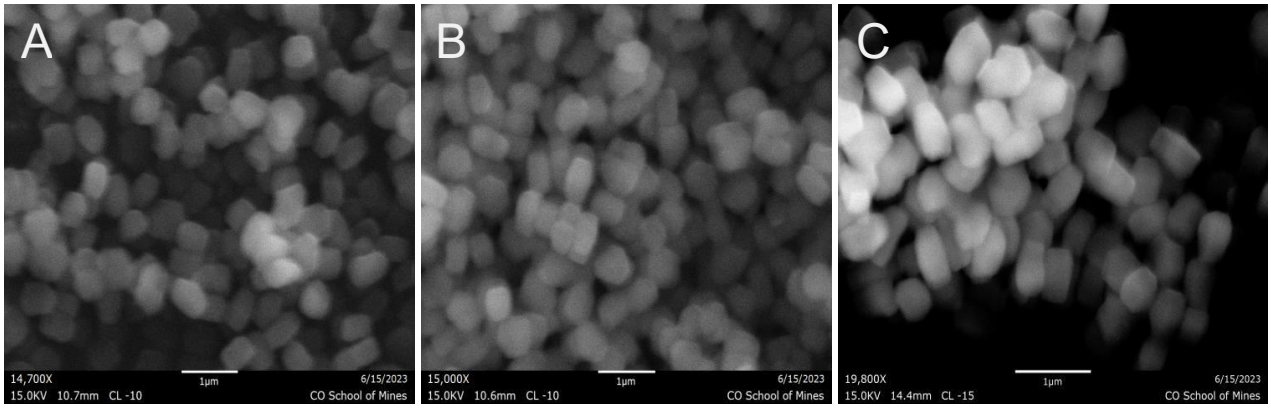

Figure B.8. Scanning electron microscope (SEM) images of chitosan coated MSN-10. Scale bar is 1 μm.

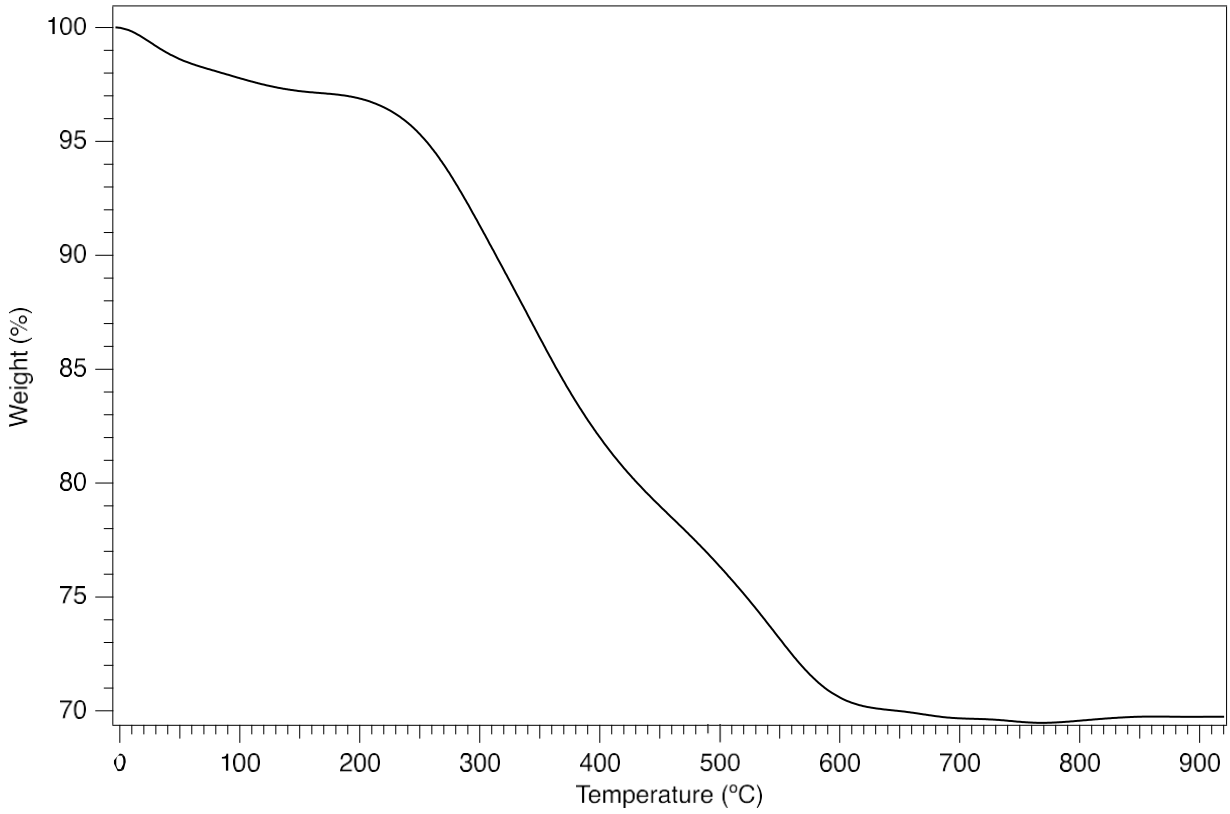

Figure B.9. Thermogravimetric analysis (TGA) of chitosan coated MSN-10.

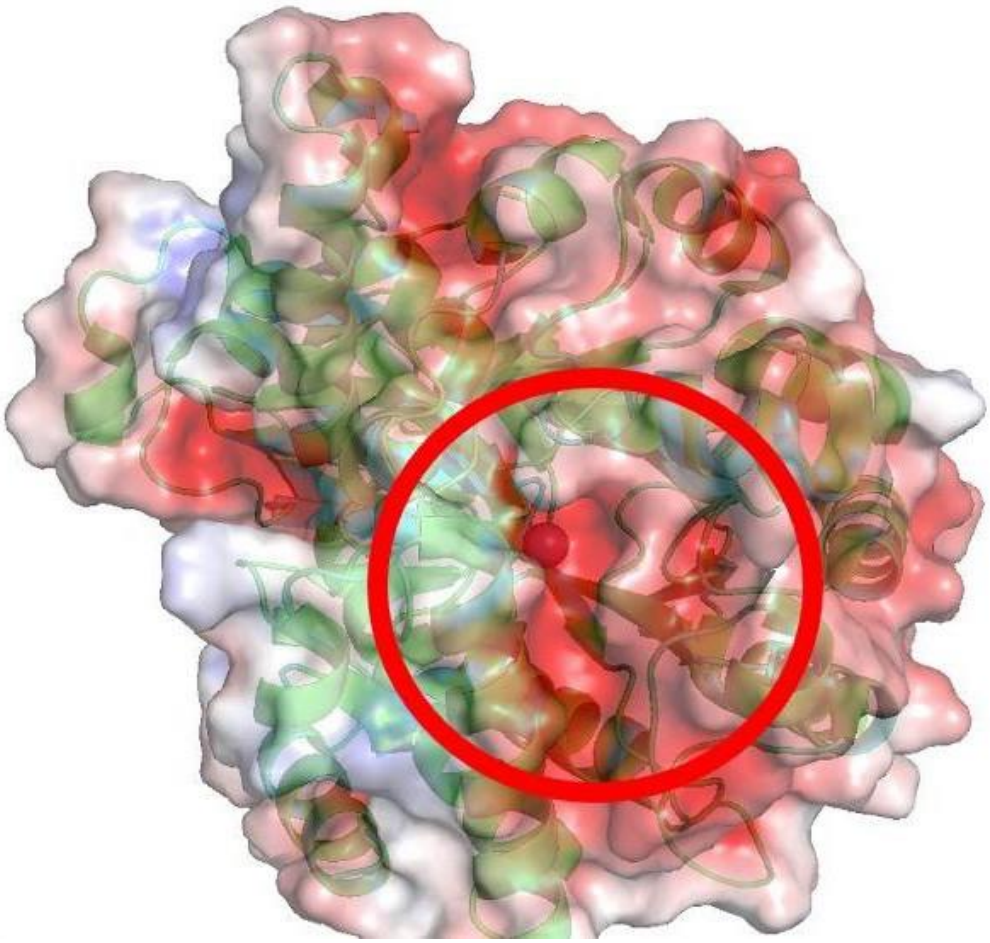

Figure B.10. PYMOL rendered image of TrzN with a red circle indicating the active site pocket. A gradient color scale is used to show areas of negative (red) or positive (blue) charge.

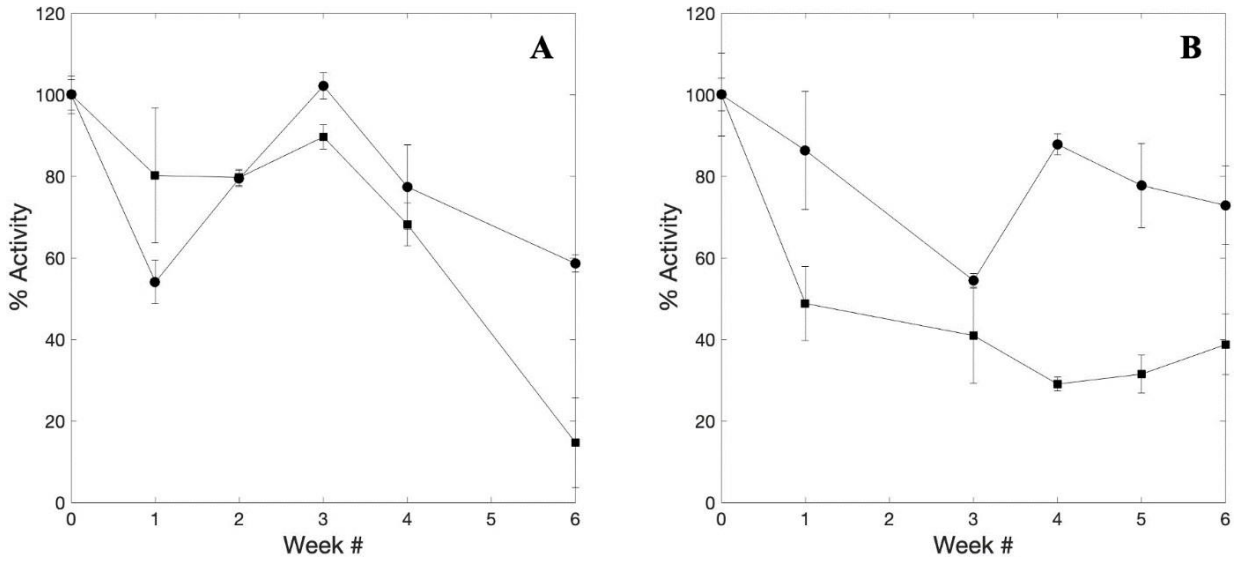

Figure B.11. Long-term stability of TrzN immobilized in MSN (black squares) and chit:MSN (black circles) measured of a six week period. The degradation of atrazine was evaluated at 25°C with 50 µM atrazine in 50 mM HEPES buffer pH 7.0 for 1 hour followed by their respective storage methods. **A.** samples were stored with no buffer at 4°C. **B.** Samples were stored with no buffer at -80°C.

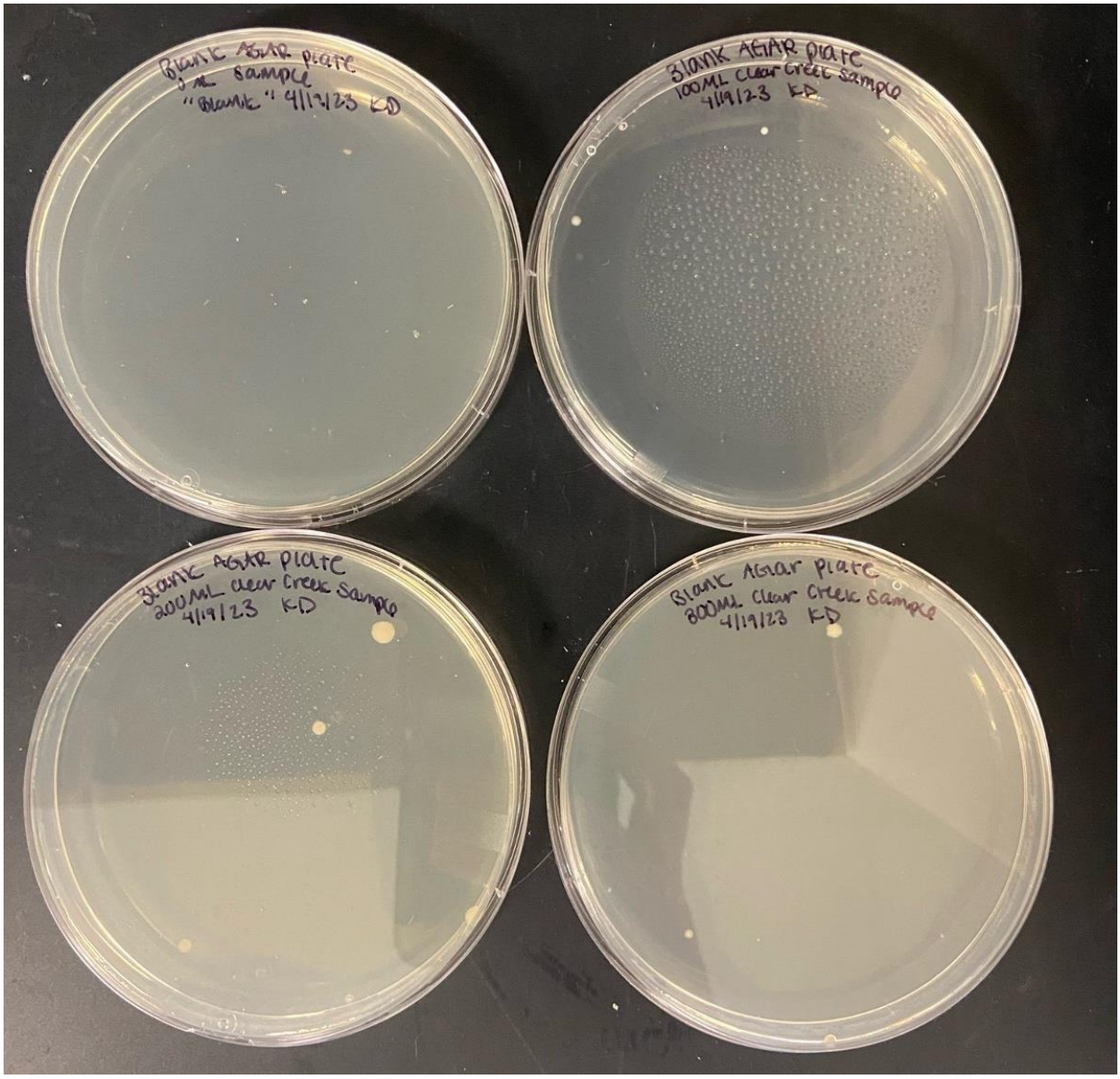

Figure B.12. Clear creek water samples were plated on agar plates and incubated for 48 hours. Top left: the "blank" agar plate had 0 µl of sample and showed no bacterial growth. Top right: 100 µl of clear creek sample was plated and there are 2 small observable colonies. Bottom left: 200 µl of clear creek sample was plated and there are 4observable colonies. Bottom right: 300 µl of clear creek sample was plated and there are 2 observable colonies.

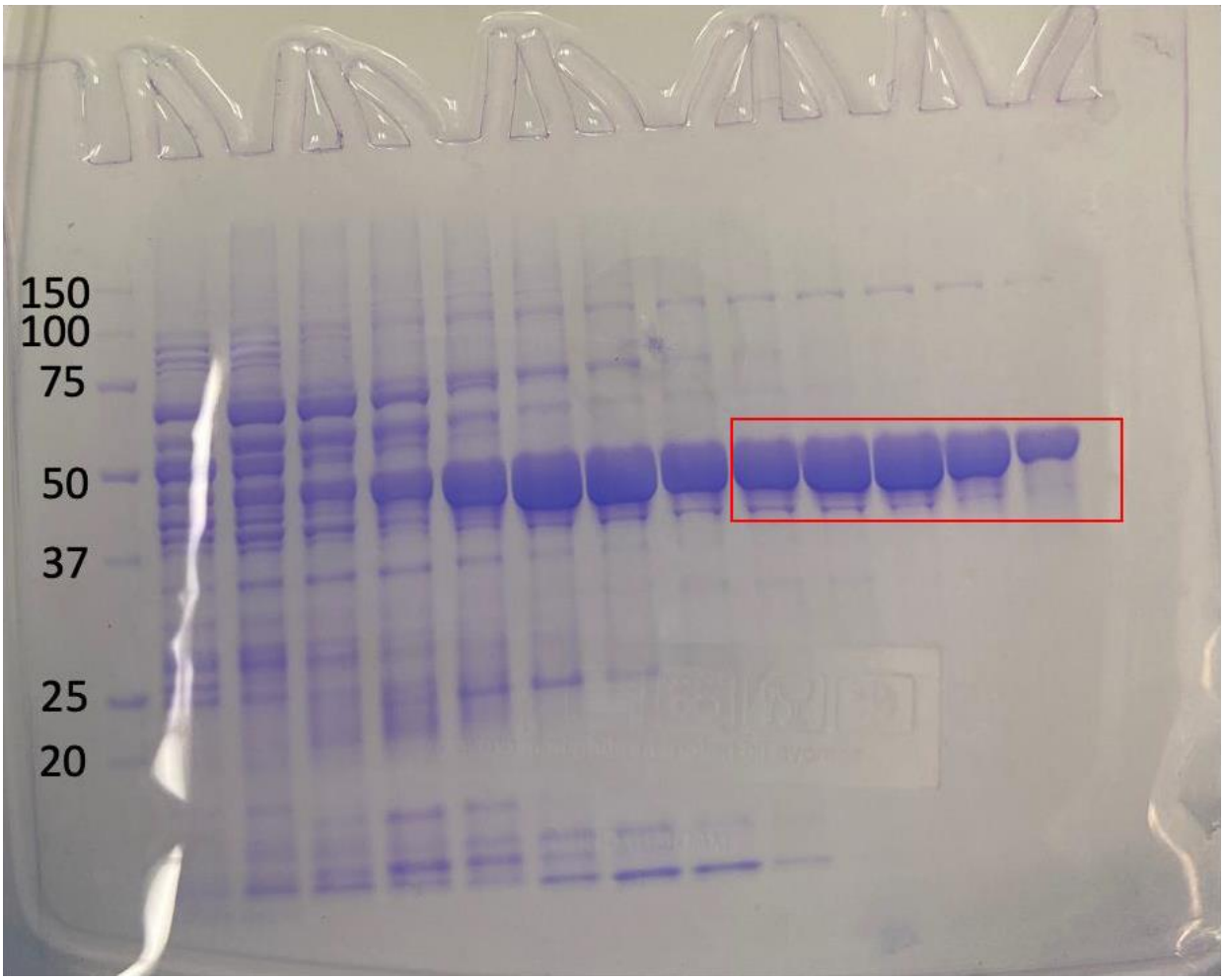

Figure B.13. SDS-PAGE gel showing pure TrzN (red box) at ~51 kDa.

APPENDIX C

COPYRIGHT PERMISSION FROM PUBLISHED JOURNALS

Catalysis and *ACS Environmental AU* are open access journals and do not require explicit permission from the publisher to include the published manuscripts in this thesis.